CONSIDERATIONS FOR THE DEVELOPMENT AND IMPLEMENTATION OF STRUCTURES FOR LOSSLESS ION MANIPULATIONS (SLIM) PLATFORMS

By

ZACKARY R. KINLEIN

A dissertation submitted in partial fulfillment of
the requirements for the degree of

DOCTOR OF PHILOSOPHY

WASHINGTON STATE UNIVERSITY
Department of Chemistry

MAY 2024

To the Faculty of Washington State University:

The members of the Committee appointed to examine the dissertation of ZACKARY R. KINLEIN find it satisfactory and recommend that it be accepted.

Brian H. Clowers, Ph.D., Chair

Qiang Zhang, Ph.D.

Jeffrey G. Bell, Ph.D.

Yehia M. Ibrahim, Ph.D.

ACKNOWLEDGMENT

I consider myself incredibly lucky to have had countless remarkable people in my life. Beginning with my family, I'd like to thank them for fostering an environment which led me to become what I am today. I'd also like to extend a special thank you to my brother Scott for being brave enough to blaze the path which I now walk, and which has led me to a life which I'd never imagined possible. I of course have to acknowledge those mentors who guided me through the early phases of my career; Dr. Kathryn Kautzman, Dr. Sheena Young, and Dr. Benedict Capacio. My admiration and gratitude towards their willingness to guide and aid those at the start of their journey has only grown with time and I will be forever grateful for their contributions to my life.

Aside from those who got me started on my journey, I must also acknowledge the people who were instrumental in my success as a graduate student. To begin, I'd like to thank the NIH for funding my research for the majority of my time at WSU. Moving on, I'd like to extend a special thank you to my group members for both their advice over the years as well as their willingness to provide a distraction when needed. I also want to acknowledge my committee members, in particular the late Dr. Peter Reilly, for their guidance throughout my journey as a graduate student. Additionally, I need to acknowledge the substantial contributions to my success made by Gordon Anderson as well as the kindness and generosity which he showed me over the years. Lastly, I need to acknowledge my graduate advisor, Dr. Brian Clowers. As I mentioned previously, I consider myself a lucky person. Given that I had the opportunity to work with him over the last five years, I don't think that's up for debate. Dr. Clowers provided me with

everything I could ask for, enabling me to flourish professionally while remaining sympathetic to the challenges that I faced not only as a graduate student, but as a human being as well.

Up until this point, I've taken the time to address those who prepared and propelled through my graduate journey. That being said, there are a few names which have yet to be mentioned. Anyone who has gone through this process or something similar will know that what ultimately differentiates success from failure, above all else, is the ability to endure. With that in mind, I'd like to acknowledge the following individuals whose companionship uplifted me and enabled me to endure all that the last 5 years have thrown at me; Connor Auth, Corey Brewer, and Zachary Lassack. All the success in the world would mean nothing without people to enjoy it with, and I will forever be grateful for your places in my life. Thank you.

CONSIDERATIONS FOR THE DEVELOPMENT AND IMPLEMENTATION OF STRUCTURES FOR LOSSLESS ION MANIPULATIONS (SLIM) PLATFORMS

Abstract

by Zackary R. Kinlein, Ph.D.
Washington State University
May 2024

Chair: Brian H. Clowers

Owing to its unique geometry, traveling wave structures for lossless ion manipulations (TW-SLIM) is able to maneuver ions at elevated pressures (2-4 Torr) without incurring significant ion loss. Building upon this unique capability, TW-SLIM has shown promise as a technique which can redefine the limits of ion mobility separations and potentially serve as a platform for gas-phase ion experiments. While the ultimate fate of the technique remains unknown at the time of this work, the greatest obstacle at present is clear: limited access to the technique. Motivated by a desire to expand both access to TW-SLIM and the scope of its capabilities, the work outlined herein outlines numerous approaches that simplify TW-SLIM implementation, optimize TW-SLIM analyses, and showcase the technique's ability to aid in experiments outside of traditional separations. Regarding implementation, technologies that reduce the cost of TW-SLIM experiments were evaluated, and tools that enable individuals with limited skill sets to develop TW-SLIM platforms were disseminated. Concerning experimentation, observations that pertain to the concurrent analysis of disparate species as well as the transmission of

dynamic biomolecules are explored and used to inform strategies to optimize TW-SLIM methodologies. Lastly, utilization of TW-SLIM as a platform for gas-phase ion chemistry showcases the ability of TW-SLIM to address complex chemical phenomena.

TABLE OF CONTENTS

Page

LIST OF TABLES

Page

LIST OF FIGURES

Page

Dedication

For Dougie

CHAPTER ONE: GENERAL INTRODUCTION

Ion mobility spectrometry (IMS) is an analytical technique which separates gas-phase ion populations based on their differing mobilities. An ion's mobility (K) is typically defined as a proportionality coefficient between its velocity (v_d) and the magnitude of an applied electric field (E) which drives the ion through a neutral colliding gas (eq. 1.1).

$$K = \frac{v_D}{E} \tag{1.1}$$

Differences in mobility arise from differential interactions with the neutral colliding gas and are often associated with collisional cross section, which loosely relates to the size of the ions. For this reason it is often said that IMS is a technique which separates ions based on their size, though it should be noted that this statement is a gross oversimplification of the complex chemical and physical factors which ultimately govern IMS experiments.[1–3]

The most common form of the IMS experiment is drift tube IMS (DTIMS) in which ions are driven through a counterflow of buffer gas by a linear electric field (Figure 1.1a).[3] Larger ions (lower mobility) will undergo a greater number of collisions with the buffer gas and thus reach the end of the drift tube later than the smaller (higher mobility) ions, enabling mobility-based separations which are observed in the time domain. Given the relatively simple design, limited material consumption, and rapid analysis times associated with DTIMS, it is unsurprising that the technique has seen significant use as a tool for onsite threat detection.[4–6]

While DTIMS continues to see use in the field of threat detection,[7,8] it's important to recognize that much of the ongoing IMS research now focuses on different approaches and applications. Owing to the development of techniques such as electrospray ionization[9] and the ever growing interests in the omics' fields,[10–12] IMS has seen increasing use as a tool for the analysis of biologically relevant molecules.[13,14] Due to the complex organization of biomolecules, those interested in analyzing these species are often met with numerous challenges such as the differentiation of isomeric species.[15,16] Given that IMS separation relates to ion size, isomeric differentiation is possible assuming the instrument is able to distinguish between closely related species.[16,17]

The ability of analytical instrumentation to separate similar species is often quantified as resolving power (R_p), where higher R_p corresponds to more powerful separations. For DTIMS systems, diffusion limited R_p is defined as:

$$R_p = \frac{t_D}{\Delta t} \approx \frac{1}{4}\left(\frac{qLE}{k_b T ln(2)}\right)^{1/2} \quad (1.2)$$

where t_D is an ion's drift time, Δt is the peak width at half-maximum, q is the ion charge, L is the length of the drift tube, E is the electric field, k_b is Boltzmann's constant, and T is the temperature.[2,18] Equation 1.2 suggests that R_p can be enhanced by elongating the drift tube, increasing the field strength within the drift tube, or lowering the temperature of the system. While equation 1.2 may make the solution to isomeric separations in DTIMS appear straightforward, each of the aforementioned means of increasing R_p suffer from practical limitations. Temperature modulation complicates instrument design, can compromise electrical components, and is often difficult to measure accurately,

particularly over extended periods.[19] With regards to DTIMS length and field strength, increasing these parameters can quickly spiral into endeavors which require specialized power supplies and increase the likelihood of electrical breakdown. To give an example, a typical DTIMS operating at atmospheric pressure will often utilize an electric field gradient in the range of 300-600 V/cm. For a modest 20 cm DTIMS, this requires the application of a 6-12 kV bias to be placed at the start of the DTIMS. If either the field strength or length were to be doubled, this would require 12-24 kV to be applied to the start of DTIMS. While certainly achievable, biases of this magnitude are best avoided for both financial and safety reasons.

In order to work around the limitations of DTIMS, a number of different IMS techniques have been developed such as trapped IMS (TIMS),[20] field asymmetric IMS (FAIMS),[21] and traveling wave IMS (TWIMS).[22,23] While distinct in their approaches, each of these IMS approaches utilize nonlinear, dynamic electric fields which enable for enhanced separations while avoiding many of the pitfalls associated with DTIMS. In the case of TWIMS, the introduction of local minima and maxima with regards to potential allow for extended separation pathlengths without accompanying increases in voltage. These local minima and maxima are provided via dynamic electric fields which have been dubbed “traveling waves” (TW). Explained simply, TW are transient potential wells which “move” at a rate defined by the user. The depth of the wells is often defined as “TW amplitude” and the rate at which the wells move is defined as “TW speed” (Figure 1.1b).

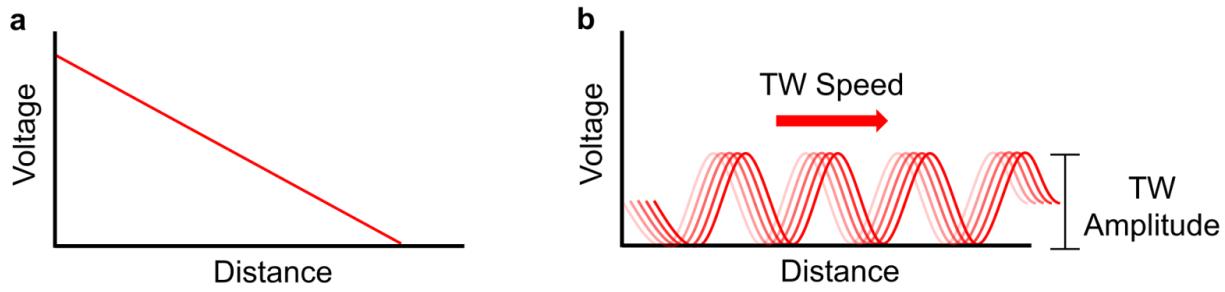

Figure 1.1. Variation in voltage as a function distance along the drift region for DTIMS (a) and TWIMS (b) systems. The linear voltage drop across DTIMS systems creates a static, homogeneous electric field which drives ions through the drift region. The electric fields within TWIMS systems are transient, shifting as a function of TW speed. The bias between the crests and troughs of the TW defines the TW amplitude.

The movement of the potential wells is made possible by defining a repeating set of electrodes and sequentially stepping which electrodes are biased “high” or "low” in a given instance. In response to the motion of the TW, ions will be pushed in the same direction that the TW is being stepped as they are driven towards the centers’ of the wells. Ions which are fast enough to keep up with the TW (i.e., higher mobility species) will simply ride at the front of the wave and are said to be “surfing”. In contrast, lower mobility species which cannot keep up with the TW will begin to rollover the TW and fall into preceding wells, subsequently taking longer to reach the detector. Given that the frequency of ion rollover defines an ions arrival time at the detector and is inversely related to mobility, TWIMS is able to provide mobility based separation that can be observed in the time domain. More in-depth discussion regarding TW fields and ions’ response to said fields are detailed elsewhere.[24–26]

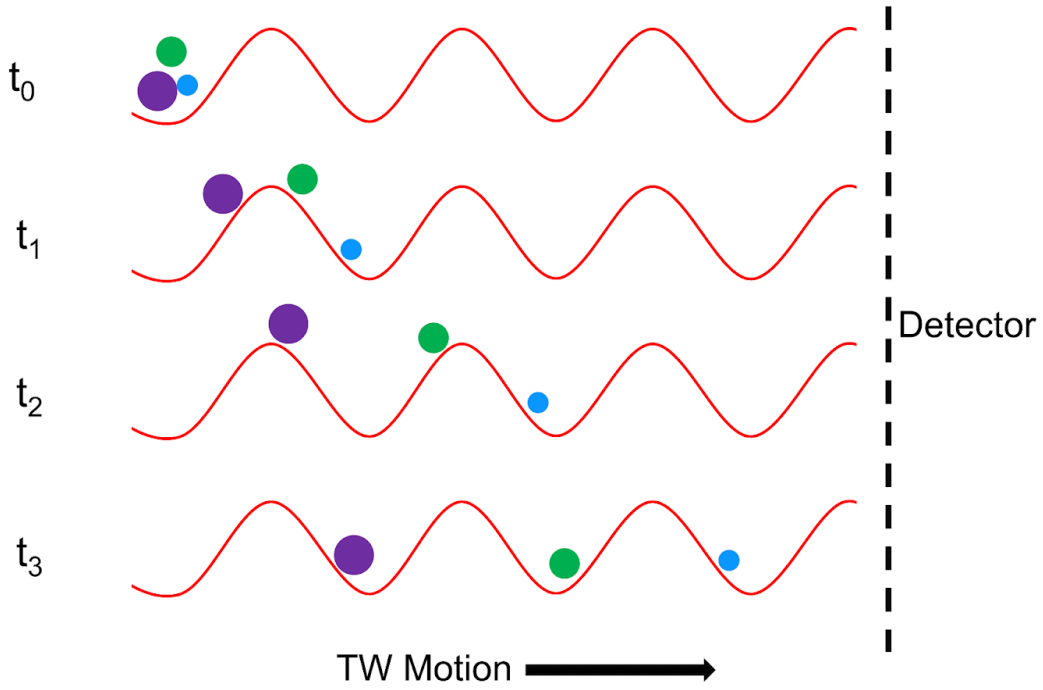

Figure 1.2. Visualization of ion separation in TWIMS systems. In this scenario, the highest mobility ions (light blue) are surfing at the front of the waves, not rolling over, and consequently arriving at the detector first. The lowest mobility ions (purple) are unable to keep up with the TW and repeatedly rollover, causing them to reach the detector last. Ions whose mobilities fall between the others (green) arrive somewhere in between the other ion species.

For many years, TWIMS instrumentation was largely limited to the Synapt systems produced by Waters (Milford, MA).[23,27] Applying TW technology to a geometry which is similar to that of traditional DTIMS, the Synapt line provided a means for many to explore TWIMS for the first time. While significant in the greater context of TWIMS, it should be noted that the resolving power of the Synapt line was rather limited, due in part to the modest length of the TWIMS region (18.5-24.5 cm).[27] While not restricted in

the same way as DTIMS systems, the length of the Synapt TWIMS region was nonetheless bound by the necessity to package the instrument in a way that is conducive to a commercial laboratory setting. Put differently, while a cylindrical TWIMS system could be extended to several meters in length without running into the electrical breakdown issues associated with DTIMS, such a system would nonetheless be overly cumbersome. Fortunately, future developments in the field of TWIMS instrumentation would remedy this issue via the implementation of alternative geometries.

In 2015, the first publication regarding a new TWIMS technique, traveling wave structures for lossless ion manipulations (TW-SLIM) was published out of Pacific Northwest National Laboratory (PNNL).[28] Building upon the original SLIM instruments which implemented linear electric fields,[29,30] the TW-SLIM systems leveraged the modular, planar geometry of its predecessor to produce a highly flexible TWIMS platform. Constructed using printed circuit boards (PCB), TW-SLIM systems lend themselves to a high degree of design variability while undercutting the cost of traditional materials such as stainless steel. While not as inert or robust as traditional materials, PCB has nonetheless proven a feasible material for the assembly of analytical instrumentation and has seen growing use in the field of IMS.[31]

In order to assemble TW-SLIM, two mirror-image TW-SLIM PCB (TW-SLIM boards) are placed in parallel to create a space between the boards which is typically around 3 mm (Figure 1.3). Each of these TW-SLIM boards are equipped with three primary types of electrodes; guard, RF, and TW, which collectively form the TW-SLIM “track” in which ions are confined and separated (Figure 1.4a). Guard electrodes border

the TW-SLIM track and are biased with DC to prevent ion loss in the lateral direction. RF electrodes are placed throughout the central region of the track and provide radial confinement which prevents ion termination at the board surfaces.

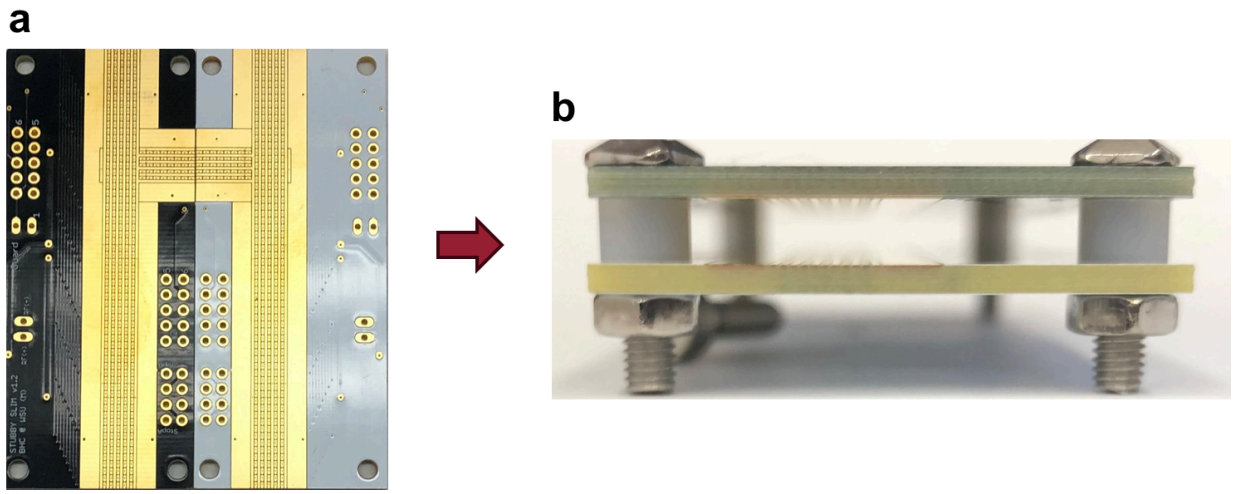

Figure 1.3. Mirror-image TW-SLIM boards (a) which are placed in parallel (b) to create a space between the boards in which ion populations are manipulated.

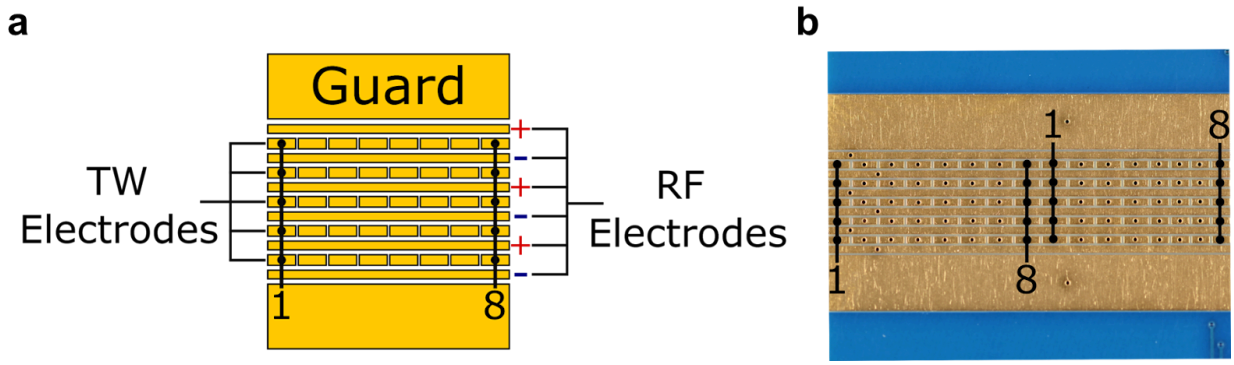

Figure 1.4. Schematic of a TW-SLIM monomer (a) and a photograph of a TW-SLIM segment which consists of 2 monomers.

As with any ion guide which relies on RF for ion confinement, the range of mass-to-charge ratios (m/z) which can be concurrently transmitted effectively is limited for a given set of RF conditions (i.e., RF frequency and amplitude).[32] While often glossed-over in the literature, this constraint placed on TW-SLIM experiments via the RF is of significant importance to those interested in utilizing TW-SLIM for broader analyses. To further complicate matters, the combination of the guard and RF fields creates a pseudo-quadrupolar environment in which variation in one of either the guard or RF biases impacts the ion's response to the other. For example, an increase in guard bias will compress an ion packet laterally and subsequently cause the packet to expand radially towards the board surfaces altering the RF fields that the ions feel. Located between the RF tracks, the TW electrodes are responsible for generating the TW which enables ion separation. The TW electrodes are typically numbered off (TW electrode 1, TW electrode 2,...) and laid out in repeating sets (TW electrodes 1-8, TW electrodes 1-8,...). The TW is generated by varying which electrodes are high or low in a given instance. An example of how this variation creates a TW is shown in Figure 1.5.

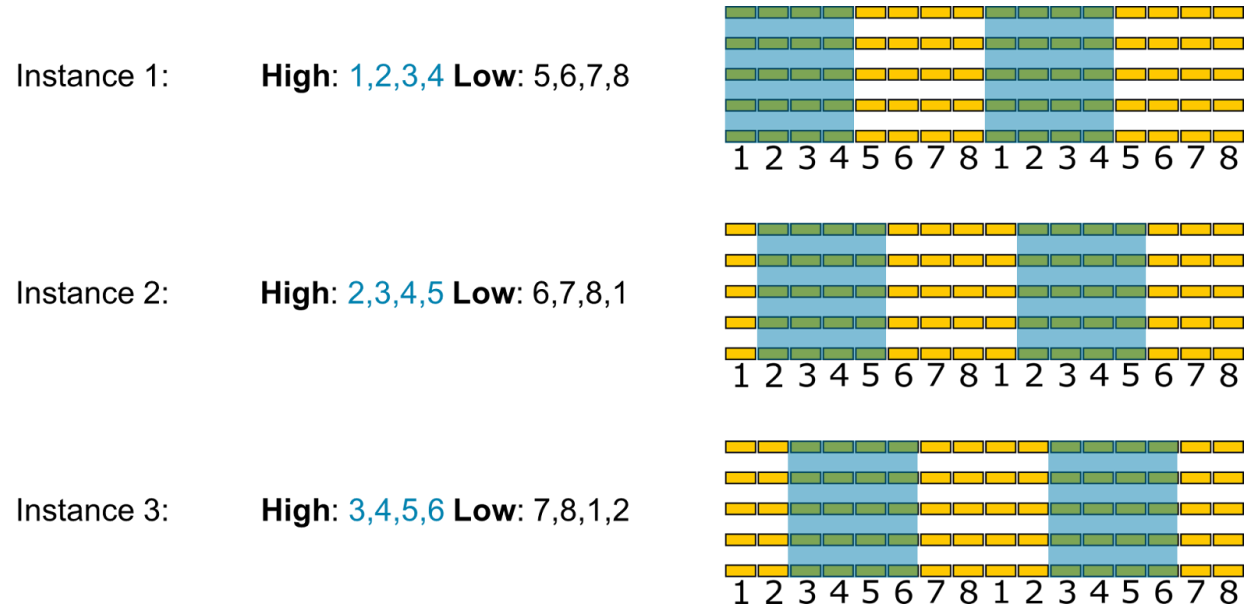

Figure 1.5. Visualization of electrode stepping which creates traveling waves. Electrodes highlighted in blue represent those in the "high" state, whereas the other electrodes are "low". The bias between the high and low is defined as TW amplitude. The time in between the instances is controlled by varying the TW speed.

While variations in electrode layout have been explored,[26,33] most TW-SLIM configurations subscribe to a number of standard conventions. RF and TW tracks are typically organized in a 6:5 configuration in which 5 TW tracks are located in the spaces between 6 RF tracks (i.e., each TW track is bordered by two RF tracks). Adjacent RF tracks are 180° out-of-phase to one another. TW electrodes are laid out in repeating sets of 8 and operate using a "4 high, 4 low" system in which an equivalent number of electrodes are high or low in a given instant. Square waves are the most common style of TW, though other waveforms such as sin waves have been used.[25,34] While an in-depth discussion regarding board design will be provided in Chapter 3, it is worth

noting that a full set of electrodes (1-8) defines the TW-SLIM monomer (Figure 1.4a) which is then propagated to create highly complex TW-SLIM paths.

While the fundamentals of TW-SLIM have remained largely the same, the complexity and utility of TW-SLIM boards has evolved rapidly since the technique's inception. The first TW-SLIM system reported in the literature was a linear design which provided a 30 cm TW-SLIM path for separation.[28] The next major advancement came shortly after which showcased the ability of TW-SLIM to maneuver ions around 90° turns without significant losses in sensitivity or separation.[35] Though important in the context of TW-SLIM's development, it should be noted that this feat is also of profound significance to the broader IMS community. With exception to the cyclic IMS system developed by the Clemmer group[36] and the original non-TW SLIM systems,[30,37] ion turning was primarily limited to high vacuum instruments wherein ion manipulation is more facile.[38,39].

Pairing the extended linear paths showcased in the original TW-SLIM publication[28] with the ability to perform 90° turns,[35] PNNL then unveiled what would quickly become the predominant TW-SLIM profile: the serpentine path. The serpentine design enables for extensive TW-SLIM paths (>10 m) to be laid out on boards which themselves have limited footprints. [40] The last major TW-SLIM development by PNNL which will be discussed in depth is the ion switch.[41] Ion switches are electronically isolated TW electrodes which can transition between a static DC potential which prevents ion progress, or a TW potential which enables ions to continue along a path. The two primary functions of an ion switch are rerouting and blocking. Rerouting

enables TW-SLIM to aid in complex experiments such as multiplexing, tandem IMS, and cyclic separations which enable theoretically infinite pathlengths for separation.[41,42] Blocking enables the TW-SLIM to both accumulate and inject ions, removing the need for additional gating hardware such as ion funnel traps.

Aside from PNNL, a select few entities have delved into TW-SLIM research and development. On the commercial side of things, Mobilion (Chadds Ford, PA) unveiled their “SLIM-based ion mobility product” in the summer of 2020. Targeting markets such as biomarker research, food and environmental analysis, and therapeutic characterizations, Mobilion has published a number of articles that showcase how TW-SLIM could aid in clinical environments.[34,43,44] While not a TW-SLIM platform, it is important to acknowledge the cyclic-IMS system developed by Waters, which draws many parallels to TW-SLIM and has seen an impressive degree of growth and implementation.[45] In the academic sphere, the first research group to publish work utilizing an independently developed TW-SLIM platform was the Rizzo group at the Swiss Federal Institute of Technology in Lausanne (EPFL). Building upon a wealth of experience with regards to infrared spectroscopy[46,47] and glycan analysis,[48,49] the work performed by the Rizzo group showcased the capability of TW-SLIM to slot into complex instrumental configurations and aid in differentiating highly similar species.[50,51]

In the Fall of 2019, the Clowers group at Washington State University (WSU) began independently developing TW-SLIM platforms. Starting with TW-SLIM boards that could fit in the palm of your hand, TW-SLIM research at WSU has rapidly expanded to include a vast array of configurations, investigations, and collaborations.[52–54] Though

the totality of TW-SLIM research at WSU can be attributed to a number of individuals, much of the foundational work will be covered in this dissertation. Having been involved in the development of TW-SLIM at WSU from the start, my work addresses many of the challenges associated with beginning TW-SLIM research and is particularly valuable to those interested in developing their own TW-SLIM systems.

One of the broader goals of the work I performed at WSU was to increase the accessibility of TW-SLIM. While the rapid growth of TW-SLIM has been staggering, greater access to the technique represents the next major step in its development. Increased access enables new and valuable perspectives to advance and mold TW-SLIM in ways yet unseen. Considering that TW-SLIM has already shown the ability to redefine the limits of a field (IMS) which is becoming increasingly involved in tackling complex analytical challenges, the work outlined herein is of great significance to the analytical community.

Beginning with the issue of limited access to TW-SLIM instrumentation, Chapters 2 and 3 will discuss efforts to lower the practical barriers to TW-SLIM implementation. More specifically, Chapter 2 will outline strategies and technologies which not only reduce the cost of TW-SLIM experiments, but also simplify the instrumental setup as a whole. Chapter 3 takes aim at remedying perhaps the most significant hindrance to TW-SLIM adoption: limited knowledge of PCB design and instrument assembly. Given that the skills and knowledge associated with designing and assembling instrumentation are often excluded from traditional chemistry programs, this work may enable otherwise highly qualified individuals to begin experimenting with TW-SLIM. Recognizing that the

complexity of TW-SLIM analysis may deter those without prior knowledge of the technique, Chapters 4 and 5 outline work which delves into the complexities of TW-SLIM analysis and informs strategies for method development. Chapter 4 seeks to address the issue of concurrently analyzing disparate species in TW-SLIM while Chapter 5 provides insights into the analysis of labile biomolecules.

In addition to improving access to TW-SLIM, the efforts outlined in Chapters 2-5 were also building towards another goal: the evaluation of TW-SLIM as a platform for probing gas-phase ion chemistry. Recognizing that experiments of such complexity require not only advanced instrumentation but also a robust understanding of TW-SLIM analysis, our eventual exploration of these matters represents a culmination of all the lessons learned over the course of my time at WSU. Chapter 6 will cover how we built towards gas-phase ion chemistry experiments, discuss some preliminary results concerning hydrogen-deuterium exchange (HDX) in TW-SLIM, and conclude with some discussions regarding future work in this area.

CHAPTER TWO: ACCELERATING PROTOTYPING EXPERIMENTS FOR TRAVELING WAVE STRUCTURES FOR LOSSLESS ION MANIPULATIONS

Reprinted (adapted) with permission from Kinlein, Z. R.; Anderson, G. A.; Clowers, B. H. Accelerating Prototyping Experiments for Traveling Wave Structures for Lossless Ion Manipulations. *Talanta* 2022, *244*, 123446. doi: 10.1016/j.talanta.2022.123446.

2.1 Attributions

The authors whose work contributed to the following manuscript include Zackary R. Kinlein, Gordon A. Anderson, and Brian H. Clowers. Zackary R. Kinlein is credited with conducting the investigation and was the primary author of this work. Gordon A. Anderson is credited with contributions to software and methodology. Brian H. Clowers is credited with conceptualization, supervision, funding acquisition, contributions to software, and writing.

2.2 Preface

The work presented in this chapter was adapted from the first manuscript detailing a TW-SLIM system developed at WSU. While published in 2022, this work represents a culmination of efforts that began in 2019 with regards to building a TW-SLIM system from scratch. While the experiments outlined in this chapter may be the simplest, it’s important to recognize that this work represents a major milestone for both WSU and TW-SLIM as a whole. For WSU, the lessons learned on the path to publishing this work provided the foundation upon which numerous future TW-SLIM platforms would be built. More broadly, in spite of limited experience and resources, a

fully functional TW-SLIM system was developed and implemented which suggests that similar efforts at other institutions and research teams is possible.

2.3 Manuscript

Abstract

Traveling wave structures for lossless ion manipulation (TW-SLIM) has proven a valuable tool for the separation and study of gas-phase ions. Unfortunately, many of the traditional components of TW-SLIM experiments manifest practical and financial barriers to the technique's broad implementation. To this end, a series of technological innovations and methodologies are presented which enable for simplified SLIM experimentation and more rapid TW-SLIM prototyping. In addition to the use of multiple independent board sets that comprise the present SLIM system, we introduce a low-cost, multifunctional traveling wave generator to produce TW within the TW-SLIM. This square-wave producing unit proved effective in realizing TW-SLIM separations compared to traditional approaches. Maintaining a focus on lowering barriers to implementation, the present set of experiments explores the use of on-board injection (OBI) methods, which offer potential alternatives to ion funnel traps. These OBI techniques proved feasible and the ability of this simplified TW-SLIM platform to enhance ion accumulation was established. Further experimentation regarding ion accumulation revealed a complexity to ion accumulation within TW-SLIM that has yet to be expounded upon. Lastly, the ability of the presented TW-SLIM platform to store ions for extended periods (1 s) without significant loss (<10%) was demonstrated. The aforementioned experiments clearly establish the efficacy of a simplified TW-SLIM platform which promises to expand adoption and experimentation of the technique.

Introduction

Ion mobility spectrometry (IMS) is an analytical technique which separates gas-phase ions via their mobility, which is loosely related to physical size, as they traverse the medium while being driven by an electric field.[1,2] Renowned for their speed of analysis and relative simplicity, IMS techniques have seen widespread implementation in the fields of threat detection[6,55,56] and the investigation of physiologically relevant biomolecules.[13,14,57] More recent analyses have even leveraged IMS for the separation of isomeric species, something that has proved troublesome for many analytical techniques.[58–60]

The most common implementation of IMS is drift tube IMS (DTIMS) which uses a linear, homogeneous electric field to measure gas-phase mobility coefficients. The ability of a DTIMS to separate ions of similar mobility is quantified as resolving power (Rp) which, when limited only by diffusion, is defined as:

$$R_p = \frac{t_D}{\Delta t} \approx \frac{1}{4}\left(\frac{qLE}{k_b T ln(2)}\right)^{1/2} \quad (2.1)$$

where t_D is an ion's drift time, Δt is the peak width at half-maximum, q is the ion charge, L is the length of the drift tube, E is the electric field, k_b is Boltzmann's constant, and T is the temperature.[2,18] Like many analytical techniques, the ability to separate increasingly similar species remains a focal point of experimentation and investigation in the field of IMS. According to equation 2.1, Rp can be improved by increasing the strength of the electric field, elongating the drift tube, or decreasing the temperature. While conceptually simple, these approaches to increasing resolving power suffer from practical limitations.[3,61,62] Given that implementing temperature controls requires more

complex instrumentation and robust electronics, lowering the temperature of the system is not always feasible nor practical for many experimental scenarios.[19] While increasing the field strength could, in theory, simply be accomplished by “turning a knob” it is important to note that higher fields require highly specialized power supplies and can contribute to electrical breakdown. Likewise, given the linear nature of the fields within a DTIMS, increasing the length of the system would require increasing the voltage at the start of the drift region to maintain the desired electric field, once again requiring capable power supplies and contributing to electrical breakdown.

While certainly the most recognizable, the DTIMS is not the only IMS technique in use today. Debuting in the early 2000s,[22] traveling wave IMS (TWIMS) has seen commercial implementation and widespread application.[23,63,64] Unlike DTIMS which applies a static linear electric field, the electric fields in a TWIMS are transient and dynamic.[24,65] In TWIMS, separation is achieved as the frequency at which ions “roll over” waves is dependent upon their mobilities.[24] The more frequently an ion rolls over, the greater its arrival time at the detector. Perhaps one of the biggest advantages of TWIMS is that the length of the separation region can theoretically be increased without increasing the voltage at the start of the region. This is due to the transient nature of the waves which leads to local minima and maxima, as opposed to absolute minima and maxima required for DTIMS.

While promising, there remain several hurdles surrounding the advancement of TWIMS. For instance, while the length of a TWIMS is not limited by issues of electrical breakdown, there remains practical limitations on length with regards to the physical

size of the instrument. These limitations are of particular concern for commercial instrumentation which must be assembled and housed in a fashion that makes for reasonable placement/storage in a laboratory. Additionally, the electrode structure of commercially available TWIMS limit the range of traveling wave and RF amplitudes that can be applied during analysis, which ultimately constrains the range of *m/z* values that can be simultaneously analyzed with the system.[27] Behaving in a fashion similar to a stacked ring ion guide, there is a window of m/z and mobility values that allow for stable ion motion within the TW-SLIM system.[32,66]

A potential solution to the shortcomings of traditional TWIMS, known as traveling wave structures for lossless ion manipulation (TW-SLIM), debuted in 2015 and has already seen a wide range of applications and modifications.[28,35,67–69] Comprised of inexpensive and readily customizable printed circuit boards (PCB), TW-SLIM offers a simplified electrode structures which, when paired with the low cost of PCBs, lends to rapid and creative prototyping. One of the most significant advancements in TW-SLIM has been the implementation of serpentine ultralong paths with extended routing (SUPER) which enable for theoretically infinite pathlengths for separation.[41] Having remedied the issues of length and electrode structure that hamper traditional TWIMS techniques, the possibility for TW-SLIM to catalyze the advancement of TWIMS and IMS as a whole, is apparent.

Despite showing great promise, there remains a series of obstacles that stand between TW-SLIM and its ultimate potential as a high-powered, low-cost gas phase separation technique. While SLIM may be constructed of inexpensive materials, the

technology used to generate the waveforms in the SLIM requires a degree of sophistication which manifests both applicative and financial barriers to its implementation. Additionally, more simplistic TW-SLIM experiments typically rely on ion funnel traps (IFT) for injection which require levels of fabrication precision that are not readily available to most laboratories. Lastly, the primary means of detection in TW-SLIM experiments are mass spectrometers (MS). While MS is undoubtedly a powerful analytical tool, the issue of cost as well as compliance with pressure requirements can limit implementation and slow prototyping efforts.

Recognizing the obstacles to TW-SLIM implementation, the following manuscript outlines an instrumental platform capable of performing the basic operations typical of a TW-SLIM, while utilizing an expansive array of techniques which reduce the practical, financial, and intellectual barriers to experimentation. With regards to TW generation, the efficacy of a simple and inexpensive multifunctional traveling wave generator (MFT) was evaluated, and was found to perform comparably to more traditional approaches. Concerning ion injection, an on-board injection mechanism (OBI) was employed which mitigated the need for an IFT, simplifying the experiment. The ability of this OBI to simultaneously aid in on-board ion accumulation (OBA), as outlined elsewhere,[70] was evaluated as well. Regarding ion detection, this report details the use of an appropriately shielded Faraday plate designed specifically for the TW-SLIM experiment serving as an inexpensive alternative to the MS techniques or highly complex charge detection schemes previously reported.[71] Lastly, the potential for this simplified

TW-SLIM platform to aid in more complex experimentation was evaluated as it proved capable of storing ions for extended periods of time (1 s) with minimal loss.

Experimental

Tetraoctyl ammonium bromide (T8, nominal mass: 466 Da) and tetradodecyl ammonium bromide (T12, nominal mass: 690 Da) were purchased from Sigma-Aldrich (St. Louis, MO). Morphine (nominal mass: 285 Da) standards were purchased from Cerilliant (Round Rock, TX). All data presented were collected using a solution of 10 μM morphine and 1 μM each of T8 and T12 prepared in methanol (HPLC grade, Fisher Chemical, Fair Lawn, NJ) with 0.1% formic acid (Honeywell-Fluka, Muskegon, MI).

A schematic of the instrument used throughout the presented work is shown in Figure 2.1A. Ions were generated via electrospray ionization (ESI) using a 75 μm ID glass capillary emitter with a sample flow rate of 3 μL/min, controlled by a Model 11 Syringe Pump from Harvard Apparatus (Holliston, MA). The ESI emitter was biased 2.2 kV relative to an adjacent stainless-steel inlet capillary (560 μm i.d., 1600 μm o.d.) purchased from McMaster-Carr (Elmhurst, IL). Having traversed the heated (160 ^{o}C) capillary, ions were focused by an ion funnel (897 kHz, 240 V_{p-p}) housed in a low pressure (2.45 torr) chamber before being transported to a second, smaller ion funnel (1.1 MHz, 140 V_{p-p}) housed in a slightly higher pressure (2.50 torr) chamber. The gas inside each of the chambers was ambient air as the focus was on the characterization of the drive electronics and not theoretical ion-neutral cross section accuracy. Pressure was measured in each chamber using Setra Model 730 capacitance manometers

(Boxborough, MA). The disparate chamber pressures and offset of the capillary as depicted in Figure 2.1A were implemented to limit the transmission of neutral solvent molecules into the second chamber. After traveling through the second ion funnel, ions arrived at the first TW-SLIM segment referred to as the “drag” board. Electrodes designated as blocks A, B, and C (Figure 2.1B) on the drag board could be operated either as TW electrodes or as blocking electrodes, in which case they were biased above the adjacent electrodes using a static DC potential. In the context of the presented work, block B was used as a point of ion packet injection, serving the role of an ion gate found in traditional ion mobility experiments. Upon switching from the block to the TW state, block B would permit the transmission of ions. The width of the injection is defined as the period in which block B operated as TW electrodes. The use of block A as either TW or blocking electrodes was varied between experiments and will be discussed in further detail when appropriate. For all the experiments discussed, block C remained in the TW state.

Having navigated the drag board, ions then reached the interface between the drag board and a second TW-SLIM segment, referred to as the zipper board in reference to the track design (Figure 2.1C). The zipper design was implemented as it provides enhanced pathlenghts for separation without greatly increasing the length of the PCB. Unlike previous iterations of the TW-SLIM experiment, this setup uses two distinct sets of SLIM segments, located adjacent to each other, as opposed to a singular set of SLIM boards. The impact of this multi-segmented approach and the flexibility associated with its implementation will be explored in future publications. The total

pathlength used for separation from the point of injection to the end of the zipper was approximately 70 cm. A custom Faraday plate was placed directly adjacent to the end of the zipper board and served as the primary detector. A detailed schematic of the custom Faraday plate is provided Figure 2.S1. Current detected at the Faraday plate was amplified using a Keithley Model 427 current amplifier (10^9 Gain, Rise time: 1 ms, Cleveland, OH) and the signal was recorded as a function of time using an Analog Discovery 2 (Digilent Inc., U.S). All data presented in this manuscript were derived from spectra averaged 100 times. Each data point represents an average of 5 spectral replicates with the standard deviation of those 5 replicates representative of the uncertainty of the measurement. Peak identities were assigned by analyzing individual standards of each of the 3 analytes (morphine, T8, and T12). Data were processed using Python notebooks developed in-house. A sample notebook is provided in the supporting information.

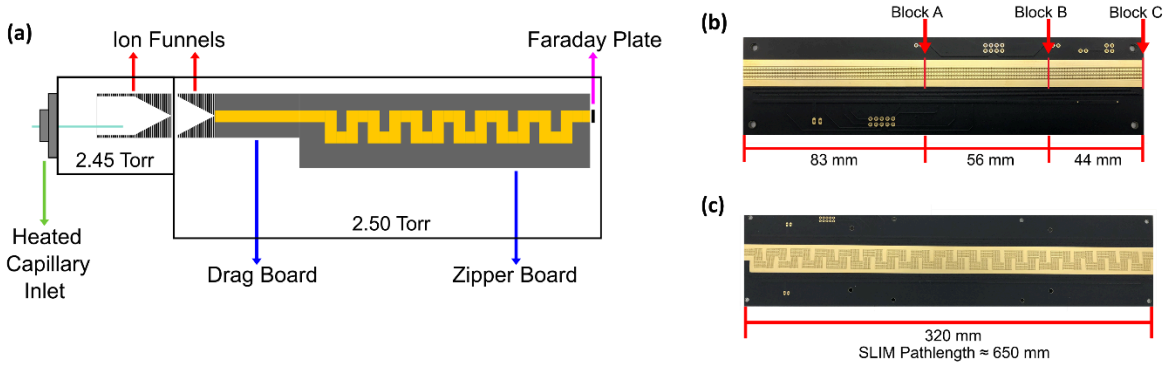

Figure 2.1. (a) Schematic of the instrument used throughout the presented work. (b) Annotated images of the "drag" board and (c) "zipper" board. Images are not to scale.

The following TW-SLIM conditions were used throughout all the presented experiments and were controlled using a modular intelligent power source (MIPS) from GAA Custom Electronics (Kennewick, WA) unless otherwise stated. Ions were confined laterally by guard electrodes biased 11 V to the TW, and radially by RF electrodes operating at 1.27 MHz, 300 V_{p-p}. The TW amplitude was 22 V_{p-p} and the TW speed was 128 m/s. Further details regarding the configuration of the SLIM boards can be found in the supporting information. To be clear, the outlined TW conditions were selected for optimized ion transmission and storage experiments and were not optimized for resolving power. While conditions which reduce peak width and subsequently enhance resolving power are achievable, it is worth noting that observed peak widths did not differ substantially from those predicted by theory for a single pass TW-SLIM experiment and the minimal path length used (Figure 2.S2).[18]

Compared to the MIPS system, which uses 8 different DC channels to generate the associated TW, the MFT uses a single DC supply to generate *all* of the TW signals. For experiments involving the MFT, a SPD3303X-E programmable DC power supply purchased from Siglent (Solon, OH) was used to provide the DC bias which was modulated by the MFT to produce the TW. Key to the MFT functionality is the multi-channel switch that is commonly used for medical ultrasound applications (e.g., Maxim 14803). Interestingly, the electrical requirements for ultrasound applications and the modulation of multiple electrodes are directly analogous to the TW experiments. Additionally, it is worth noting that the MFT in its current configuration is controlled by a M0 microcontroller (Adafruit Trinket M0) and contains the same core functionality as the

MIPS including TW generation, frequency adjustment, forward and backward TW movement, float capacity, and TW halt functionality. The system additionally accommodates an external trigger to cycle through pre-programmed events.

Results and Discussion

In order to evaluate the efficacy of the MFT as a TW generator, its performance was placed in the context of its more traditional counterpart, the MIPS. This was accomplished by operating the TW-SLIM in two modes: “MIPS mode” where both the drag and zipper TW were generated by the MIPS, and “MFT mode” where the drag TW was generated by the MIPS and the TW of the zipper was provided by the MFT. Mobility spectra collected when operating the instrument in these different modes provided the foundation for analyses of the MFT performance. While preliminary data indicates that both the drag and zipper TW can be effectively generated by a single MFT, an emphasis was placed on evaluating the ability of the MFT to work in tandem with a MIPS in the presented analyses. For all comparisons between the MIPS and MFT mode, block A remained in the TW state throughout the analyses and no TW conditions that favor accumulation were implemented. Initial testing revealed an apparent variation between spectra collected in the MIPS and MFT modes, as there was a noticeable shift to later arrival times and subsequent increases in peak width when operating in MFT mode (Figure 2.2A). This shift is attributed to subtle but real deviations (~ 0.3 V) from the desired TW amplitude present in each system, which when compounded, resulted in the behavior shown in Figure 2.2A. It is worth noting that if analyses hinge on tightly aligned TW generated within a system in which MFT and MIPS work in tandem, it is possible to

tune the TW amplitude of either the MIPS or MFT so that the system performs similarly to how it would with just MIPS or MFT (Figure 2.2B). For clarity, the spectra shown in Figure 2.2B correspond to actual spectra where the MFT TW amplitude was tuned to match that of the MIPS, and not alignment through digital signal processing.

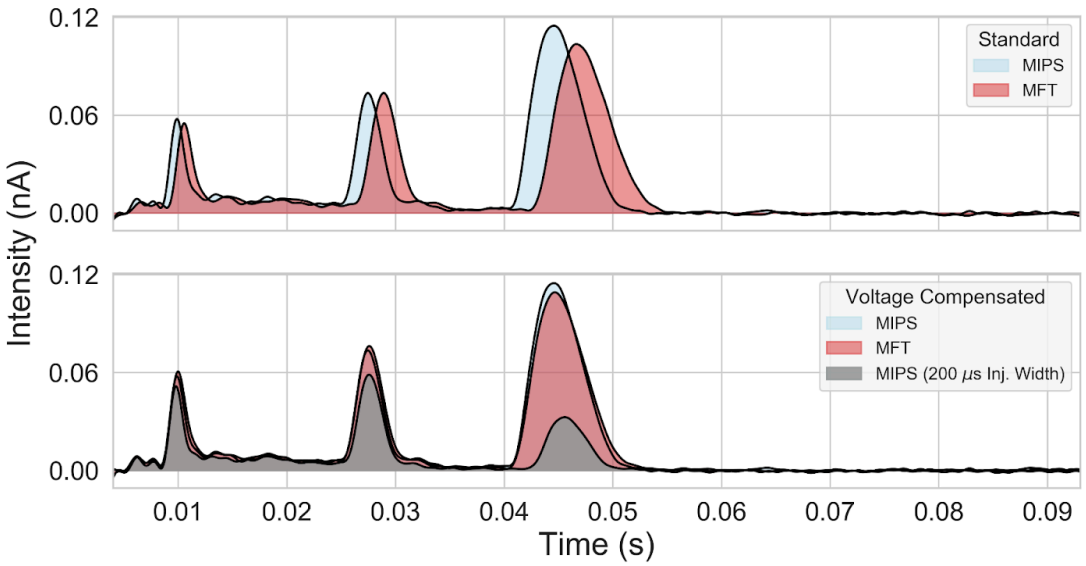

Figure 2.2. Mobility spectra collected when TW were generated in MIPS mode (blue) and MFT mode (red). The spectra on the top (a) are misaligned due to variations in TW amplitude which, once corrected for, produce the spectra on the bottom (b). The injection width used when collecting the presented spectra was 1 ms, with the exception of the spectra labeled "MIPS (200 µs Inj. Width)." Peaks at (approximately) 10, 27, and 45 ms correspond to morphine, T8, and T12, respectively.

A more thorough analysis of the MFT's performance was accomplished by comparing numerous spectral metrics for each analyte, across different injection widths, when operating in MFT mode relative to MIPS mode (Figure 2.3). For these analyses, the amplitude of the TW generated by the MFT was not corrected to align with that

corresponding MIPS spectra. Consequently, as observed in Figure 2.2, the arrival times are consistently greater when operating in MFT mode relative to MIPS mode. This increased arrival time naturally coincides with the observed attenuation in peak amplitude as peaks broaden due to ion populations undergoing diffusion for a longer period. It is important to note that while peak amplitudes were slightly diminished when operating in MFT mode, peak areas remained comparable, with no peak area varying more than 10% relative to its respective value generated when operating in MIPS mode. This suggests that the diminished peak amplitudes are in fact the result of diffusion and not ion loss. The most substantial difference between the two modes is observed for T12 when operating with a 100 μs injection width. This pronounced deviation is attributed to an observed high mobility bias of the injection mechanism which limited the population of the injected T12 ion packet (Figure 2.2b). This type of behavior is well within expected levels of performance as mobility bias is well documented for modulated ion populations.[72–74] Unsurprisingly, the diminished ion population exhibited greater run-to-run variability which manifested as greater deviations from the corresponding MIPS mode values and greater deviations between measurements. Considering that the deviations observed in Figure 2.3 can be largely attributed to the TW amplitude generated by the MFT differing from that of the MIPS (which can be mitigated relatively easily) and the presence of a mobility bias in an injection method, the comparable performance of the MFT mode relative to that of the MIPS is extremely promising. Given the relative simplicity and low cost of the MFT, its ability to operate in-tandem with a MIPS expands the suite of simultaneous TW-SLIM experiments to augment future TW-SLIM configurations and increasingly complex TW-SLIM designs.

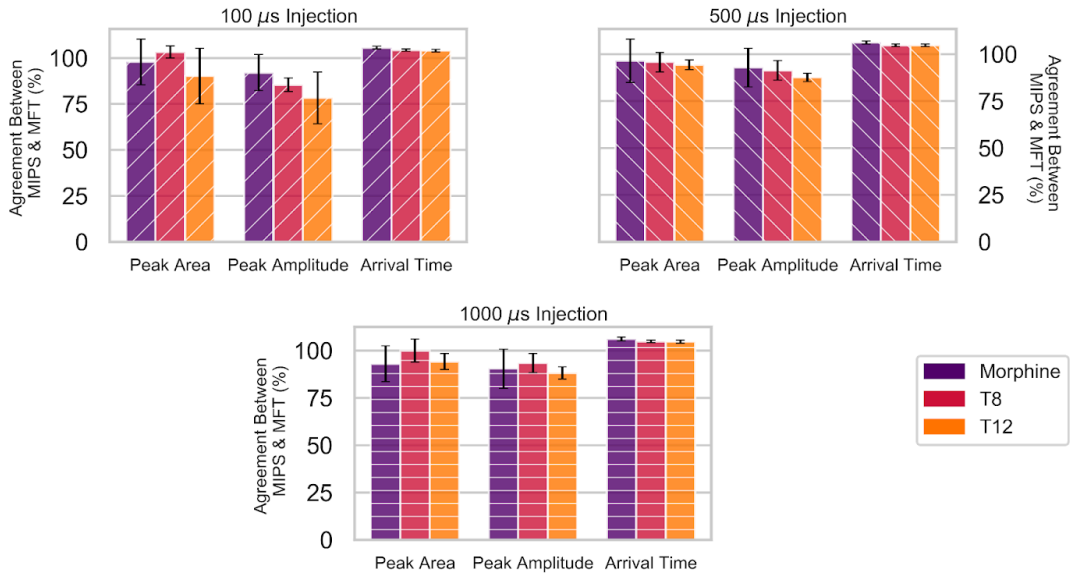

Figure 2.3. Spectral metrics for each analyte, across different injection widths, when operating in MFT mode relative to MIPS mode. An agreement of 100% would indicate that the value attributed to MFT mode is identical to that which was collected when operating in MIPS mode. Raw data associated with these plots can be found in Table S1.

Much like the MFT, the use of OBA and OBI offers a simple and serviceable alternative to a more traditionally used technique: the ion funnel trap.[32,53] While used in the context of ion injection in the MFT evaluation, static potentials have been used in other TW-SLIM experiments which exploit the nature of TW to allow for the accumulation of high density ion populations relative to the continuous current generated by an ESI emitter.[70,75,76] Given the apparent benefits to sensitivity that come with ion accumulation, experiments were performed to characterize the ability of the presented instrument to accumulate large ion populations. For simplicity, the MFT was excluded from these analyses as the emphasis was on ion accumulation, not TW

generation. Prior to injection, the TW operates under conditions aimed at increasing the likelihood of ion roll over (lower TW amplitude and or higher TW speed) akin to the approach outlined by Deng et al. which has shown to increase ion accumulation in TW-SLIM.[70] Per the nomenclature established by Deng et al., these conditions are referred to as a “gentle” traveling wave (GW).[70] In our implementation, after some period defined as “accumulation time,” block A is raised to a static DC bias, block B transitions to a typical TW electrode for some period (i.e., injection width), and the TW returns to its usual conditions used for separation (22 V_{p-p}, 128 m/s). These separation conditions are maintained until the SLIM has been cleared of all injected ions after which point the timing cycle repeats. The transition of block A to a static DC bias during the injection period was done to ensure that the ion population being injected consisted only of ions accumulated when the GW was implemented.

The first set of experiments regarding accumulation were aimed at evaluating how different GW conditions impact the accumulation of different ion species. GW conditions in which TW amplitude was held constant while TW speed was increased, and conditions in which TW speed was held constant while TW amplitude was lowered, were applied. Variations in the observed peak areas for morphine and T12 as a function of different GW conditions are presented in Figure 2.4. The accumulation time used for these experiments was 15 ms and the injection period was 3.2 ms. The 3.2 ms injection was chosen as it provided enough time across all conditions to allow for the region between blocks A and B to be cleared of ions. Data recorded at 22 V_{p-p} and 128 m/s represent a baseline in which no GW was applied and ions were accumulated under

normal TW conditions. When achieving GW conditions using increased TW speed, both morphine and T12 show an increase in peak area relative to their baseline values. Interestingly, morphine observed greater relative gains to its peak area using the reduced TW speed approach compared to T12 which showed modest and, in some cases, negligible gains. In agreement with results published by Deng et al., decreasing TW amplitude proved to have the greater impact on the accumulated ion populations compared to varying TW speed.[70] Peak areas for both compounds were consistently greater when using the reduced amplitude GW, except for that of T12 when a TW amplitude of 12 V_{p-p} was applied. The noticeable depreciation of the T12 peak area as the TW amplitude decreased from 18 to 12 V_{p-p} is attributed to poor confinement of T12 ions. In contrast, morphine shows only a minor decline in peak area and only at the lowest TW amplitude evaluated (12 V_{p-p}). These distinctly different trends in peak area for morphine and T12, suggests that considerations should be made regarding factors that influence confinement (guard bias and RF amplitude/frequency) as well as the range of mobilities being analyzed when accumulating ions in TW-SLIM.

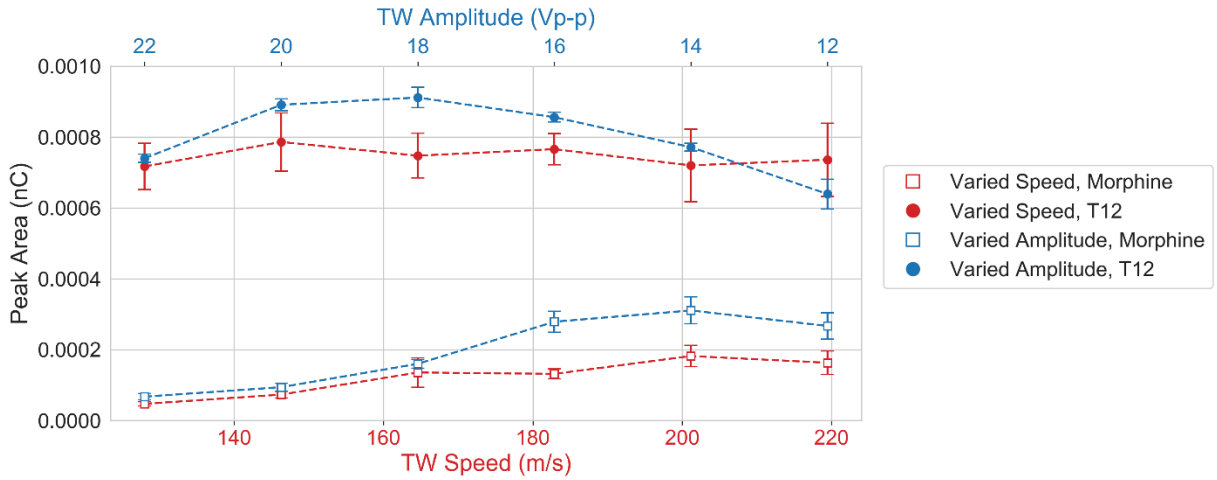

Figure 2.4. Plot of peak area vs TW amplitude and speed. Data collected when the TW amplitude was held constant (22 V_{p-p}) while TW speed was increased are shown in red. The data shown in blue were collected when the TW speed was held constant (128 m/s) and the TW amplitude was reduced.

Having established that the presented instrument could effectively accumulate ions, an additional round of experiments was performed in which the impact of accumulation time on the population of differing ion species was evaluated. The same experimental workflow for accumulation outlined previously was used for these analyses as well; however, the GW conditions used this time were static, 16 V_{p-p} and 128 m/s, and the injection width was 2 ms. The GW conditions were selected based on the results shown in Figure 2.4. An injection width of 2 ms was chosen as it had proven capable of providing ample time to clear all ions from the region between blocks A and B for the GW conditions chosen for these analyses. The impact of accumulation time on ion populations is presented in Figure 2.5A. Similar to observations made by Deng et al., the total ion current (approximated here as the sum of the peak areas of morphine,

T8, and T12) increases as a function of time until eventually plateauing.[70] Interestingly, plots of peak area vs accumulation time for each compound individually reveal behavior that deviates from that of the total ion population. With exception of the largest species, T12, ion populations reach a local maximum at a given accumulation time (10 ms for morphine, 30 ms for T8), after which point the ion population begins to decrease before eventually stabilizing. Figure 2.5B displays peak areas for each of the 3 compounds, normalized to their apex, as a function of accumulation time. Both the accumulation time at which the local maxima is reached for each compound and the magnitude of the decrease that follows appears to be related to the size of the ion species. Morphine, being the smallest of the ion populations, reaches its maxima before T8 and experiences a decline of 49±2% relative to its apex, a decline far greater than that of T8 (16±2%). The apex for T12, the largest species, coincides with the plateau of the total ion current and shows no significant decline. While limited in scope, these results suggest that as ions are allowed to accumulate for longer and longer periods, space charge effects begin to play a considerable factor in determining which ion species dominate the accumulation space, with higher abundance species “pushing out” those with smaller contributions to the total charge in the system. While not surprising given reports and personal experience with ion funnel traps,[77,78] these results remain notable when considering OBA and OBI approaches for TW-SLIM experiments. Similar to the results of the GW condition experiments, this evaluation of the impact of accumulation time suggests that when accumulating species of disparate size in a TW-SLIM, it is imperative to recognize that a “one size fits all” approach may be detrimental to select ion populations.

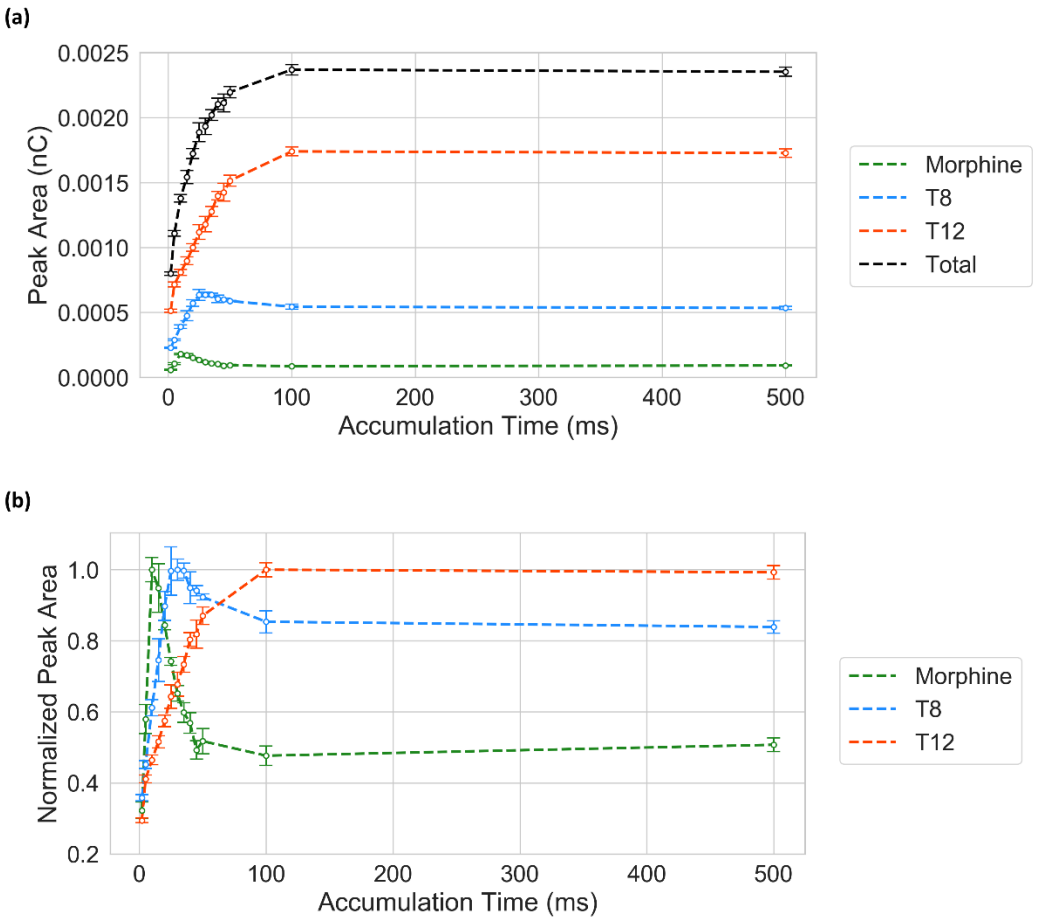

Figure 2.5. (a) Plot of Peak area vs accumulation time for the 3 analytes individually, as well as the sum of the three ("Total"). For this experiment "Total" is used to approximate the total ion current, given that the three analytes are the only ones present in the solution. (b) Plot of peak area for each of the three compounds normalized to their greatest value as a function of accumulation time.

The results of the experiments discussed previously suggest that the presented instrument can perform many of the basic operations typical of a TW-SLIM experiment. As a final assessment of the presented TW-SLIM platform, the potential for this set-up to be used for more complex TW-SLIM experiments was evaluated. More specifically,

the ability of this instrument to store ions for extended periods of times, a technique that could enable a user to probe issues of gas-phase chemistry, was evaluated. For these experiments, ion storage was accomplished by first allowing ions to enter the TW-SLIM and then subsequently halting the TW entirely, creating a series of static ion traps throughout the SLIM. Two different approaches to ion storage were evaluated: a post-injection halt in which ions were injected, allowed to separate for 5 ms, and then halted, as well a pre-injection halt in which the TW was halted while ions were trapped between blocks A and B prior to injection. Normal TW conditions were resumed after the halt period. The conditions for these experiments were identical to those of the accumulation time evaluation but with a static accumulation time of 15 ms and the added halt step. For both the pre- and post-injection experiments, the TW amplitude was 22 $V_{p\text{-}p}$ during the halt period.

During the initial evaluation of ion storage within TW-SLIM, the MIPS was used to halt and store ions within the system. These experiments served as the baseline for comparison to the MFT. With the capacity to accept an external trigger to adjust TW parameters, the MFT has the ability to mimic the functionality of the standardized MIPS platform. For the sake of brevity, the full complement of storage experiments was not repeated as the capacity to match the MIPS functionality with the MFT was effectively demonstrated in Figures 2.2 and 2.3. Storage experiments conducted using the MFT demonstrated the capacity to control the TW modulations required for extended ion storage. Figure 2.S3 illustrates the recorded ion signal using the MFT for a condition

where no halting was observed and an ion population held within the SLIM system for 1 s using a post-injection halt.

Results showing the impact of storage time on the observed area and intensity of the T12 peak are shown in Figure 2.6. For both peak area and amplitude, the reported values were normalized to their respective values when no storage was implemented. Sample spectra collected with no halt and a 1 s halt period are shown in Figure 2.S4. After halting the ions for a period of 1 s, the post-injection data for both peak area and amplitude depreciates less than 10% relative to the unhalted data, whereas the pre-injection data shows losses of approximately 50%. It's also worth noting that both peak areas and amplitudes from the post-injection halt experiment remained relatively static, whereas the pre-injection data decreases as a function of accumulation time until 50 ms, at which point the values begin to plateau. Considering that the pre-injection experiment does not allow for ions to separate prior to storing them, the most likely cause of the significant loss and the trend of said loss is space charge effects, as a large population of ions is confined between blocks A and B. When ions are allowed to spread out on the board (i.e., the post-injection halt) these detrimental effects are not observed. While some loss of ions appears inevitable when storing with the presented approach, allowing ion populations to disperse prior to storing them mitigates the losses, indicating that the proposed platform could potentially serve as a tool for the exploration of gas phase ion chemistry.

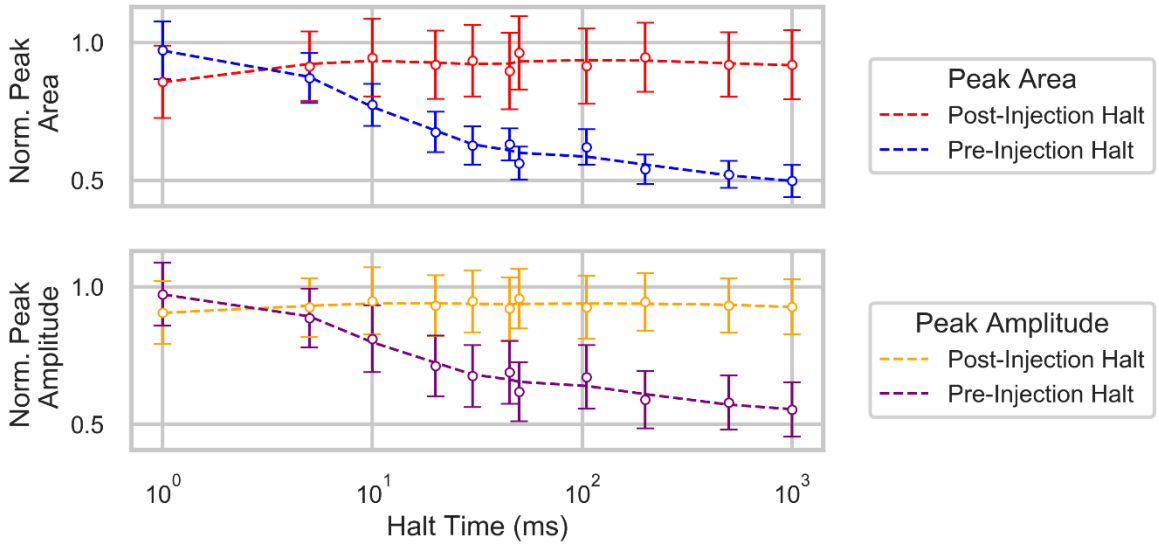

Figure 2.6. Variation in peak area (top) and amplitude (bottom) as a function of halt time. "Post-injection halt" refers to data collected when the ions were stored post injection, after 5 ms of separation. "Pre-injection halt" data was collected when ions were stored in the region between blocks A and B, prior to injection.

Conclusions

The presented multi-board TW-SLIM platform realizes the fundamental operations typically performed in single-board TW-SLIM experiments, while offering several simplifications that lower the barriers to its implementation. Recognizing that the MFT as a TW generator is considerably less complex and more economical than its traditional counterpart, the MIPS, its impressive performance implies it may play a role in augmenting future TW-SLIM experiments. By using MFTs, one could perform TW-SLIM experiments in which numerous distinct TW are generated within a single TW-SLIM, allowing for more complex experiments with a wide range of functionality. Like the MFT, the use of OBA and OBI simplifies the TW-SLIM experiment, removing

the need for an ion-gating mechanism independent of the TW-SLIM. While the nature of the OBA and OBI does produce a mobility bias, optimization of the TW conditions during the injection period could potentially allow a user to fine-tune the range of mobilities effectively injected by the OBI. While not explored in the context of this manuscript, the use of distinct SLIM segments does not appear to adversely impact the TW-SLIM experiment. A more thorough investigation on the impact of distinct SLIM segments will be presented in a future publication. The use of multiple distinct SLIM segments could allow a user to construct a diverse array of TW-SLIM configurations using a series of interchangeable SLIM boards of varying functionality. Lastly, to our knowledge, the presented TW-SLIM platform is the first to use a shielded Faraday plate as a detector to collect raw spectra. More sophisticated charge detection mechanisms have been reported previously but have yet to demonstrate spectra with comparable signal to noise ratios.[71] While limited in its functionality, the Faraday plate is far more economical than other detectors and eliminates concern regarding the process of venting a mass analyzer. The ability to rapidly bring the instrument to and from vacuum allows for more frequent adjustments to this system which affords considerable benefits when prototyping new TW-SLIM designs.

Though the scope of the experiments conducted with this simplified TW-SLIM platform is limited, the value of such a system has been shown already as it has enhanced our understanding of the underlying mechanics of SLIM accumulation. While a simple approach to accumulation may degrade the quality of analysis for some species, understanding how accumulation conditions affect given ion species may allow

a user to selectively improve the abundance of a given species of interest. Furthermore, this TW-SLIM platform has shown potential as a tool for the exploration of ion chemistry as it is capable of storing ions for extended periods (1 s), allowing a user ample time to introduce reactants into the region where these ion populations are stored. The implementation of storage times that exceed 1 s were precluded from the presented work but will be explored in future publications as the trends shown in Figure 2.6 suggest greater storage times are achievable. The development of TW-SLIM platforms such as the one presented in this manuscript are critical as they allow for more widespread implementation of the technique by introducing a modular assembly approach and reducing costs while increasing flexibility using the MFT.

Acknowledgments

This work was supported by NIH (NIGMS R01GM140129).

Supporting Information

SLIM Configuration

TW electrodes (1 mm long x 0.4 mm wide) were laid out in repeating sets of 8, with each electrode in the set assigned a number (1-8). The TW was generated by modulating the 8 electrode sets in a 4 high, 4 low pattern. For each electrode number, 5 electrodes were laid out across the width of the SLIM path with RF electrodes (0.4 mm wide) placed in between them, creating a 6:5 rf:TW configuration. Each RF electrode was 180^{o} out-of-phase to adjacent RF electrodes. Guard electrodes were 3.1 mm wide. The space between the top and bottom boards for both the drag and zipper section was

maintained at 3.2 mm using nylon spacers purchased from McMaster-Carr (Elmhurst, IL).

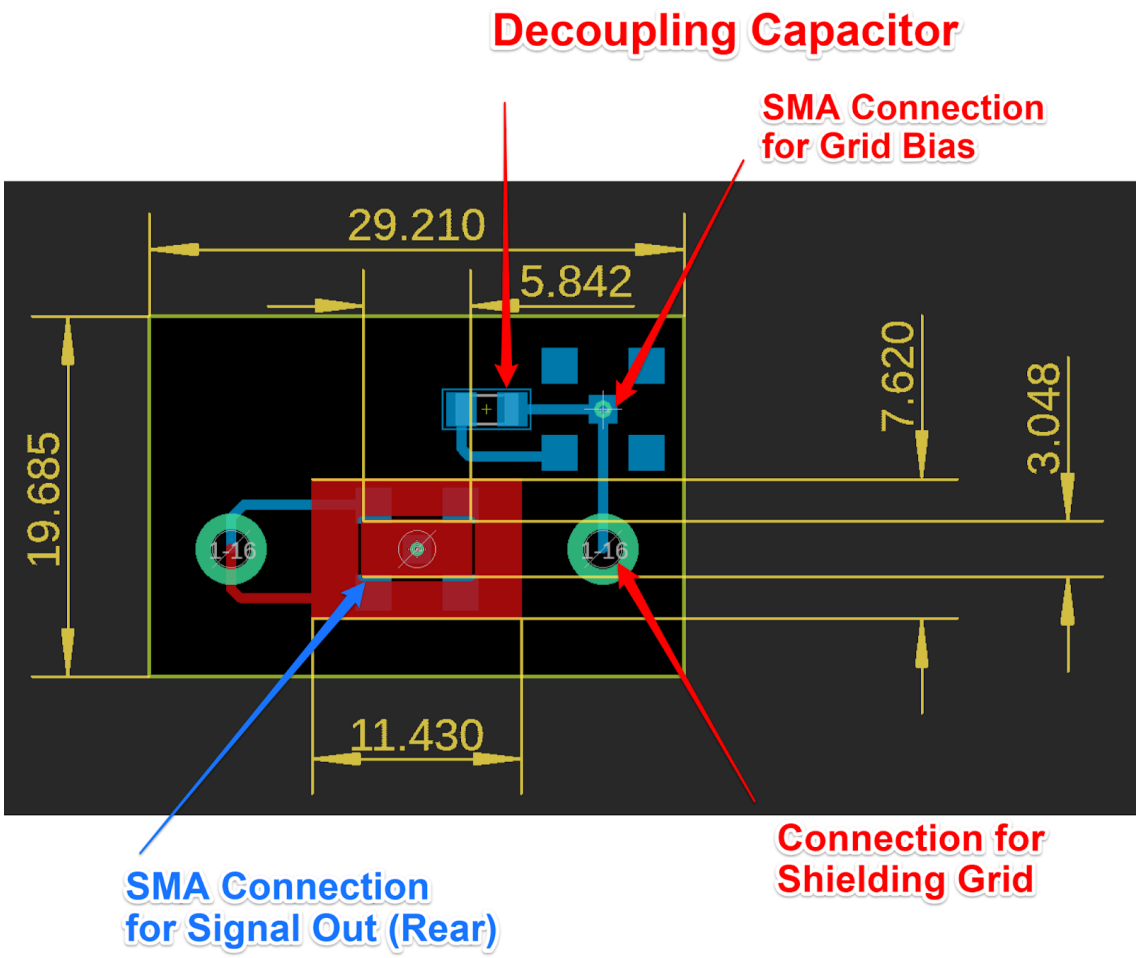

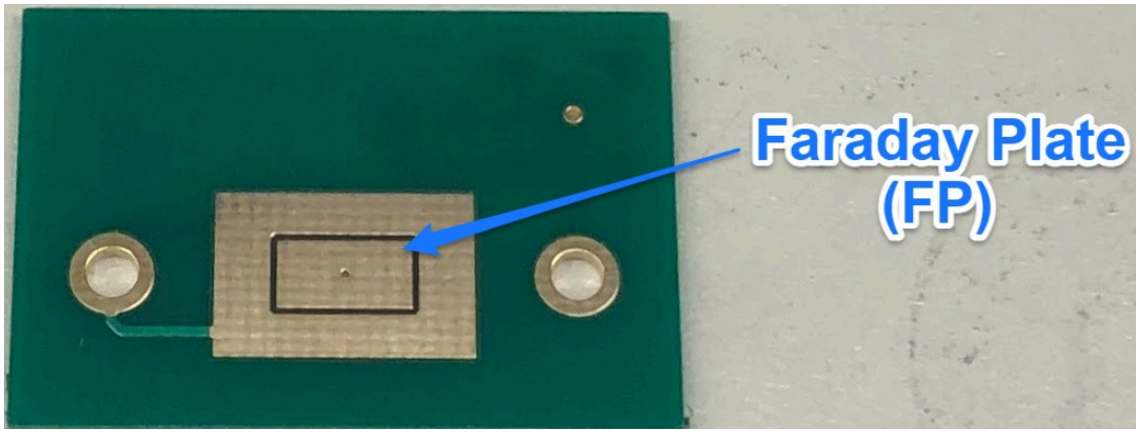

Figure 2.S1. Schematic and photo of the custom Faraday plate used throughout all presented experiments.

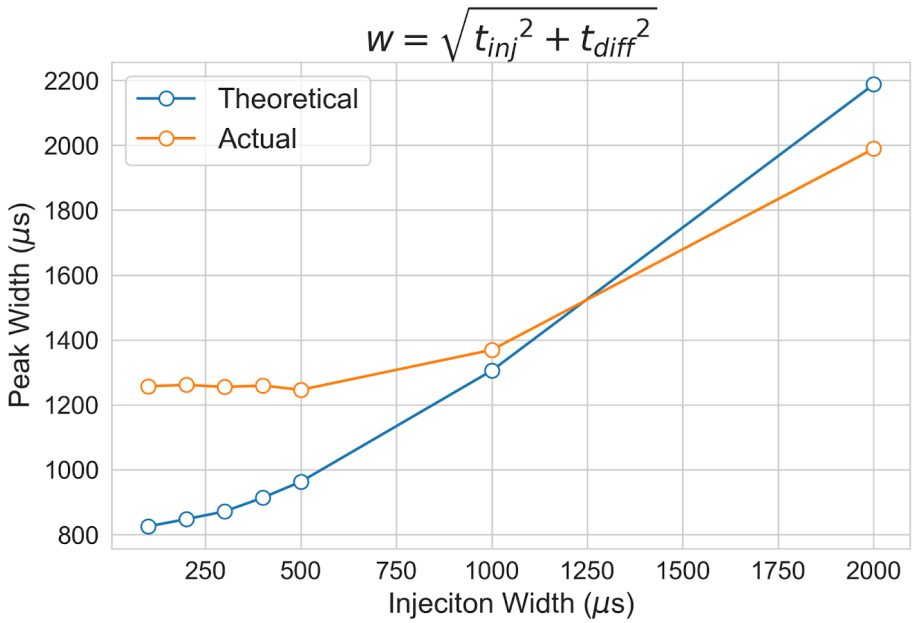

Figure 2.S2. Plots of theoretical[12] and actual peak widths observed for morphine as a function of injection width.

Table 2.S1. Data associated with the evaluation of the MFT mode performance relative to that of MIPS mode, at injection widths of 100 µs (a), 500 µs (b), and 1000 µs (c).

a)

100 µs Injection

Analyte	Metric	MIPS	MFT	Agreement (%)
Morphine	Peak Area (C*10^{-14})	6.3 ± 0.5	6.2 ± 0.6	98 ± 12
	Peak Amp. (nA)	0.037 ± 0.002	0.034 ± 0.003	92 ± 10
	Arrival Time (ms)	9.63 ± 0.04	10.17 ± 0.06	105.7 ± 0.8
T8	Peak Area (C*10^{-14})	7.2 ± 0.2	7.5 ± 0.1	103 ± 3
	Peak Amp. (nA)	0.0301 ± 0.0006	0.026 ± 0.001	85 ± 4
	Arrival Time (ms)	27.6 ± 0.1	28.8 ± 0.1	104.4 ± 0.6
T12	Peak Area (C*10^{-14})	4.7 ± 0.7	4.2 ± 0.4	90 ± 15
	Peak Amp. (nA)	0.011 ± 0.001	0.008 ± 0.001	78 ± 14
	Arrival Time (ms)	45.8 ± 0.1	47.6 ± 0.3	104.0 ± 0.7

b)

500 µs Injection

Analyte	Metric	MIPS	MFT	Agreement (%)
Morphine	Peak Area ($C*10^{-14}$)	7.9 ± 0.8	7.7 ± 0.5	97 ± 12
	Peak Amp. (nA)	0.048 ± 0.005	0.044 ± 0.003	93 ± 10
	Arrival Time (ms)	9.66 ± 0.06	10.25 ± 0.05	106.1 ± 0.8
T8	Peak Area ($C*10^{-14}$)	20.8 ± 0.8	19.9 ± 0.8	96 ± 5
	Peak Amp. (nA)	0.070 ± 0.003	0.064 ± 0.002	91 ± 5
	Arrival Time (ms)	27.3 ± 0.1	28.57 ± 0.08	104.7 ± 0.6
T12	Peak Area ($C*10^{-14}$)	47.1 ± 0.6	45 ± 1	94 ± 3
	Peak Amp. (nA)	0.091 ± 0.002	0.080 ± 0.002	88 ± 2
	Arrival Time (ms)	44.3 ± 0.2	46.4 ± 0.0001	104.7 ± 0.6

c)

1000 µs Injection

Analyte	Metric	MIPS	MFT	Agreement (%)
Morphine	Peak Area ($C*10^{-14}$)	10 ± 1	9.3 ± 0.4	93 ± 9
	Peak Amp. (nA)	0.054 ± 0.005	0.049 ± 0.003	90 ± 10
	Arrival Time (ms)	9.78 ± 0.06	10.39 ± 0.07	106 ± 1
T8	Peak Area ($C*10^{-14}$)	25 ± 1	25.5 ± 0.7	100 ± 6
	Peak Amp. (nA)	0.078 ± 0.004	0.073 ± 0.001	93 ± 5
	Arrival Time (ms)	27.3 ± 0.2	28.68 ± 0.09	104.9 ± 0.7
T12	Peak Area ($C*10^{-14}$)	71 ± 1	67 ± 3	94 ± 4
	Peak Amp. (nA)	0.126 ± 0.003	0.111 ± 0.003	88 ± 3
	Arrival Time (ms)	44.2 ± 0.2	46.2 ± 0.2	104.7 ± 0.7

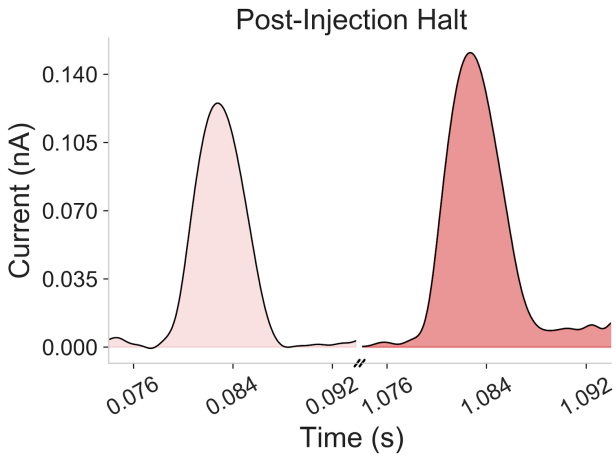

Figure 2.S3. T12 peak when no halt is implemented (left) and after a 1 s post-injection halt (right) using the MFT. The position of the T12 peak does not align with spectra shown elsewhere as this data was collected while prototyping a different SLIM configuration.

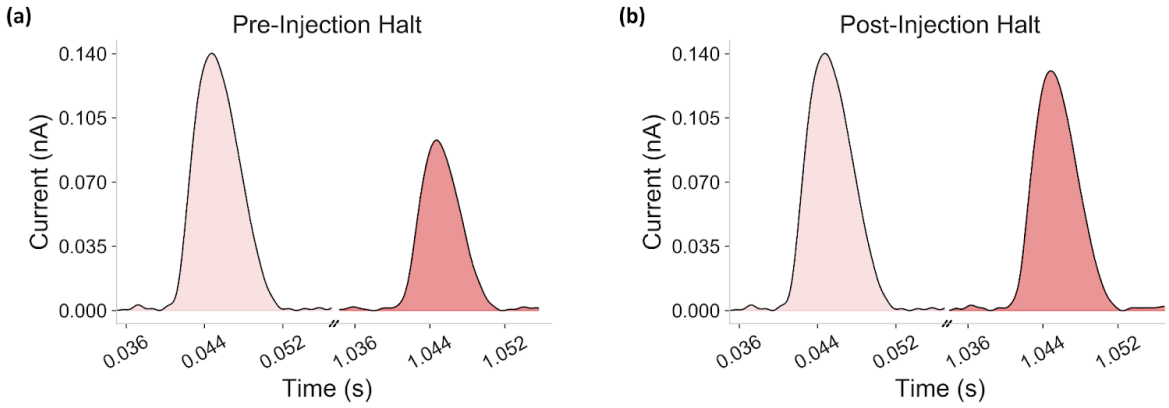

Figure 2.S4. (a) T12 peak when no halt is implemented (left) and after a 1 s pre-injection halt (right). (b) T12 peak when no halt is implemented (left) and after a 1 s post-injection halt (right). Spectra shown was collected when using the MIPS for TW modulation.

2.4 Broader Impact

The acquisition and utilization of funding is a major factor in determining the success of a project. With that in mind, approaches which reduce the cost of implementation may be the deciding factor on whether or not a particular research endeavor is pursued. Offering a cost-effective alternative to traditional TW electronics, the MFT reduces the financial commitment of beginning TW-SLIM research and may assuage concerns associated with committing to an emerging technology. It is our hope that groups interested in developing their own TW-SLIM platforms will incorporate MFTs into their prototyping efforts and that this technology will ultimately lead to the increased adoption of TW-SLIM. Since this work was published, more sophisticated versions of the MFT have been developed and are currently in use at WSU. While the more sophisticated ARBs remain in use for the more complex TW-SLIM systems, the MFTs have seen repeated use when prototyping and evaluating new platforms.

CHAPTER THREE: PRACTICAL CONSIDERATIONS FOR TW-SLIM DEVELOPMENT

3.1 Preface

This chapter will reference work published by Greer et al. titled: *SLIM Tricks: Tools, Concepts, and Strategies for the Development of Planar Ion Guides*.[79] Given that substantial contributions were made by all authors, it would be unreasonable to insert the full manuscript into this dissertation. Instead, I will briefly summarize the work as a whole and then focus on my contributions to the manuscript. Readers are strongly encouraged to read the manuscript in its entirety.

Similar to Chapter 1, this work represents the culmination of years of experimentation, namely the trial and error that comes along with building a TW-SLIM platform from the ground up. While not apparent in many of the TW-SLIM publications out of WSU, the way in which we've designed and assembled our instruments has varied significantly over the years as we've gained insight into the world of TW-SLIM. Some innovations have stemmed from a need to streamline our implementation and others from unforeseen challenges that come with scaling a TW-SLIM system to face increasingly challenging analyses. Regardless of what prompted the evolution of our research, this work outlines our development in a way that may ease the journey of those beginning upon a similar path and hopefully will increase TW-SLIM adaptation.

3.2 Contributions to *SLIM Tricks* Manuscript

SLIM Tricks: Tools, Concepts, and Strategies for the Development of Planar Ion Guides by Greer et al[79] outlines a series of tools which aid in all phases of TW-SLIM development from conceptualization to assembly. Beginning with conceptualization, SIMION is the most commonly used software for the modeling of ion optics and has proven a valuable tool for TW-SLIM development.[28,71,80,81] Though popular, fully leveraging the capabilities of SIMION often involves a higher degree of training and preparation than many are interested in committing to. Recognizing the need to make TW-SLIM modeling in SIMION more accessible, Brian Clowers and Cullen Greer outline and provide tools which aid in these endeavors. Assuming modeling efforts suggest that a TW-SLIM design is feasible, the next step is to design the TW-SLIM boards using computer aided design software (CAD), a skillset which is very limited amongst chemists. In order to make CAD more palatable, Brian Clowers developed *SLIM Pickins*, a Python-based tool which automates much of the board layout process. Additionally, individual board components such as TW-SLIM monomers and wiring templates were released to further simplify the process of designing TW-SLIM boards.

Up until this point, we've exclusively discussed the preparatory elements of TW-SLIM development. However, as the TW-SLIM transforms from an idea to a tangible object, numerous practical considerations come into play which can heavily influence the success of a TW-SLIM platform. Seeing as my work was at the forefront of TW-SLIM development at WSU, I was directly involved in many of the practical improvements to our TW-SLIM systems and will discuss those elements of *SLIM Tricks*

in greater detail. Select portions will be excluded from this discussion as they are covered more thoroughly elsewhere in this dissertation (e.g., the MFT in Chapter 2).

One of the major differences between the original TW-SLIM boards we used and the later generations is board thickness. When operating with smaller TW-SLIM paths (<2 m), the 1.6 mm thick boards provided no cause for concern. However, as we scaled to larger boards (>8 m), the boards began to sag in regions which lacked sufficient support. We attribute this sagging to two main factors: a lack of board rigidity and insufficient support towards the center of the boards. To address the board rigidity, we shifted from board thicknesses of 1.6 mm to 2.4 mm. Fortunately, this shift was not only effective, but also inexpensive. In order to both support the TW-SLIM boards and maintain a consistent gap between them (i.e., avoid board sagging/bowing) holes are placed throughout the boards to allow nylon spacers (McMaster-Carr) to be secured between them (Figure 1.3). For smaller TW-SLIM boards, spacer placement was limited to the board perimeter to simplify the layout of the TW-SLIM path. When scaling to larger boards, this perimeter-only approach proved insufficient and boards were modified to allow for centrally located spacers to be installed (Figure 3.1).

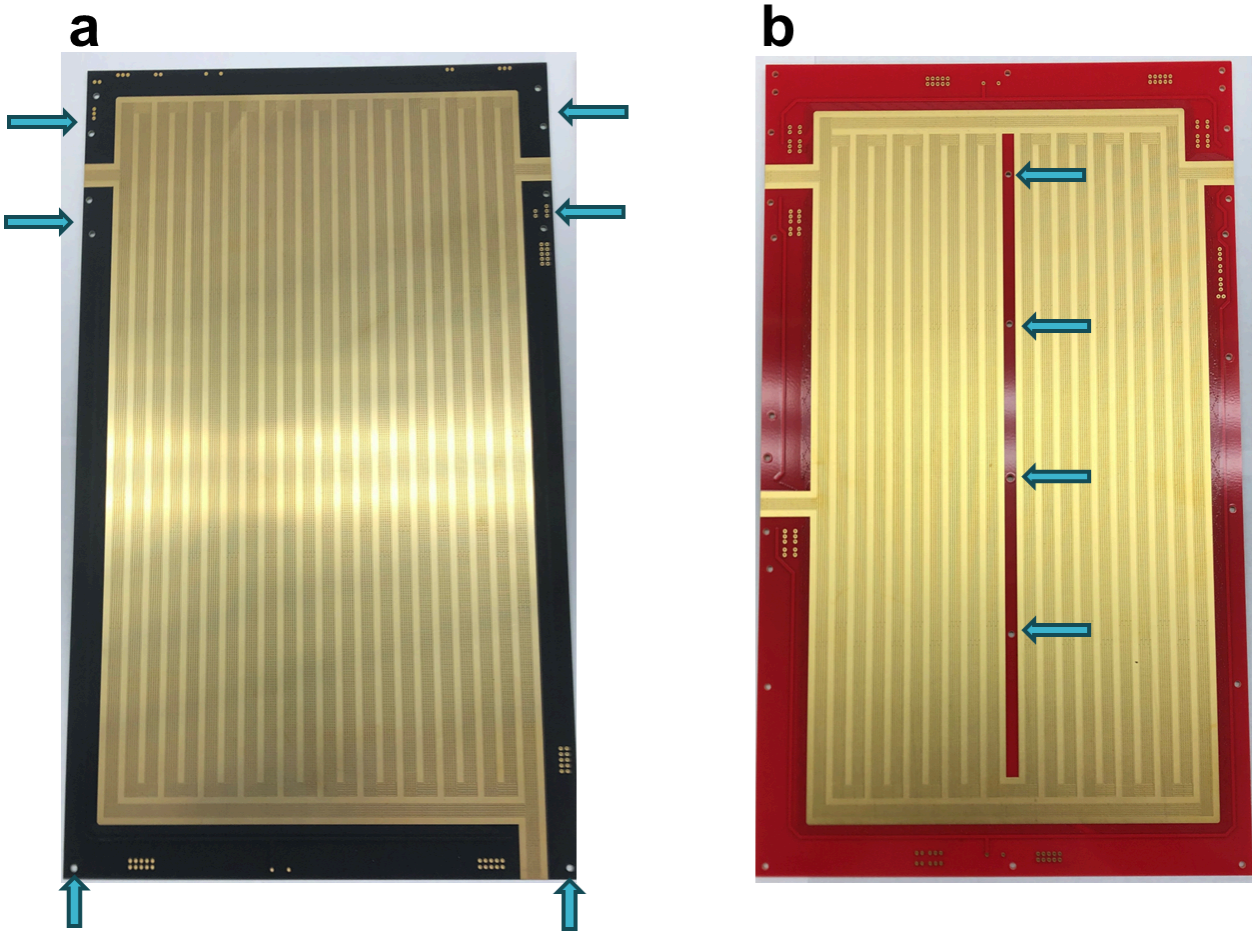

Figure 3.1. Photographs of the first large (>2 m pathlength) TW-SLIM board developed at WSU (a) and a later version which was utilized for the work discussed in Chapters 5 & 6. The board shown in (a) only had holes for spacers around the perimeter (blue arrows) and sagged towards the board center, reducing the quality of analysis. In later versions of our big boards (b), we added spacer holes in the center to remedy this issue in addition to increasing the board thickness.

Another issue we encountered as we scaled to larger TW-SLIM systems was crosstalk between the TW and RF signals. Put simply, crosstalk is the unintentional coupling of traces within a PCB.[82] To be clear, the TW and RF traces are not in physical contact with one another, but are instead capacitively coupled throughout the PCB.

Where crosstalk becomes an issue is when it becomes so excessive that it causes electronics to fail, namely the TW generators. Recognizing that crosstalk increases with TW-SLIM pathlength (longer path, more overlapped traces), TW amplitude, TW speed, RF amplitude, and RF frequency, those working with TW-SLIM can quickly find themselves unable to access certain experimental conditions which may limit the quality of their analysis. From a design standpoint, there are two primary solutions to limiting crosstalk: increasing the spacing between RF and TW layers in the TW-SLIM boards, and careful consideration for the layout of traces within the PCB. Fortunately, the use of thicker boards not only helps with sagging, but also allows for a greater distance between RF and TW traces. With regards to trace layout, minimizing trace overlap and avoiding parallel trace placement are great ways to limit crosstalk (Figure 3.2).

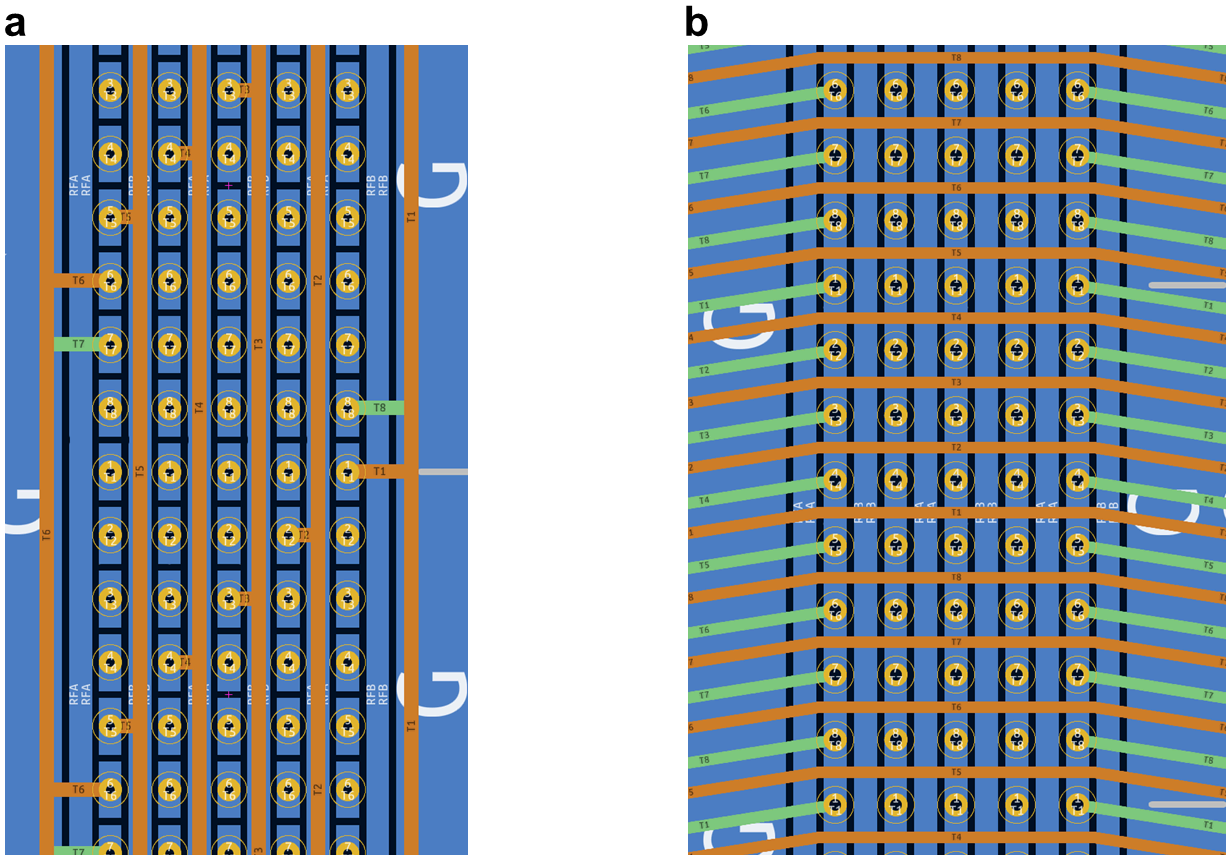

Figure 3.2. Screenshots from KiCAD (CAD software we use to design our SLIM boards) show TW traces (orange and green lines) which run parallel (a) and non-parallel (b) to the RF traces. Boards that are laid out like (a) will have greater crosstalk and are at an increased risk of electronics failure.

One of the fundamental principles of TW-SLIM research of WSU has been an emphasis on designs which lend to flexibility and rapid prototyping. Perhaps the greatest reflection of this has been our commitment to multi-board systems. Multi-board systems consist of multiple TW-SLIM board sets which are joined together to create increasingly complex TW-SLIM configurations. To be clear, a board set refers to the mirrored top and bottom boards which are joined together. In the case of a multi-board

setup with 2 board sets, the total number of PCB used to assemble the system would be 4. While the multi-board setup does require extra effort to join and align the boards, we have found that simple Delrin cutouts are more than capable of solving this issue (Figure 3.3). One of the primary benefits of the multi-board approach is that it allows for various TW-SLIM configurations to be rapidly evaluated. One can theorize a situation where, having designed numerous boards capable of performing different functions, a user can “mix and match” these boards in ways that would enable complex experiments without having to create a singular, costly board set. The benefits of the multi-board systems also extends to troubleshooting, wherein problematic board sets can be identified and removed without having to redo an entire TW-SLIM setup.

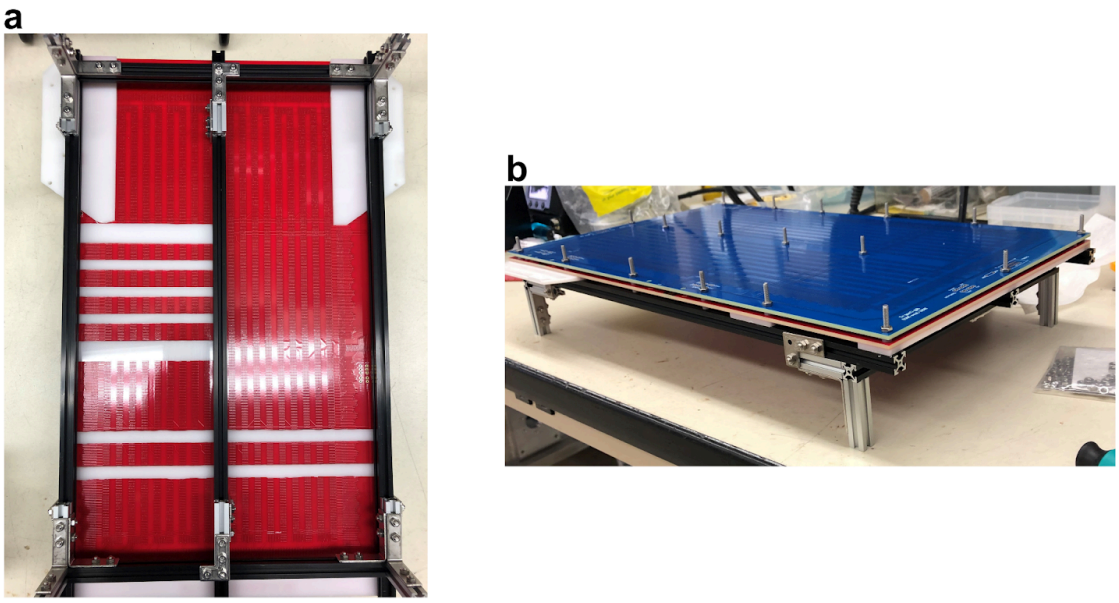

Figure 3.3. Photographs showing how our TW-SLIM boards are mounted onto MakerBeam (Utrecht, Netherlands) structures which enable them to be secured in the TW-SLIM chamber. The view from beneath the boards (a) shows the Delrin cutouts (white) which secure the TW-SLIM boards to the MakerBeams. A side view of the structure (b) shows how the boards are oriented when placed into the TW-SLIM chamber. The portions of the Delrin cutouts which extend beyond the TW-SLIM boards serve as a platform for other board sets to be mounted, enabling for multi-board systems to be easily assembled.

Though not unique to TW-SLIM, a discussion about the reduced pressure environment (2-4 Torr) in which experiments are conducted warrants a brief discussion. Beginning with the simplest configuration (no mass spectrometer) which was used for the work shown in Chapters 2&4, it's possible to operate a TW-SLIM system using only two vacuum pumps: one for the inlet chamber and one for the SLIM chamber. Using this configuration, the only gas entering the system is that which travels through the inlet

(i.e., ambient air), greatly simplifying the instrument at the cost of greater control over the environment within the SLIM chamber. Using this setup, the only condition which requires fine adjustments is the pressure differential between the SLIM and inlet chambers which is offset by approximately 50 mTorr to discourage the transmission of neutral molecules into the SLIM chamber. Though not appropriate for complex chemical analyses which require controlled environments, this configuration is great for simple prototyping experiments and has seen continued use at WSU when testing out new TW-SLIM platforms.

Upon pairing a TW-SLIM system with a mass spectrometer (MS), the simplistic nature of the prototyping setup quickly dissolves and is replaced with a far more complex environment. The pressure range at which MS operate ($<10^{-3}$ Torr) means that the SLIM chamber now exists as a middle ground between high pressure (ambient conditions where ESI occurs) and low pressure (MS) regions. Depending upon factors such as orifice sizes, pumping speeds, and pressure gradients, the setup for this type of system (i.e., number of pumps, additional gas leaks, etc.) will vary greatly. While variability in instrument design is acceptable and expected, it's vital that conditions within the SLIM chamber remain static. Recalling that TW-SLIM is capable of enabling ion manipulation over extended pathlengths and timescales, minor fluctuations in pressure can result in significant shifts in arrival time which decreases the reproducibility of measurements.

A significant advantage of TW-SLIM technology is the relatively low cost of TW-SLIM board production. While tempting to promote TW-SLIM as a low-cost

technique, it would be disingenuous to ignore the significant cost of the auxiliary components of TW-SLIM experiments, namely the power supplies (discussed in Chapter 2) and vacuum equipment such as pumps and housing. The traditional approach to vacuum housing is to design custom chambers which are made to fit a particular instrument. The benefit of this approach is that the design of the instrument is not dictated by the housing, alleviating the need to compromise on experimental capabilities. Recalling that TW-SLIM research at WSU emphasizes flexibility and rapid development, the use of traditional vacuum chambers is problematic as it isn't feasible to frequently design and pay for custom housing on a regular basis. Recognizing a need for vacuum housing which can match the flexibility of our TW-SLIM platforms, we have opted to assemble all of our housing using modular vacuum chambers purchased from Ideal Vacuum Products LLC (Albuquerque, New Mexico). While perhaps more expensive to purchase up-front, these modular chambers represent a cost-effective alternative to traditional housing as they can be repurposed for any number of experimental configurations in the future. Furthermore, the use of these modular chambers eliminates the wait times associated with manufacturing custom housing, enabling more rapid prototyping. The primary drawback of using these modular chambers is that they will ultimately dictate the dimensions of the TW-SLIM boards they house. While this restraint is unfortunate, we have found this issue easy to work around and have provided tools (SLIM Pickens) which can help others do the same.

3.3 Broader Impact

In many ways, this work represents a major stepping stone for TW-SLIM research at WSU. While other entities may showcase more complex instruments, none of them have provided our community with the degree of insight into TW-SLIM development that we have. Recognizing that instrumentation experience is uncommon amongst analytical chemists, the work outlined in this chapter extends a much needed invitation to those without the prerequisite skill sets to engage with TW-SLIM research. When paired with some of the cost-saving approaches outlined in this dissertation, a path to widespread TW-SLIM adaptation quickly takes form.

Aside from aiding in the adoption of TW-SLIM, it's also worth acknowledging the underlying story that is being told in this chapter with regards to our journey with TW-SLIM development. Each of the recommendations and considerations we discussed stem directly from issues and pitfalls that we endured as we got our TW-SLIM systems up and running. Had these issues been reported in the literature by those who have cleared such hurdles already, far more time could have been spent on improving and expanding TW-SLIM instead of solving problems whose solutions were already known. It is our hope that those who develop their own TW-SLIM systems in the future will use *SLIM Tricks* as a guide for navigating the early stages of the process wherein many well intentioned individuals may otherwise fall short.

CHAPTER FOUR: EVALUATING DYNAMIC TRAVELING WAVE PROFILES FOR THE ENHANCEMENT OF SEPARATION AND SENSITIVITY IN TRAVELING WAVE STRUCTURES FOR LOSSLESS ION MANIPULATIONS

Reprinted (adapted) with permission from Kinlein, Z.; Clowers, B. H. Evaluating Dynamic Traveling Wave Profiles for the Enhancement of Separation and Sensitivity in Traveling Wave Structures for Lossless Ion Manipulations. *J. Chromatogr. A* 2023, *1706*, 464207. Doi: 10.1016/j.chroma.2023.464207. Copyright 2023 Journal of Chromatography A

4.1 Attributions

The authors whose work contributed to the following manuscript include Zackary R. Kinlein and Brian H. Clowers. Zackary R. Kinlein is credited with method development, conducting the investigation, and was the primary author of this work. Brian H. Clowers is credited with conceptualization, supervision, method development, funding acquisition, and contributions to writing.

4.2 Preface

Shortly following the work discussed in Chapter 2, we designed and tested our first serpentine board with the ability to perform cyclic separations. Something that became apparent upon utilizing extended TW-SLIM pathlengths was that TW conditions which enabled for the separation of closely related species did not effectively transmit disparate species present in the sample. Put differently, TW settings optimized for the analysis of species within a select mobility window resulted in poor transmission (i.e., loss of sensitivity and resolving power) of species outside of that window. Though not

surprising that a one-size-fits-all approach was unachievable considering that RF confinement will always impose a bias on ion transmission,[32,66] the observation that certain TW conditions were problematic warranted further investigation.

Utilizing a unique capability of the arbitrary TW generator developed by GAA Custom Electronics (Kennewick, WA) to “ramp” through TW speeds and amplitudes, we envisioned a solution to disparate analysis akin to gradient elutions in chromatography. As I began working up the data which would eventually turn into in the manuscript adapted for this chapter, I quickly came to two major conclusions: the ramp was not the perfect solution that we had envisioned and that I had been greatly underestimating the complexity of TW analysis. Nonetheless, the work outlined in this chapter will provide insight into how an individual can tune their analysis to improve particular experimental metrics for select species and also provides a broader commentary on TW-SLIM analysis as a whole

4.3 Manuscript

Abstract

The amenability of traveling wave ion mobility spectrometry (TWIMS) to extended separation pathlengths has prompted a recent surge of interest concerning the technique. While promising, the optimization of ion transmission, particularly when analyzing increasingly disparate species, remains an obstacle in TWIMS. To address this issue, we evaluated a suite of dynamic TW profiles using an original TW structures for lossless ion manipulations (TW-SLIM) platform developed at Washington State University. Inspired by the range of gradient elution profiles used in traditional chromatography, three distinct square TW profiles were evaluated: a static approach which represents a traditional waveform, a dual approach which consists of two distinct TW profiles within a given separation event; and a ramp approach which varies TW speed and amplitude at a fixed rate during separation. The three waveform profiles were evaluated in terms of their impact on separation (quantified as resolution) and sensitivity (quantified using signal-to-noise ratio (SNR), and ion abundance). Concerning separation, the highest resolution (R) was observed when operating with the static waveform (R=7.92); however, the ramp waveform performed comparably (R=7.70) under similar conditions. Regarding SNR, optimum waveform profiles were species dependent. Bradykinin^{2+} displayed the largest gains in SNR (36.6% increase) when ramping TW speed, while the gains were greatest (33.5% increase) for tetraoctylammonium when modulating TW amplitude with the static waveform. Lastly, significant (>10%) increases in the abundance of tetraoctylammonium ions were observed exclusively when utilizing a ramped waveform. The present set of experiments

outline the results and challenges related to optimizing separations using alternative TW profiles and provides insight concerning TW-SLIM method development which may be tailored to enhance select analytical metrics.

Introduction

Ion mobility spectrometry (IMS) is a gas-phase analytical technique that separates analytes based on their ionic mobilities as they are propelled through a gas under the influence of an externally applied electric field.[1,2] Lending to relatively simple construction and rapid analysis, much of the early implementations of IMS concerned matters of threat detection and field deployment.[4,5,83] However, developments in the field of IMS, particularly those concerning its coupling with mass spectrometry, have led to an expansion of IMS applications to include the investigation of biomolecules and even the separation of isomers.[17,84,85]

While the most commonly deployed IMS approach is drift tube IMS (DTIMS) which separates ions using linear, homogeneous fields, other iterations of IMS instrumentation exist, such as field asymmetric IMS (FAIMS),[86] trapped IMS (TIMS),[87,88] and traveling wave IMS (TWIMS).[3,23] TWIMS in particular has seen a recent spike in interest in part due to the development of traveling wave structures for lossless ion manipulations (TW-SLIM), which utilizes planar printed circuit boards (PCB) to effectively confine and separate ions.[28] While TW-SLIM differs from other TWIMS approaches in terms of construction, the nature of ion separation via traveling waves remains relatively consistent across the techniques. In-depth explanations of ion behavior in response to traveling waves are outlined elsewhere.[22,24,25] Briefly, ions

exposed to dynamic electric fields, which are in essence transient potential wells, attempt to “keep up” with the wells which are moving at a user-defined rate. This rate is often referred to as TW speed (s). The ability of ions to remain within a given well and not fall to a preceding well is dependent upon their velocity (v), which is a function of the ions’ mobilities and the depth of the well. Well-depth is defined by the user and is often referred to as TW amplitude. The ratio of ion velocity to traveling wave speed is often expressed as c (eq. 4.1):

$$c = \frac{v}{s} \tag{4.1}$$

Ions whose velocities approach the TW speed will fall over to preceding wells less frequently than those with lower velocities (i.e., lower mobility species), which leads to mobility-based separations that are related to the rate of ion rollover.

A profound benefit of TWIMS is its use of electric fields which are defined by localized minima and maxima, as opposed to the absolute maximum and minimum field strengths found in DTIMS systems, which ultimately limit their length and subsequent separation power. Recent work has seen this unique flexibility with regard to field strengths leveraged to achieve separation pathlengths in excess of 10 m, far exceeding the length of a typical DTIMS system.[40,89] Additionally, TWIMS experiments using cyclic separations continue to grow in popularity, with both the Waters Cyclic-IMS and TW-SLIM platforms enabling theoretically infinite pathlengths for separation.[41,45] While the unique nature of TWIMS may appeal to those interested in performing mobility separations, it is important to note that the technique is by no means a solution to all

IMS shortcomings and presents its own inherent issues. Concerning issues inherent to TWIMS, the concurrent transmission of increasingly disparate species remains an obstacle. This issue stems from the use of RF confinement[32,66] and the dependence of ion motion (i.e., bobbing or riding wavefronts) on mobility (eq 4.1). In the greater context of IMS, an issue analogous to the general elution problem often associated with chromatography exists as static conditions which enable the separation of early “eluting” species do not necessarily provide for optimum transmission of later “eluting” species.

Recognizing the aforementioned issues concerning TWIMS, we sought to evaluate a suite of TW profiles that seek to simultaneously remedy issues of ion transmission as well as address the general elution problem. Taking inspiration from the gradient elutions employed in chromatography, we implemented a ramped waveform in which TW speed and amplitude were varied at a fixed rate during separation in hopes of providing optimum conditions for transmission and separation of both early and later arriving (i.e., higher and lower mobility) species. In order to evaluate the performance of the ramped waveform against a more traditional waveform, we performed similar experiments with a static waveform analogous to isocratic approaches in chromatography. Lastly, a third waveform was implemented in which a sudden change in conditions was implemented immediately following the arrival of the first species. This was theorized as an approach that would enable the optimum transmission of one species before modulating to conditions that provide ideal transmission of another species.

The following discussion provides insight into the impact of the various waveforms on matters of both separation and sensitivity. Acknowledging issues associated with resolving power as a metric for evaluating TWIMS separations,[28,90] resolution was used instead (eq. 4.2):

$$Resolution = 1.18 * \frac{t_2 - t_1}{(w_2 + w_1)} \quad (4.2)$$

where t_2 and t_1 correspond to the arrival times of two species, and w_2 and w_1 are the species' full widths at half maximum (FWHM). The optimum resolution was obtained by operating with the static waveform and modulating TW amplitude, though it is worth noting that the ramped waveform did not perform significantly (>10%) worse than its static counterpart. With regard to sensitivity, signal-to-noise ratio (SNR) and ion abundance (which relates to peak area) were used to characterize the performance of the waveforms. For the two compounds used throughout the presented analyses, bradykinin^{2+} and tetraoctylammonium (T8), a combination of a ramped waveform and TW speed modulation provided optimal SNR for T8, whereas static TW amplitude modulation performed best for bradykinin^{2+}. Akin to observations made regarding SNR, ideal conditions for ion abundance were not consistent amongst the analytes, with T8 benefiting most from the use of the ramped waveform and bradykinin^{2+} reporting the lowest ion abundance when using the ramp.

Experimental

Tetraoctyl ammonium bromide and bradykinin acetate salt were purchased from Sigma-Aldrich (St. Louis, MO). All data presented were collected using a solution of 1

μM each T8 and bradykinin prepared in methanol (HPLC grade, Fisher Chemical, Fair Lawn, NJ) with 0.1% formic acid (Honeywell-Fluka, Muskegon, MI). T8 was selected in order to gauge how the various experimental conditions would impact simpler analytes (singly charged, lack of conformers), which are popular within the field of ion mobility (e.g., explosives and narcotics).[4,83,91] Bradykinin was chosen as a representative biomolecule, though it is important to note that the peptide is neither particularly large nor complex and that further experiments would be necessary to explore how the presented methods impact increasingly complex species.

A schematic of the instrument used throughout the presented work is shown in Figure 4.1. The instrument used throughout the presented analyses is analogous to one reported in detail elsewhere.[54] Briefly, ions were generated via electrospray ionization (ESI) using a 75 μm ID glass capillary emitter biased 2.2 kV relative to an adjacent heated (160 °C) stainless-steel inlet capillary (560 μm i.d., 1600 μm o.d.) purchased from McMaster-Carr (Elmhurst, IL). The sample flow rate used throughout the analyses was 3 μL/min, controlled by a Model 11 Syringe Pump from Harvard Apparatus (Holliston, MA). After traversing the inlet capillary, ions were focused by an ion funnel (897 kHz, 240 V_{p-p}) housed in a low-pressure (2.45 torr, ambient air) chamber before being transported to a second, smaller ion funnel (1.1 MHz, 140 V_{p-p}) housed in a slightly higher pressure (2.50 torr, ambient air) chamber. The pressure in each chamber was monitored using Setra Model 730 capacitance manometers (Boxborough, MA).

After traveling through the second ion funnel, ions arrived at the first TW-SLIM segment, referred to as the “drag” board, which was used for ion packet injection. The

injection of stored ion packets was achieved utilizing a series of electrodes capable of switching between a blocking state, in which they were biased above the adjacent electrodes using a static DC potential, and a TW state which enabled ion transmission (i.e., injection). Throughout all experiments, the injection width was 1 ms. Immediately following the drag board was a second, distinct SLIM board dubbed the "separation board." An investigation concerning the impact of two distinct sets of SLIM boards, as opposed to the traditional single set, will be expounded upon in future publications. While capable of enabling more advanced separation techniques, such as multi-pass and compression ratio ion mobility programming (CRIMP),[70,81] the secondary track of the separation board was not used in the presented analyses. The total path length used for separation was approximately 1.5 m. A custom Faraday plate served as the primary detector.

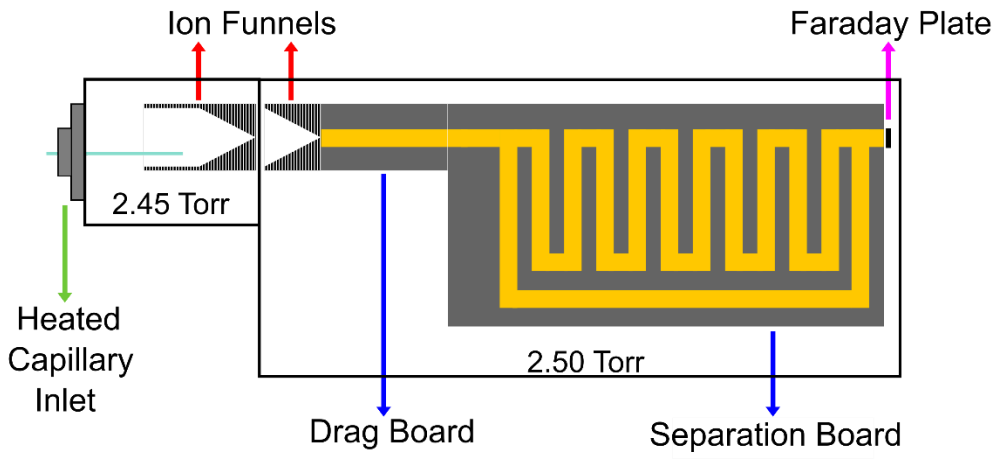

Figure 4.1. Schematic of the instrument used throughout the presented work. A photo of the instrument is shown in Figure 4.S1.

Current detected at the Faraday plate was first amplified using a Keithley Model 427 current amplifier (10^9 Gain, Rise time: 1 ms, Cleveland, OH) and then subsequently recorded as a function of time using an Analog Discovery 2 (Digilent Inc., U.S). Data were processed using Python notebooks similar to those released in a previous publication.[54] Arrival time distributions (ATD) were averaged 75 times, and each presented data point represents an average of 5 ATD replicates. The standard deviation of the 5 replicates is representative of the measurement's uncertainty. "Noise," as it pertains to SNR calculations, was defined as the baseline immediately preceding and following each peak. "Ion abundance" refers to the total number of charges associated with each species and was calculated via integration of the ion signal detected at the Faraday plate. Peak identities were assigned by analyzing the individual standards of each analyte.

TW-SLIM conditions were controlled using a modular intelligent power source (MIPS) from GAA Custom Electronics (Kennewick, WA). Ions were confined laterally by guard electrodes biased to the TW at half its amplitude. Radial confinement was achieved using RF electrodes operating at 1.07 MHz, 300 V_{p-p}. The square TW was generated using a 4 high, 4 low electrode configuration. Control conditions for the TW were defined as 23 V_{p-p}, 183 m/s. Further details regarding the configuration of the SLIM boards are reported elsewhere.[54]

Three waveform profiles were evaluated as a means of optimizing peak profiles within TW-SLIM: a static waveform (static), a waveform with two distinct segments (dual), and a ramped waveform (ramp). A visual representation of the three waveform

profiles is provided in Figure 4.2. The static waveform represents the simplest TW profile in which all species reach the detector under identical conditions (analogous to isocratic elutions in LC). The dual waveform consists of two distinct profiles: control conditions (maintained until after the first species (bradykinin^{2+}) reaches the detector) and conditions in which either the TW amplitude was increased or the TW speed was decreased. The transition between the conditions in the dual profile occurred as rapidly as the MIPS would allow (~300 μs). Regarding the ramp, 5 ms after injection, TW conditions were ramped to either higher amplitudes or lower speeds over the course of 120 ms. Information regarding ramp rates can be found in Table 4.S1. Across all waveform profiles, the TW was operated at conditions that enhanced ion accumulation (TW amplitude was reduced to 16 Vp-p) for 60 ms prior to injection.

Regardless of the waveform profile implemented, the TW-SLIM operated under control conditions for the first 5 ms from the point of injection. This was done to avoid any confounding effects stemming from the impact of TW parameters on ion injection, which have been reported elsewhere.[54] Additionally, despite preliminary modeling efforts suggesting that varied TW parameters do not significantly impact ions traversing the gap between board sets, the 5 ms control period enabled ions to traverse this gap prior to any waveform modulation, once again avoiding any potential confounding effects.

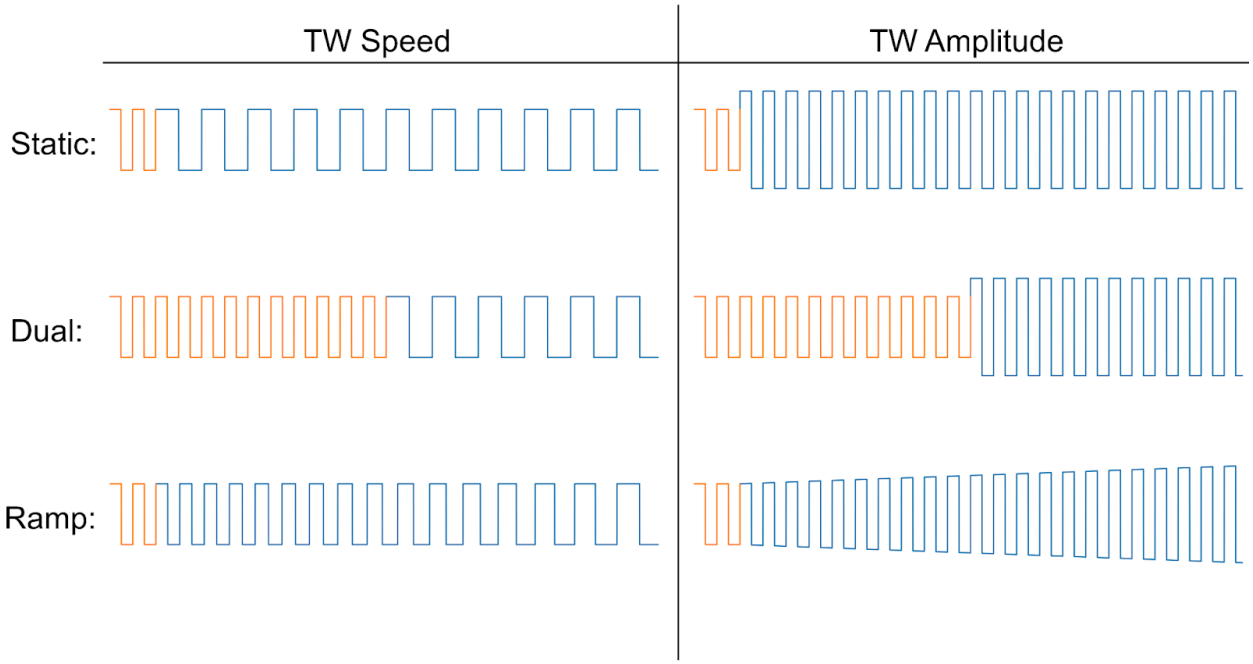

Figure 4.2. Visualization of the waveform profiles evaluated. The orange portion of each waveform represents control conditions. The "static" approach is representative of a typical TW in which all species arrive at the detector under identical conditions. The "dual" waveform was theorized as an approach that could enable the optimum transmission of one species before switching to the conditions that provide the idealized transmission of another species. Lastly, the "ramp" waveform modulates TW speed or amplitude at a fixed rate during separation and was hypothesized as a middle-ground for the transmission of disparate species.

Results and Discussion

Prior to evaluating the dual and ramp waveforms, preliminary experiments were conducted to validate results reported elsewhere[28] concerning the relationship between resolution and TW conditions. In agreement with Hamid et al.,[28] over a given range of values, decreasing TW speed and increasing TW amplitude coincide with gains in resolution between T8 and bradykinin^{2+} (Figure 4.3). Having established that the presented TW-SLIM platform performed as expected when operating with the static

waveform, the previous analysis was repeated, this time with the dual and ramp waveforms (Figure 4.3). For both the amplitude and speed experiments, similar trends were observed for the static and ramp waveforms which demonstrated gains in resolution associated with decreases in TW speed and increases in TW amplitude, while the dual waveform behaved inversely. Interestingly, the experiments varying amplitude provided greater gains in resolution for the static and ramp waveforms and mitigated the decrease in resolution associated with the dual approach. While a direct comparison cannot be made between the presented results and those published by Hamid et al.,[28] it is interesting to note that in both cases, modulating TW amplitude appears to have a more profound impact on separation than TW speed. With exception to the TW speed experiments concerning the static and ramp waveforms, the data presented in Figure 4.3 show distinct trends associated with resolution as a function of waveform profiles (static, dual, and ramp). It is worth noting, however, that aside from select conditions (TW speed: 110 m/s, TW amplitude: 29-31 $V_{p\text{-}p}$), no significant (>10%) variation between resolution values was observed.

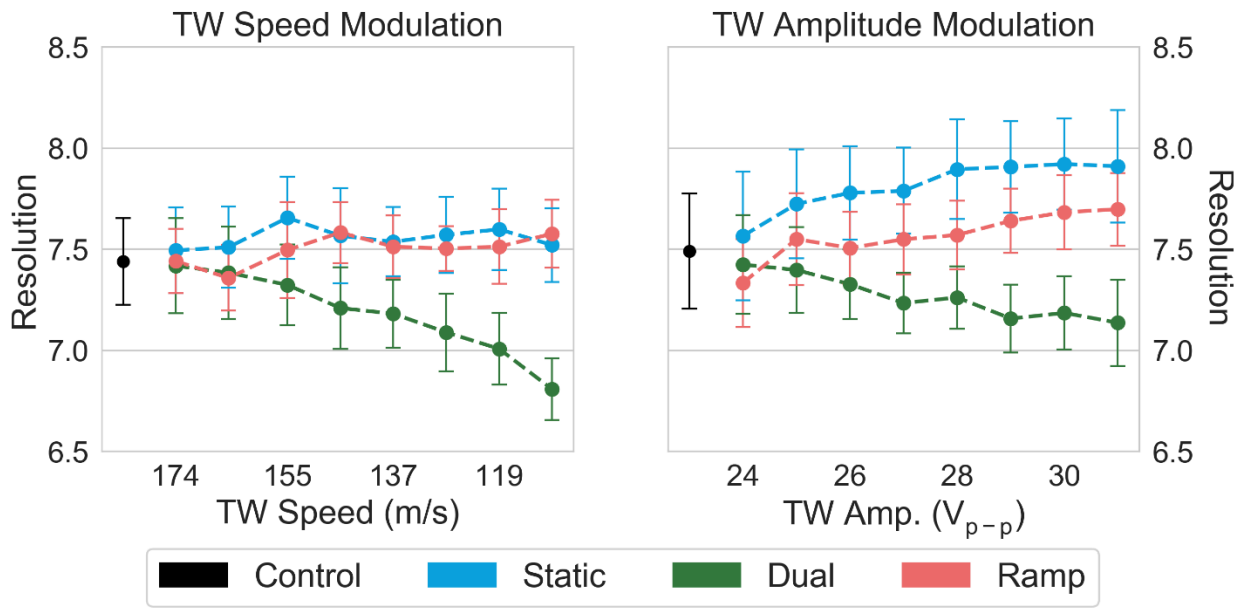

Figure 4.3. Variations in resolution between T8 and bradykinin^{2+} as a function of TW speed (left) and amplitude (right). Values on the x-axis represent conditions that followed the control period of the static and dual waveforms, and the value that was ramped to in the ramp waveform.

Despite the comparable resolutions observed across various conditions, a more in-depth analysis of the data associated with Figure 4.3 reveals substantial differences between the ATDs collected using the different waveform profiles (Figure 4.4). A qualitative assessment of the ATDs presented in Figures 4.4b and 4.4c suggests that each of the three waveform profiles has a distinct impact on factors concerning both separation and sensitivity. Regarding separation, a quantitative evaluation of peak widths and the temporal separation between T8 and bradikinin^{2+} is presented in Figure 4.5. Recalling that gains in resolution were observed when increasing TW amplitude and decreasing TW speed, it is interesting to note that these gains in resolution coincide with decreases in temporal separation (i.e., more tightly spaced peaks). Ultimately, so

long as the reduction in peak width is more significant than the loss of temporal separation (eq. 4.2), the quality of separation will improve. While similar results and discussions have been published elsewhere,[28,92] it is important to acknowledge this behavior as it provides insight regarding TW method development, suggesting that optimal separation is achieved within some range of rollover events in which ions are sufficiently separated but not subject to excessive diffusion. Regardless of whether TW speed or amplitude is being modulated, the rates of peak width reduction and loss of temporal separation are more profound when operating in static mode relative to ramp mode (values associated with the lines of best fit are provided in Table 4.S2), as ion populations are exposed to conditions which discourage ion rollover, for longer periods. Interestingly, despite comparable behavior between the speed and amplitude data (Figure 4.5), a clear disparity in the nature of these trends (linear for speed, quadratic for amplitude) is apparent. We attribute the linear nature of the speed data to a steady-state separation mechanism proposed by May and Mclean,[92] which occurs as a result of ions undergoing numerous rollover events and thus experience a range of field strengths. Regarding the amplitude data, we ascribe this nonlinear behavior to the quadratic relationship between drift time and KE proposed by Shvartsburg and Smith,[24] where K is an ion's mobility and E is the field intensity (which relates to TW amplitude) experienced by the ion.

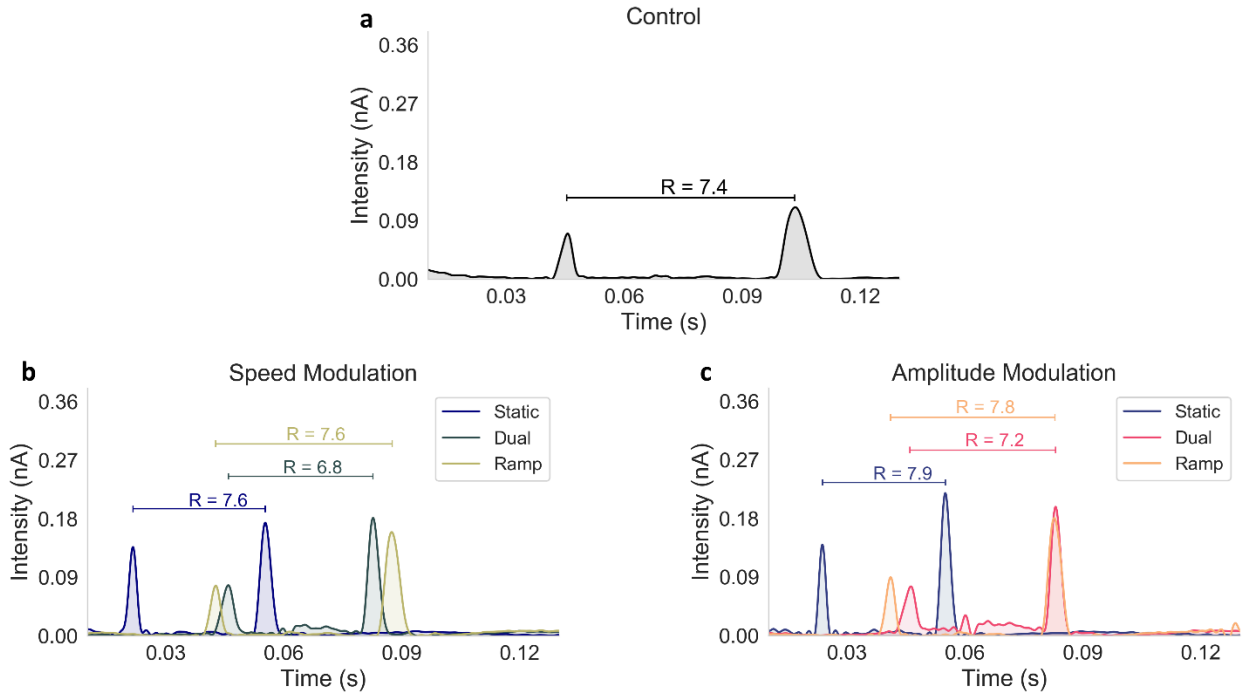

Figure 4.4. Baseline corrected ATD of bradykinin^{2+} (first peak) and T8 (second peak) under control conditions (a) and conditions in which TW speed (b) and amplitude (c) were modulated. The TW speed was modulated to 110 m/s for all ATD shown in (b). The TW amplitude was modulated to 31 $V_{p\text{-}p}$ for all ATD shown in (c).

In the context of method development, the data presented in Figures 4.3 and 4.5 illustrate the tradeoffs when choosing different TW profiles. Beginning with a simple comparison between the modulation of TW speed and amplitude, the presented data suggest that modulating TW amplitude has a greater impact on resolution. It is important to note that the full range of TW amplitudes evaluated represented a 35% deviation from the control value (Control: 23 $V_{p\text{-}p}$, highest amplitude evaluated: 31 $V_{p\text{-}p}$) compared to a 40% deviation for the TW speed experiments (Control: 183 m/s, lowest speed evaluated: 110 m/s), which further emphasizes the impact that TW amplitude has on resolution relative to TW speed. Regarding the three waveform profiles, should a

user opt to modulate TW amplitude, the static elution method provides the greatest gains in resolution, though it is worth noting that no significant (>10%) differences were observed between the static and ramp waveforms. Lastly, the dual waveform expectedly performed the worst as the arrival time of bradykinin^{2+} remains stagnant, while that of T8 decreases as a function of TW speed and amplitude.

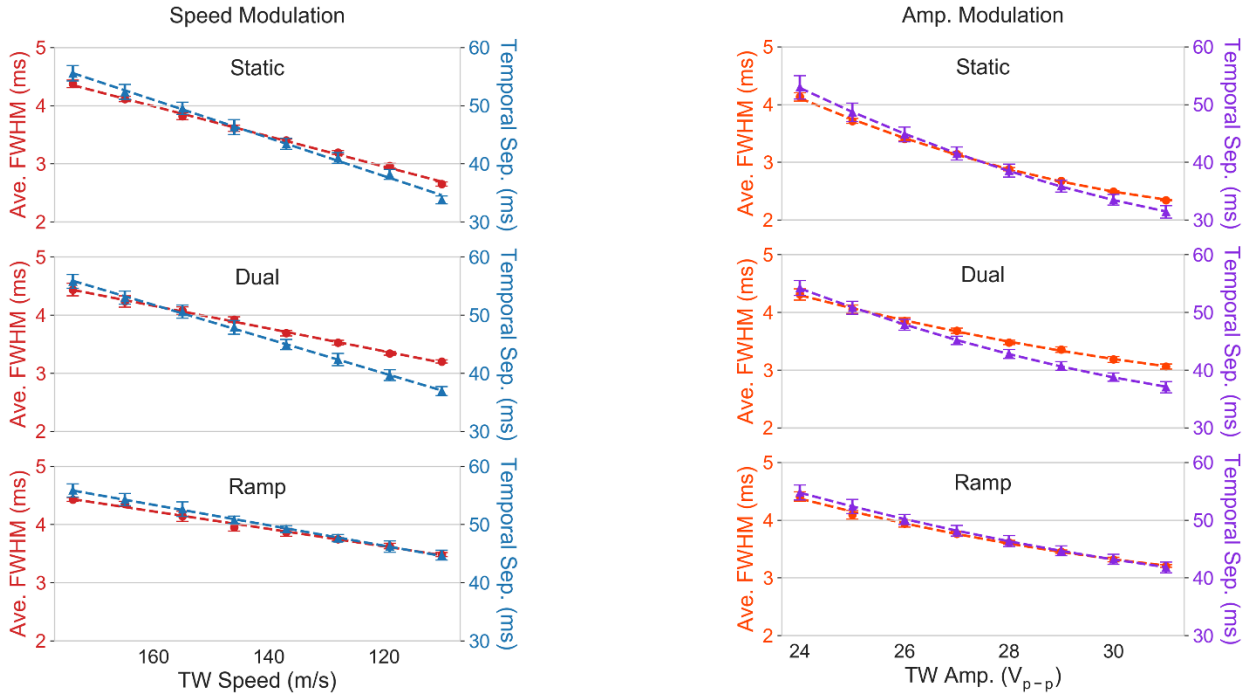

Figure 4.5. The average FWHM of bradykinin^{2+} and T8 and temporal separation between the two species as a function of TW speed (left) and amplitude (right). Values on the x-axis represent conditions that followed the control period of the static and dual waveforms, and the value that was ramped to in the ramp waveform.

While the information provided in Figure 4.5 enhances our understanding of how each waveform impacts separation, further investigation into how these waveforms impact sensitivity is required to fully understand their analytical impact. A key distinction

between the ATD presented in Figures 4.4b and 4.4c are apparent variations in peak height. While a quantitative overview of peak height variation is provided in the supplementary material (Figure 4.S2), this discussion will instead focus on SNR, which, while related to peak height, is more relevant to matters of sensitivity. Fluctuations in SNR as a function of TW speed and amplitude are presented in Figure 4.6. Unsurprisingly, the SNR of bradyikinin^{2+} does not vary significantly (>10%) for any conditions in which either the dual or ramp waveforms were used. While the cause of this minimal variation is straightforward for the dual waveform (conditions are only varied after bradykinin^{2+} exits the TW-SLIM), it is important to recognize that the ramped approach does not affect all species equally, instead having a more profound impact on later arriving species. We attribute this greater impact in part to the disparity in conditions during which ions reach the detector, leading to some degree of temporal compression as ions exit the TW-SLIM faster as the ramp progresses. To be clear, unlike the gains in peak intensity and SNR observed by Williamson and Nagy,[93] contributions from temporal compression may contribute to, but do not fully explain, the observed behavior which is also impacted by variations in c throughout the separation process.

Unlike the ramp and dual waveforms, the static approach has a greater impact on the SNR of bradykinin^{2+}, particularly when modulating TW amplitude. Interestingly, the rate at which the SNR of bradykinin^{2+} increases is similar to that of T8 when modulating TW amplitude, but shows a far greater disparity when modulating TW speed. The drastic deviations associated with the SNR of bradykinin^{2+} when modulating

to 110 and 119 m/s are attributed to bradykinin^{3+}. Bradykinin^{3+} increases the noise preceding bradykinin^{2+} for the 119 m/s data (lower SNR) and increases the signal attributed to bradykinin^{2+} as the two species reach the detector simultaneously (greater SNR) at 110 m/s.

In contrast to bradykinin^{2+}, the behavior displayed by T8 in Figure 4.6 shows less disparity between the performance of the three waveform profiles, though variations in trends between the TW speed and amplitude experiments persist. Regarding TW speed modulation, the ramp waveform consistently outperforms the other two, particularly at lower speeds, with the highest disparity observed at 174 m/s between the static (1.0 ± 0.1 relative SNR) and ramp (1.2 ± 0.1 relative SNR) waveforms. In contrast, when modulating TW amplitude, the ramp waveform outperforms the other two at lower amplitudes (<27 V_{p-p}) before being overtaken by the static waveform as TW amplitude is increased. It is also worth noting that the amplitude experiments produced the least variance between waveforms, with the greatest disparity observed at 25 V_{p-p} between the ramp (1.19 ± 0.09) and dual (1.11 ± 0.09) waveforms.

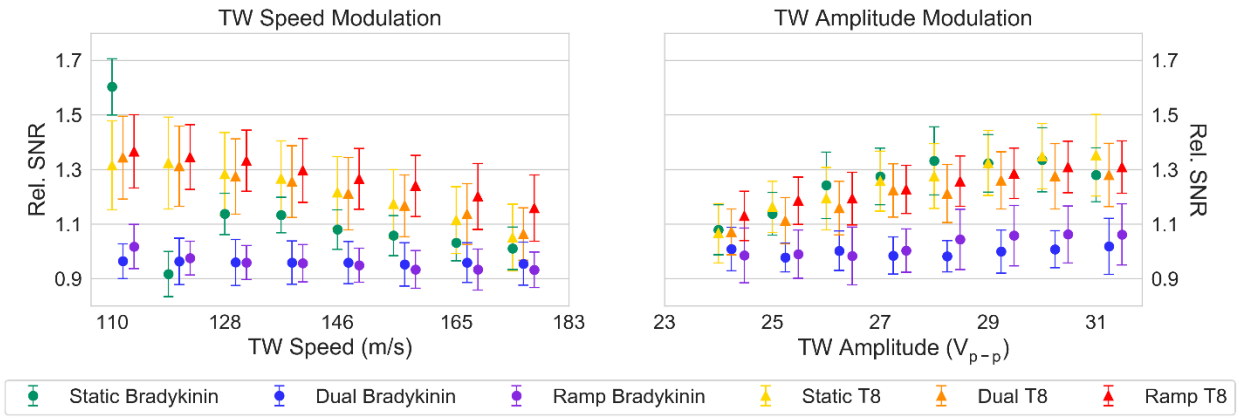

Figure 4.6. SNR of T8 and bradykinin^{2+} relative to control. An offset was added in the x-dimension for visual clarity. To be clear, all data for the static, dual, and ramp waveforms were collected using identical TW speeds and amplitudes. Values on the x-axis represent conditions that followed the control period of the static and dual waveforms and the value that was ramped to in the ramp waveform.

The results presented in Figures 4.6 and 4.S2 provide valuable guidance for those interested in optimizing the sensitivity of their TW-SLIM methods. Recalling the earlier discussion regarding separation, the modulation of TW amplitude and implementation of a static waveform proved the most effective means of increasing resolution. In contrast, when optimizing for SNR, there is no single approach that provides superior gains in SNR for both species. For T8, the ramped TW speed approach provided the greatest gains in SNR over the same range of parameters that saw this method fall short regarding separation. It is important to note however, that the performance of the ramped waveform did not differ significantly from that of the other two. When evaluating the data associated with T8, a simplistic argument could be made that the ramped TW speed approach should be used when gains in sensitivity are required, and the static TW amplitude approach could be implemented when greater

resolution is desired. However, this argument ultimately falls short as it neglects the SNR of bradykinin^{2+}, whose greatest gains did not coincide with those of T8, instead benefiting from the static TW amplitude approach. A more complete interpretation of the data presented thus far suggests that a user must consider whether earlier or later arriving species are in greater need of SNR enhancement and then select a method accordingly while ensuring adequate separation is maintained.

While metrics such as SNR are often at the forefront of discussions pertaining to sensitivity, it is important to note that SNR alone inadequately describes a method's sensitivity.[94] Figure 4.7 presents the ion abundance of both T8 (Figures 4.7 and 4.7b) and bradykinin^{2+} (Figures 4.7c and 4.7d) across various conditions, normalized to those observed under control conditions. Beginning with bradykinin^{2+}, no significant (>10%) variation in ion abundance was observed, with the exception of data associated with static TW speed modulation at 110 m/s and ramped TW amplitude modulation at 27 $V_{p\text{-}p}$. We attribute the spike in ion abundance observed at 110 m/s to the simultaneous arrival of bradykinin^{3+} (see earlier discussion regarding SNR) and the “loss” of ion abundance at 27 $V_{p\text{-}p}$ to issues of peak fitting, which arise from abnormalities in peak shape under those conditions. It is interesting to note that across all conditions, the ramp waveform performed the worst with regard to the ion abundance of bradykinin^{2+}, but provided optimal performance for T8. Aside from the performance of the ramp waveform, differences between the behavior of T8 and bradykinin^{2+} displayed in Figure 4.7 persist for all waveform profiles, as the trends for bradykinin^{2+} are relatively static in comparison to those of T8. While the exact cause of this behavior requires further

investigation, we attribute the observed disparities between T8 and bradykinin^{2+} to the fact that T8 spends a greater amount of time within the TW-SLIM during separation and is thus more sensitive to perturbations to experimental conditions.

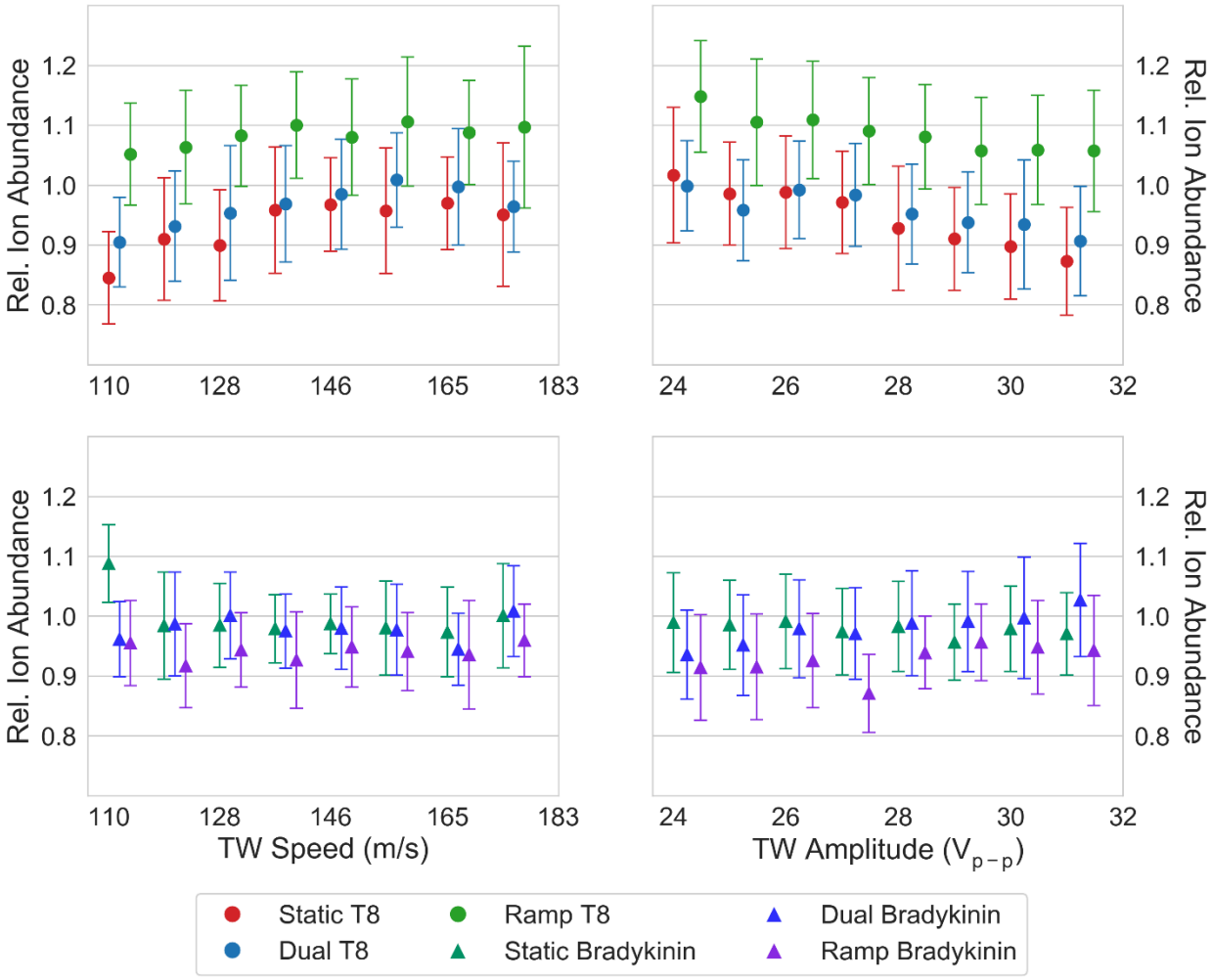

Figure 4.7. Relative (to control) ion abundances of T8 when modulating TW speed (a) and amplitude (b). Relative (to control) ion abundances of bradykinin^{2+} when modulating TW speed (c) and amplitude (d). Values on the x-axis represent conditions that followed the control period of the static and dual waveforms, and the value that was ramped to in the ramp waveform. An offset was added in the x-dimension for visual clarity.

One last point of emphasis for the data presented in Figure 4.7 is the disparate performances of the three waveforms with regard to T8. As mentioned previously, the ramp waveform provided the optimal transmission of T8 ions through the SLIM (i.e., enabled the greatest number of charges to reach the detector). Not only did the ramp outperform both the dual and static waveforms in this regard, but it also increased the observed T8 ion population relative to the control, particularly when implementing more gradual ramps wherein the value being ramped to is closer in value to control conditions. In alignment with results associated with the ramp, the static and dual waveforms provided optimal transmission of T8 ions under conditions that were closer to those of the control (TW speed: 174-146, TW amplitude: 24-27 V_{p-p}) with greater ion losses observed as conditions deviated more profoundly from the control. A possible explanation for the loss of ions when implementing the static and dual waveforms is ion activation and or collisions with SLIM surfaces during the rapid transition from control conditions (Figure 4.2). While these two events cannot be ruled out entirely at this time, the authors would like to suggest that if these events were truly the singular cause of the observed ion loss, the relative T8 ion abundances for the static and dual waveforms would be near indistinguishable across all conditions evaluated. In actuality, barring the modulation of TW amplitude at 24 and 25 V_{p-p}, the observed ion abundance of T8 is consistently less when operating with the static waveform as opposed to the dual waveform. An alternative explanation for the behavior of T8 in Figure 4.7 is that higher speed/lower amplitude conditions simply provide more optimal transmission of T8 ions based on their motion relative to the passing waves. While ion activation is not

considered a significant factor in the presented work, future investigations utilizing more labile analytes should be completed prior to expanding the presented methods to a wider range of analytes.

Aside from an enhanced perspective on the three waveforms presented, the results shown in Figure 4.7 give rise to a greater discussion of how best to simultaneously transmit ions of disparate size within TW-SLIM. Given that “ideal” confinement (namely radial confinement via RF)[32,66] and ion motion with regards to separation (eq. 4.1) are dependent upon mobility, it is unsurprising that a singular set of experimental parameters utilized throughout the presented work was unable to provide optimum analytical performance across all metrics and analytes. Though an absolute solution to optimizing separation and sensitivity for all ions present in a system is most likely unattainable, the waveform profiles implemented here, namely the dual and ramp waveforms, offer compromises that may mitigate the negative consequences of performance optimization. While not explored in this preliminary work, one could theorize a dual waveform profile which, having determined optimum transmission conditions for each analyte within a mixture, can be used to achieve optimum transmission of one species before transitioning to optimum conditions for another species. While this would inevitably limit the transmission of later arriving species, it would allow a user to enhance the performance of a particular species which may prove difficult to observe. Interestingly, the ramp waveform, which was originally hypothesized to be a middle ground for disparate ion transmission, proved to provide optimal transmission for one species (T8) and relatively poor transmission for another

(bradykinin^{2+}). Future work will evaluate more flexible implementations of the ramp waveform in which both the start of the ramp is varied (e.g., after the arrival of higher mobility species) as well as the steepness of the ramp. Additionally, the simultaneous ramping of TW speed and amplitude will be evaluated as well.

Conclusion

The presented analysis of three distinct TW waveform profiles provides insight regarding approaches to TW-SLIM method development which may be tailored to enhance select analytical metrics concerning matters of separation (resolution) and sensitivity (SNR and ion abundance). Concerning separation, the static waveform demonstrated the greatest impact on peak width and temporal separation and ultimately provided the greatest gains in resolution across all conditions analyzed when modulating TW amplitude. It is worth noting that while static TW amplitude modulation provided the greatest increase in resolution, these gains were not significantly (>10%) greater than those provided by the ramp waveform. Analyses of results pertaining to sensitivity were unable to provide a singular “optimal” approach and suggest a more nuanced approach to method development is required to achieve the desired result. Beginning with SNR, TW speed modulation utilizing the ramp waveform provided the greatest gains in SNR for T8 (though the other waveforms did perform comparably), but fell short for bradykinin$^{2+,}$ which benefited most from the static TW amplitude approach. Leveraging the use of a Faraday plate as a detector, measurements of ion abundance were conducted which provided insight into how various conditions impacted ion

transmission through the TW-SLIM. Similar to observations made concerning SNR, no singular set of parameters provided optimal ion transmission for both T8 and bradykinin^{2+}, with the former benefiting most from the ramp waveform and the latter suffering the greatest ion loss when operating with the ramp.

While not explored in this work, it is important to note that dynamic waveform profiles may complicate TW-SLIM experiments which incorporate time-sensitive events such as multi-pass separations or the targeted manipulation of select ion species.[41,51,95] Time-sensitive events are often defined by ion velocities which allow a user to predict the location of ions at a particular moment. The use of dynamic waveform profiles limits this predictive ability as ion velocity is no longer constant throughout a given separation. It's important to note that the use of dynamic waveform profiles may also complicate efforts to determine ion-neutral collisional cross sections (CCS), particularly when ion velocity is used for calibration.[96] Given the nature of TW-SLIM separations, it is unsurprising that a one size fits all approach is unable to provide ideal conditions for separation and ion transmission when analyzing ions of disparate size. That being said, given the unique capabilities of TW-SLIM,[41,70,97] much of the work concerning the technique has thus far focused on hard-to-separate isomers (i.e., ions of similar size). However, as TW-SLIM continues to grow as a technique and becomes more widely available,[34,54] the scope of TW-SLIM analyses will inevitably expand and approaches that address the issue of disparate ion analysis must expand in turn. Arguably, the results associated with our analysis of species with only modest differences in reduced

mobility (i.e., T8 = 0.816 cm^2/Vs vs. bradykinin^{2+} = 1.189 cm^2/Vs)[98,99] suggest that addressing this issue is of more immediate relevance.

With that in mind, the presented waveforms provide alternatives to traditional TW-SLIM methodologies and establish a point of comparison for future TW profiles that adopt a widening degree of profiles (e.g., square vs. sinusoidal vs. sawtooth).[25] Most importantly, these concepts will aid those implementing the technique with added flexibility which will be necessary as the technique adapts to meet an ever-increasing number of analytical demands.

Acknowledgments
Support for this effort was supplied by the NIH (NIGMS R01GM140129). The authors would also like to recognize helpful advice and electronics guidance provided by Gordon A. Anderson.

Supplementary Material

Table 4.S1. Details regarding the ramped waveforms implemented during TW amplitude (a) and speed (b) experiments

a

Amplitude Ramping

Control Value (V_{p-p})	Final Value (V_{p-p})	Ramp Duration (ms)	Ramp rate (V_{p-p}/ms)
23	24	120	0.008
23	25	120	0.017
23	26	120	0.025
23	27	120	0.033
23	28	120	0.042
23	29	120	0.050
23	30	120	0.058
23	31	120	0.067

b

Speed Ramping

Control Value (m/s)	Final Value (m/s)	Ramp Duration (ms)	Ramp rate ((m/s)/ms)
183	174	120	0.076
183	165	120	0.152
183	155	120	0.229
183	146	120	0.305
183	137	120	0.381
183	128	120	0.457
183	119	120	0.533
183	110	120	0.610

Table 4.S2. (a) Slope values associated with the linear regressions fitted to the data presented in Figure 4.5 for the TW speed experiments. (b) Coefficients of the x^2 term associated with the quadratic fits presented in Figure 4.5 for the TW amplitude experiments.

a	FWHM (ms)	Temporal Separation (ms)
Static	0.0259	0.328
Dual	0.0195	0.294
Ramp	0.0150	0.176

b	FWHM (ms)	Temporal Separation (ms)
Static	0.0189	0.181
Dual	0.00844	0.137
Ramp	0.00973	0.0871

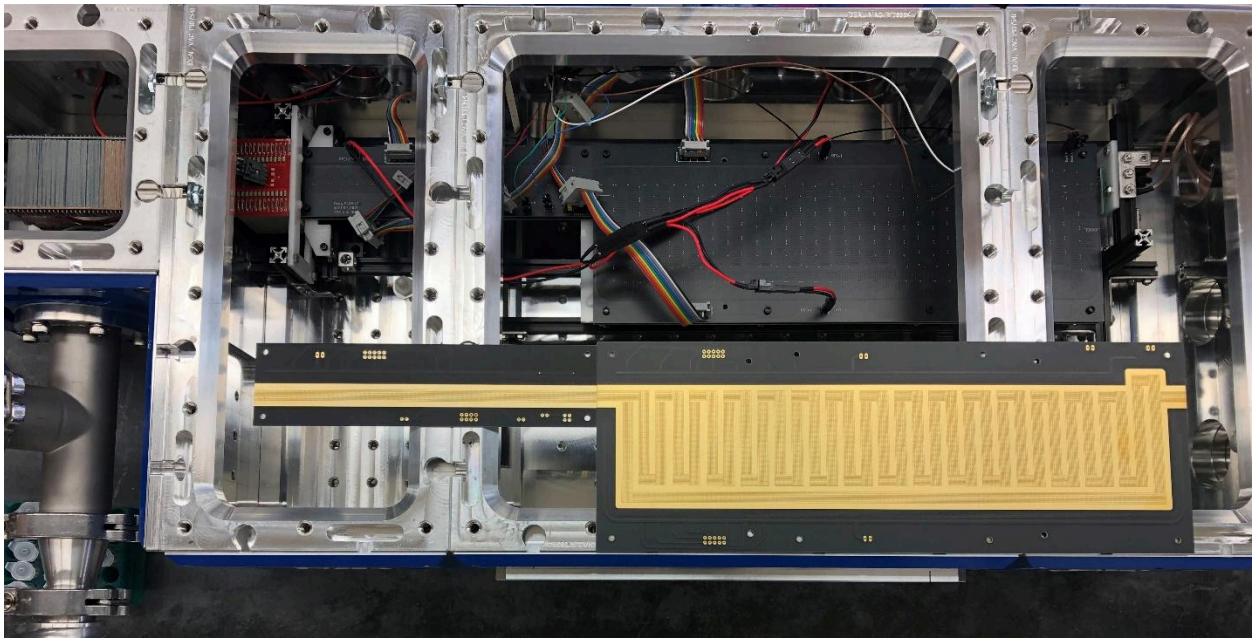

Figure 4.S1. Picture of the instrument used throughout the presented analyses.

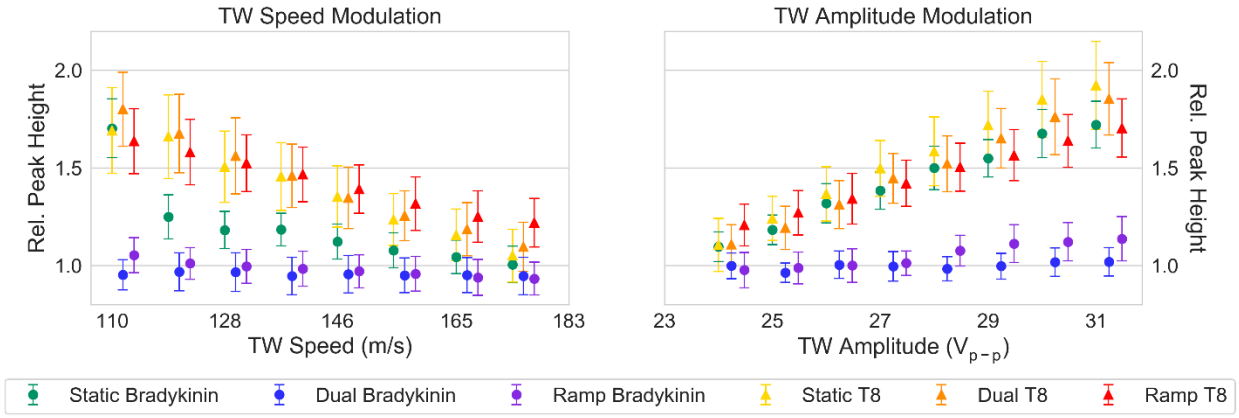

Figure 4.S2. Relative (to control) peak height of T8 and bradykinin2+. An offset was added in the x-dimension for visual clarity.

4.4 Broader Impact

Many chemical applications involve the analysis of complex matrices (e.g., environmental and biological samples) which contain numerous analytes at varying concentrations. Regardless of the technique used, a complete survey (qualitative and quantitative) of such samples will always elude the analyst due to limitations and biases inherent to the technique. In the case of TW-SLIM, the known biases imposed via the use of RF confining fields[32,66] as well as the TW conditions used to separate ions appear to limit the range of mobilities which can be concurrently analyzed. Though the work outlined in this chapter does not offer solutions which eliminate these limitations, it nonetheless informs strategies for those seeking to optimize their analyses to achieve particular analytical goals. In the grand scheme of things, we hope that these strategies may enable those interested in tackling complex samples to consider TW-SLIM as a tool for their analyses, increasing the techniques adaptation and consequently its growth.

CHAPTER FIVE: ALTERING CONFORMATIONAL STATES OF DYNAMIC ION POPULATIONS USING TRAVELING WAVE STRUCTURES FOR LOSSLESS ION MANIPULATIONS

5.1 Attributions

The authors whose work contributed to the following manuscript include Zackary R. Kinlein and Brian H. Clowers. Zackary R. Kinlein is credited with conceptualization, method development, conducting the investigation, and was the primary author of this work. Brian H. Clowers is credited with conceptualization, supervision, method development, funding acquisition, and contributions to writing.

5.2 Preface

The work discussed in the previous chapters outlines much of the foundational TW-SLIM work performed at WSU. While important, the analytical power of the platforms developed during this early period were ultimately lacking in the absence of a mass spectrometer to augment our analyses. In the summer of 2022, we acquired a time-of-flight mass spectrometer (ToF) from Ionicon (Innsbruck, Austria) which was eventually paired with one of our custom TW-SLIM platforms. While much of the work that went into developing our TW-SLIM-ToF platform remains unreported in the

literature, the manuscript from which this chapter is adapted provides insights into some of the key components which enabled us to effectively pair the two systems.

One of the primary benefits of the TW-SLIM-ToF system is the ability to analyze increasingly complex analytes and samples without encountering the ambiguity associated with Faraday plate measurements. Put differently, the ability to assign mass-to-charge (m/z) values to peaks in the mobility domain enables for more complex mobility spectra to be deciphered (i.e., assign identities to peaks) and more information to be gleaned from the analysis. Leveraging our recently developed TW-SLIM-ToF system, we sought to analyze complex biomolecules such as substance P and bradykinin which exhibit numerous charge states and conformers. Upon analyzing data associated with these complex species, it became apparent that numerous phenomena such as interconversion between conformers and charge transfer were occurring throughout TW-SLIM analysis and that further investigation into this matter was warranted.

5.3 Manuscript

Abstract

With its capacity to store and translate ions across considerable distances and times, traveling wave structures for lossless ion manipulations (TW-SLIM) provides the foundation to expand the scope of ion mobility spectrometry (IMS) experiments. While promising, the dynamic electric fields and consequential ion-neutral collisions used to realize extensive degrees of separation have a considerable impact on the empirical result and the fundamental interpretation of observed arrival time distributions. Using a custom-designed set of TW-SLIM boards (~9 meters) coupled with a time-of-flight mass spectrometer (SLIM-ToF), we detail the capacity to systematically alter the gas-phase distribution of select peptide conformers. In addition to discussing the role charge-transfer may play in TW-SLIM experiments that occur at extended time scales, the ability of the SLIM-ToF to perform tandem IMS was leveraged to confirm that both the compact and elongated conformers of bradykinin^{2+} undergo interconversion within the SLIM. Storage experiments in which ions are confined within SLIM using static potential wells suggest that factors aside from TW-induced ion motion contribute to interconversion. Further investigation into this matter suggests that the use of radio frequency (RF) fields to confine ions within SLIM may play a role in ion heating. Aside from interconversion, storage experiments also provide insight into charge transfer behavior over the course of extended periods. The results of the presented experiments suggest that considerations should be taken when analyzing labile species and inform strategies for TW-SLIM design and method development.

Introduction

The drive toward high-resolution, broadband ion mobility (IM) separations is prompted largely by the recognition that there are a host of critical molecular descriptors that transcend *m/z* measurements. Though exceptional levels of separating power have been realized for select drift cell systems,[100,101] the practical limits imposed by high-voltage power supplies when scaling drift cell systems is a considerable hindrance toward their continued expansion. More recently, the capacity to separate gas-phase ions with a high degree of resolution is enabled by the use of systems that employ time-varying electric fields for ion confinement, such as trapped ion mobility spectrometry (TIMS)[20] and traveling wave ion mobility spectrometry (TWIMS).[23] Unsurprisingly, these non-linear electric fields establish conditions where external calibration of the apparatus is required to approximate the coefficient of gas-phase ion mobility (i.e., K) for a given ion population. To further complicate the interpretation of the experimental features attributed to a suite of ion populations, the use of dynamic fields in moderate-pressure environments (e.g., 1-10 Torr) is known to alter gas-phase conformations for select species. For experiments that rely upon variations in relative conformer abundances to infer chemical or molecular properties, an understanding of the experimental factors that may alter gas-phase structures is essential.

Precisely because IM provides information that complements *m/z* measurements, the opportunity exists to capture subtle differences in ion conformation that transcend mass measurements. However, because IM approaches exploit the orientationally averaged momentum-transfer cross section for separation, only

conformations with lifetimes that approach the timescale of the experimental are captured as distinct arrival time distributions (ATDs).[102] Conversely, for ion populations where where the interconversion between conformational states is rapid, time-dispersive IM techniques will yield an ATD with a singular distribution that represents average between the states.[103] In the case of drift cell IM systems where internal ion energy may be manipulated or controlled (e.g., variable temperature systems), the ability to record the interconversion between states provides an opportunity to derive fundamental thermodynamic parameters.[102,104,105] Using these historical approaches as inspiration, similar considerations for the growing class of IM separation techniques that exploit time-varying electric fields are necessary.

Amongst the suite of ion mobility techniques that utilize dynamic fields, traveling wave structures for lossless ion manipulations (TW-SLIM) has proven an effective tool for tackling challenging chemical analyses.[42,68,97] Owing to its unique geometry and assembly, TW-SLIM possesses a degree of flexibility that has enabled the technique to not only push the limits of IMS resolving power[76,106] but also perform unique experiments[70,81,95] that deviate from traditional separations. Though broad access to the technique remains comparatively limited,[28,43,51,54] the extended pathlengths, low-voltage requirements, and capacity to sustain ion populations at appreciable pressures (i.e., 2-4 Torr) present new opportunities for gas-phase ion chemistry experiments in addition to separations.

While the potential for ion heating, which relates to the aforementioned altering of gas-phase conformations, has been explored for traditional TWIMS systems[24,107,108],

similar efforts with regard to TW-SLIM have been limited.[25,109] Arguably, the treatment of ion motion in these prior efforts is an extremely rough approximation as the velocity vector used for interpretation ignores the complex motion induced by the traveling wave and the considerable degree of ion micromotion induced by the confining radiofrequency fields. More specifically, separate works by Allen and Bush[110] and Allen et al.[111] illustrate a strategy to estimate effective temperatures using RF-confining drift cells and electrostatic SLIM configurations. However, these works do not account for the substantially differing electrode configurations present in TW-SLIM electrode design, though it should be noted that the underlying approach could be extended to account for more complex electrodes and dynamic electric fields. Continued, cross-validated efforts to evaluate the complex ion motion in TW-SLIM platforms are needed to advance the collective understanding of these experimental variables on arrival time distributions. While some of the broader conclusions regarding the relationship between TW conditions and ion heating in traditional TWIMS systems may translate to planar TW-SLIM, such as the significance of “gentle” conditions that dampen ion velocities, direct comparisons between the two should be avoided due to the vastly different electrode geometries. Nevertheless, concerns related to ion energy deposition are of primary concern as such variables can influence gas-phase conformer identities.

Recent works by Zercher et al.[112] using a SLIM system with electrostatic fields as opposed to traveling waves demonstrated the capacity to monitor the dynamics of different protein charge states in the gas phase. This effort builds upon prior work by Allen et al.,[111] who first explored structural dynamics in electrostatic SLIM systems

through both time- and energy-dependent experiments. Similarly, recent efforts by Eldrid et al.[113] using the cyclic-TW system developed by Waters (Milford, MA) evaluated the structural dynamics of protein ions. These efforts remain notable and relevant, however, these endeavors focused almost exclusively on protein charge states. While similarities exist between electrostatic SLIM, cyclic-TW systems, and TW-SLIM, direct comparisons between those techniques must be tempered due to either differing electric field profiles or geometries.

Recognizing the need to explore the impact that TW-SLIM analysis may have on labile species further, the work outlined in this manuscript utilizes an independently developed TW-SLIM platform coupled with a time-of-flight mass spectrometer. Notable observations presented in this report include the observation of bradykinin^{2+} interconversion and the subtle but differential behavior of sodiated vs. protonated species. Interestingly, the use of on-board storage revealed that interconversion occurs even when ions are not moving in response to the TW. While further investigations regarding the precise origin(s) of interconversion are required, preliminary data suggests that the RF fields in SLIM may play a role in the observed phenomena. Though it was not determined which species was/were responsible for inducing charge transfer with substance P, data regarding how charge transfer may impact species within SLIM over time was collected and may inform strategies to attenuate this behavior through altering experimental methodologies. Most importantly, however, this report highlights key experimental factors that may impact the observed distribution of conformationally flexible gas-phase ions using TW-SLIM.

Experimental

Tetrabutyl- (T4), tetrapentyl- (T5), and tetraheptylammonium bromide (T7) were purchased from Sigma-Aldrich (St. Louis, MO). Bradykinin acetate salt and substance P acetate salt hydrate were also purchased from Sigma-Aldrich. The sample used throughout the presented analyses consisted of 200 nM each T4, T5, and T7 as well as 500 nM each bradykinin and substance P in 80:20 methanol:water (HPLC grade, Fisher Chemical, Fair Lawn, NJ) with 0.1% formic acid (Honeywell-Fluka, Muskegon, MI).

Using the strategies outlined by Greer et al.[79], a multi-board SLIM system was interfaced to a compact time-of-flight (ToF) mass spectrometer (ioniToF 4000, Ionicon Analytik, Innsbruck, Austria) equipped with an analog-to-digital converter from Teledyne (Thousand Oaks, CA). A schematic of the instrument used throughout the presented work is shown in Figure 5.1. Though not shown in Figure 5.1, the vacuum chamber and mechanical construction are based upon the standard and customized versions of a modular vacuum cube chamber system (Ideal Vacuum Products, LLC, Albuquerque, New Mexico). Ions were generated via electrospray ionization (ESI) and were transmitted into the instrument via a stainless-steel inlet capillary (560 μm i.d., 1600 μm o.d.) purchased from McMaster-Carr (Elmhurst, IL). Further details regarding this process are reported elsewhere.[52,54] After traversing the inlet, ions were focused by an ion funnel (0.9 MHz, 100 $V_{p\text{-}p}$) housed in a chamber at 2.45 Torr before being transmitted to a second ion funnel (1.1 MHz, 75 $V_{p\text{-}p}$) in an adjacent chamber (2.50 Torr). The second ion funnel was responsible for transmitting ions into the SLIM, which was held in the same chamber. The SLIM chamber was filled with high-purity N_2 supplied at

a flow rate of 110 mL/min using a mass flow controller from Alicat Scientific (Tucson, AZ). The pressure in each of the two chambers was monitored using Setra Model 730 capacitance manometers (Boxborough, MA).

The SLIM consists of 3 distinct board sets, which are joined and aligned mechanically.[79] The spacing between the two planar board surfaces was 2.75 mm. The first board, dubbed the “loader” board, provides approximately 1 m of SLIM track, which, in the context of the presented work, was utilized for ion accumulation prior to injection. Injection was performed by switching a series of electrodes between a static DC potential, which blocks ion progression, and a TW, which enables ion transmission (i.e., injection). The injection width used throughout the presented work was 1 ms. The second board contains approximately 8 m of SLIM track along with the ability to cycle ions and is referred to as the “separation” board. The utilization and extent of the cycling is controlled via switching electrodes located near the exit of the board, which behave similarly to those used for ion injection. In the context of the presented work, this cycling mechanism was used to perform tandem IMS experiments in which portions of separated ion populations were selected for an additional cycle through the separation board. The third and final board, known as the “stager” board, was designed to enable the SLIM to maneuver through the vacuum chamber and accommodate a Faraday plate detector for troubleshooting purposes. Though not utilized in this work, this SLIM system is capable of operating in “bypass” mode in which ions avoid the serpentine regions of the board and are quickly transmitted through the system. The housing for all components discussed thus far was constructed using modular vacuum chambers from

Ideal Vacuum Products LLC (Albuquerque, New Mexico). Conditions within the SLIM were controlled using a modular intelligent power source (MIPS) and RFgenerator from GAA Custom Electronics (Kennewick, WA). Unless otherwise stated, the following conditions were implemented throughout all SLIM analyses. Lateral confinement of ions was achieved by biasing guard electrodes 12 V relative to the center of the TW. Confinement orthogonal to the board surfaces was maintained via RF electrodes operating at 0.97 MHz, 200 V_{p-p}. The TW was generated as a square wave using a 4 high, 4 low configuration.[28] The TW was operated at 142 m/s, 18 V_{p-p}. Further details regarding the configuration of the SLIM boards are reported elsewhere.[54] While not the focus of this work, we acknowledge that the conditions utilized throughout this work proved capable of yielding CCS values, which are in agreement with those found in the literature within 2%.[61,98]

Upon exiting the SLIM, ions traverse a custom gate-valve inspired by Esser et al.[114] which enables the SLIM to be vented while maintaining the rest of the instrument, namely the mass spectrometer (MS), at vacuum. Directly adjacent to the gate valve is a third ion funnel (0.94 MHz, 110 V_{p-p}), which transmits ions out of the SLIM chamber and into a custom stacked ring ion guide (SRIG) constructed from printed circuit boards (PCB) The RF applied to the SRIG was coupled with that of the third funnel (0.94 MHz, 110 V_{p-p}). The SRIG chamber was maintained at 0.36 Torr and acted as a buffer between the higher-pressure SLIM chamber and the MS. After traversing the SRIG, ions entered yet another chamber housing a custom PCB hexapole (1.1 MHz, 230 V_{p-p}), and subsequently entered the lens system of the MS. A more in-depth discussion and

photos detailing the components of the instrument can be found in the supporting information. Arrival time distributions (ATD) were averaged 200 times, and the resulting HDF5 file was processed using python notebooks developed in-house. The ATD displayed herein were smoothed using a Savitzky-Golay smoothing algorithm to attenuate noise stemming from the sampling frequency of the ToF (20 kHz). A comparison of smoothed and unsmoothed ATD can be found in the supporting information (Figure 5.S5). Data shown throughout this work represent the average of five replicates, the standard deviation of which is reflective of the measurement uncertainty. The term “peak area” used throughout to quantify ion abundance was calculated via the integration of ATD windows which correspond to select species.

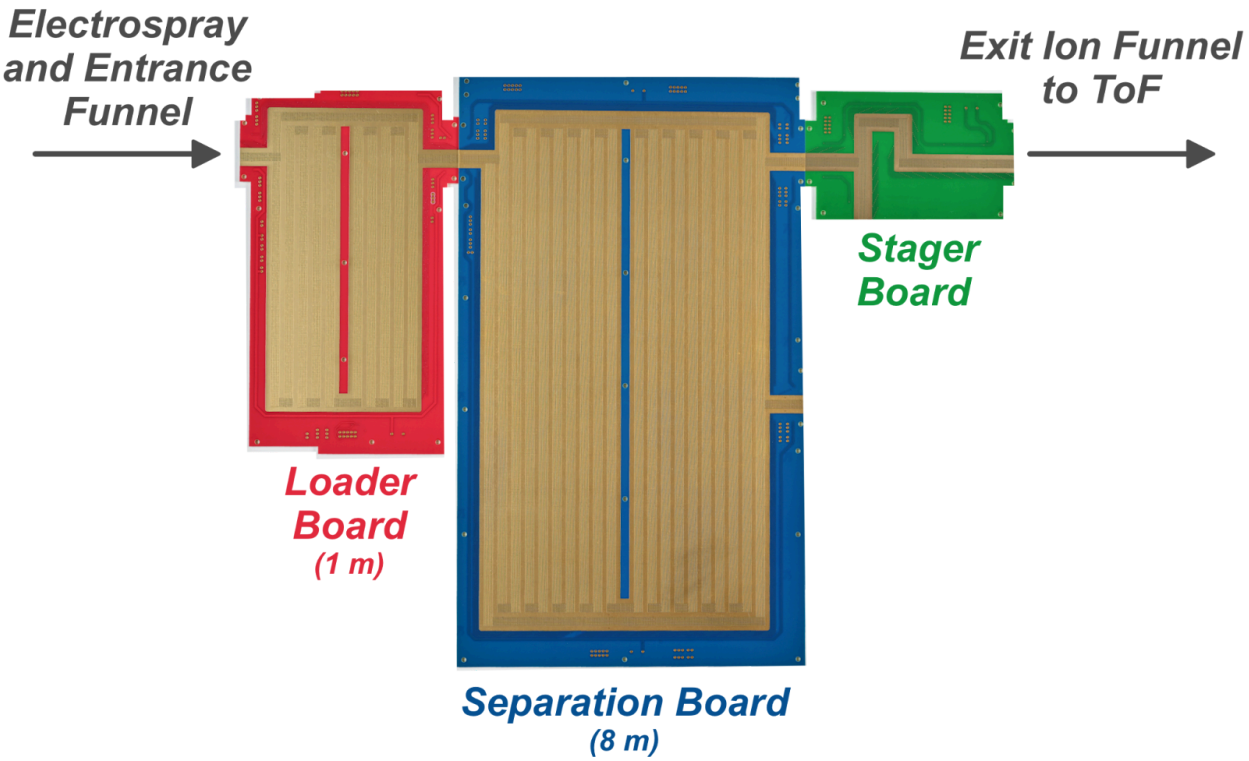

Figure 5.1. Photograph of the SLIM boards used throughout the presented work. A schematic of the system and its components can be found in the Supporting information.

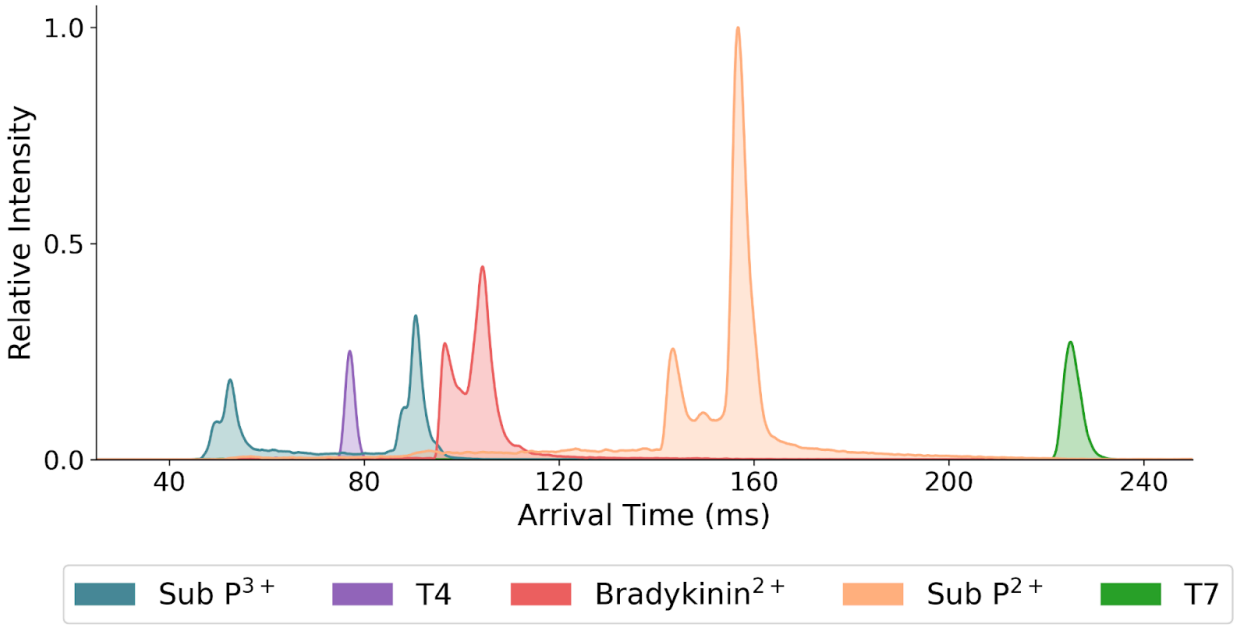

Figure 5.2. m/z-specific ATDs associated with substance P^{2+} (Sub P^{2+}), substance P^{3+} (Sub P^{3+}), bradykinin^{2+}, T4, and T7. The subtle but small increase ion +2 ion current of Sub P coincides with the +3 arrival times. These observations suggest the potential for charge reduction that occurs between the +3 and +2 charge states of substance P. A zoomed view of these data is provided in the supporting information (Figure 5.S6).

Results and Discussion

The ATD of substance P^{2+}, substance P^{3+}, and bradykinin^{2+} shown in Figure 5.2 reveal that each species exists in multiple conformers within the gas-phase. While the existence of these conformers is well documented,[15,115,116] the presence of the apparent "bridging" between conformers is interesting as it suggests that interconversion occurs

continuously throughout the separation. Using a combination of tandem ion mobility and mass spectrometry efforts, it is well-established that select ion populations can interconvert between states.[102,105,117,118] In the context of Figure 5.2, ions having spent some time in different conformational states will have arrival times that fall between the two peak maxima, which is then observed as bridging. It is important to recognize that if the bridging were the result of gate leakage, a raised baseline would be present throughout the entire ATD, as opposed to select time windows. In order to determine whether or not the observed bridging is due to the interconversion of conformers or simply poor resolving power, the ability of the presented SLIM platform to perform tandem IMS experiments was leveraged to further investigate the conformers of bradykinin^{2+}.

Figure 5.3 showcases ATD in which portions of the compact and elongated conformers of bradykinin^{2+} were sliced (i.e., selected for an additional lap in the SLIM) to further investigate their potential for interconversion. In the case of the compact conformer, the sliced bradykinin^{2+} population broadens asymmetrically, extending disproportionately to the right (Figure 5.3a). Similarly, the sliced portion of the elongated species also broadens asymmetrically but in the opposite direction (Figure 5.3b). To be clear, the “sliced” ions are rerouted for an additional dimension of IMS and arrive later than the parent population from which they originated. The ATD shown in Figure 5.3 strongly suggests that a significant degree of interconversion between the two primary conformers of bradykinin^{2+} is occurring as the species navigate the SLIM. While further investigation would be required to quantify the rates and magnitude of interconversion,

the data presented in Figure 5.3 suggest that the conversion of the elongated species to that of its compact counterpart occurs more rapidly than its inverse. Further discussions on this matter will be presented in subsequent sections of the manuscript.

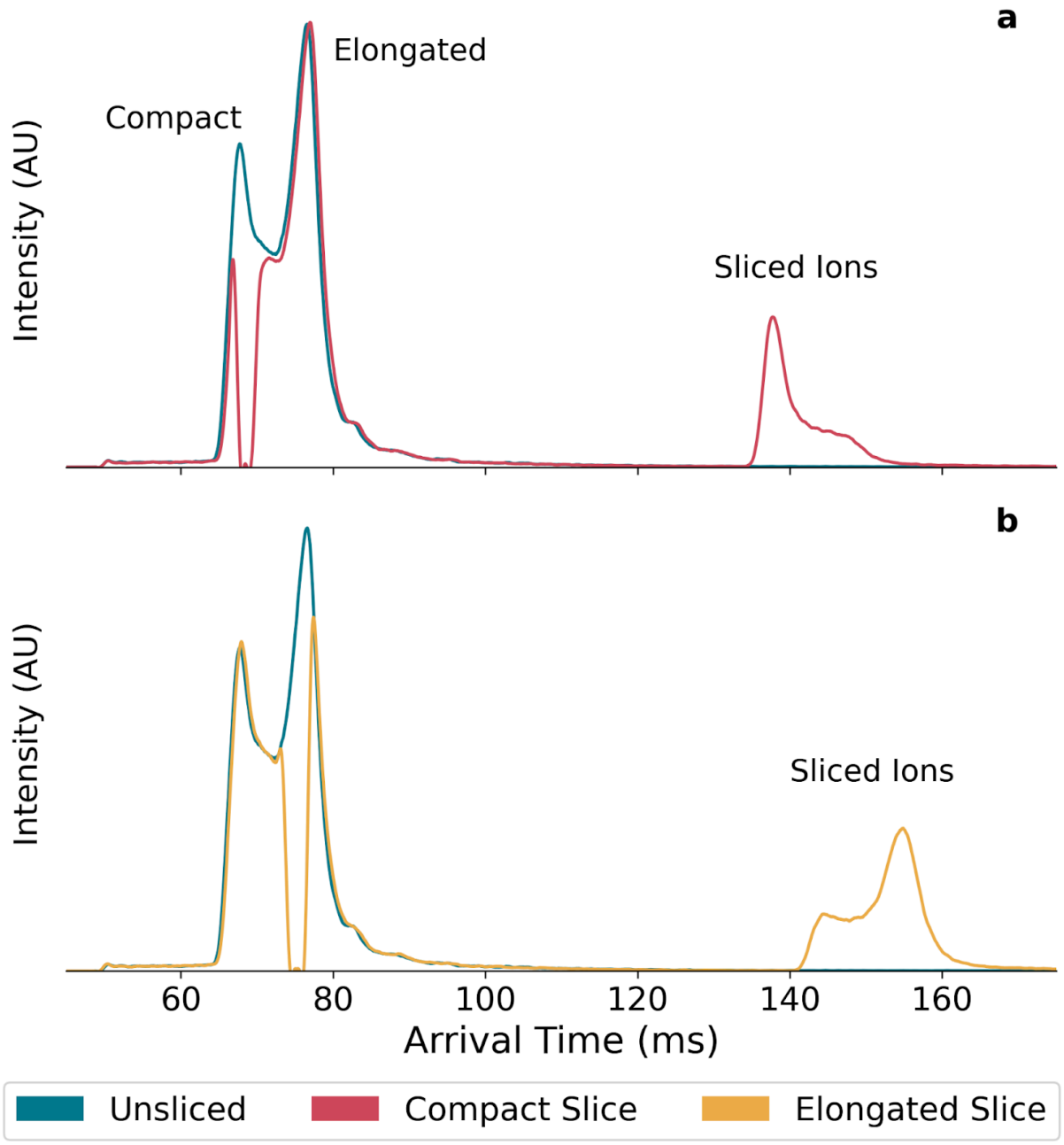

Figure 5.3. ATD of tandem IMS experiments performed on (a) the compact and (b) elongated conformers of bradykinin^{2+}. The ions which were chosen for an additional dimension of IMS analysis (i.e., an additional cycle through the SLIM) are referred to as "Sliced Ions" and arrive later due their extended separation period. Unlike experiments shown elsewhere, the following conditions were implemented during the collection of the presented data: TW speed 128 m/s, guard bias 15 V, ToF sampling frequency 25 kHz, number of averages 250. Additional data are presented in the supporting information.

Given that Figure 5.3 strongly suggests that interconversion is occurring within the SLIM, further investigation into the cause of the interconversion is warranted. One possible explanation for the observed interconversion is the heating of ion populations as they traverse the SLIM. Although the complexity of the fields experienced by ions traversing the SLIM cannot be ignored,[25,26] one can certainly theorize specific components that may expose ions to fluctuations in energy: the TW[24,107,108] and the RF fields.[119] In order to determine whether or not ion heating is related to velocity imparted by the TW, experiments were performed in which ions were stored in static potential wells after being injected into the separation region of the SLIM. This "storage" was accomplished by halting the forward advance of the TW. Under these conditions, the voltages applied to the TW electrodes are held static for as long as the storage period was implemented. If variations in interconversion are observed between experiments with and without storage, it would suggest that energy imparted in response to TW motion is not the only factor responsible for the interconversion. It is worth noting that the storage conditions used in this effort were conducted in an attempt to retain the

spatial position of the separated ion populations. Recent works by Huntley et al. demonstrated a considerable capacity to store ion populations with minimal loss.[95] However, the SLIM-based ion traps used in that effort were considerably longer and did not contain a static TW for trapping. While different from the present evaluation, the two works are not necessarily contradictory. Rather, the combined works illustrate that a choice to maximize storage efficiency may require different experimental parameters that may not always be compatible with the retention of the target conformations of flexible species.

Figure 5.4a shows a series of overlaid bradykinin^{2+} ATD collected using various storage times. From these ATD, it can be concluded that interconversion occurs even when the ions are not being exposed to the motion of the TW, as the ratio of the two bradykinin^{2+} conformers shifts as a function of storage time. Interestingly, the data shown in Figures 5.4a and 5.4b suggest that, given sufficient storage time, the compact species will become the more predominant of the two, supporting the aforementioned notion that this bidirectional interconversion seems to favor the compact state. A more expanded view of the data contributing to Figure 5.4 is shown in Figure 5.S9. Included in this latter figure are the results of fitting the data to a simple kinetic model that accounts for the observed ion loss. While the choice of fitting constraints can impact the absolute value of the rates returned by the fitting model (See the SI for details of the model), all of the numerical conditions considered further support the notion that the compact state is favored under the experimental conditions probed, even when accounting for ion loss (Figure 5.4b). It should be recognized that a variety of plausible

explanations exist that account for the observed shifts in conformer ratios, such as ion chemistry[118,120–122] and confinement issues, which can be conformer-specific. While these factors may influence the results shown in Figure 5.4, the drastic shift in conformer ratio observed between storage times of 5 and 100 ms (Figure 5.4b, purple trace) does not coincide with significant ion loss (Figure 5.4b, green trace) which suggests that depletion is not the primary cause of conformer ratio variation.

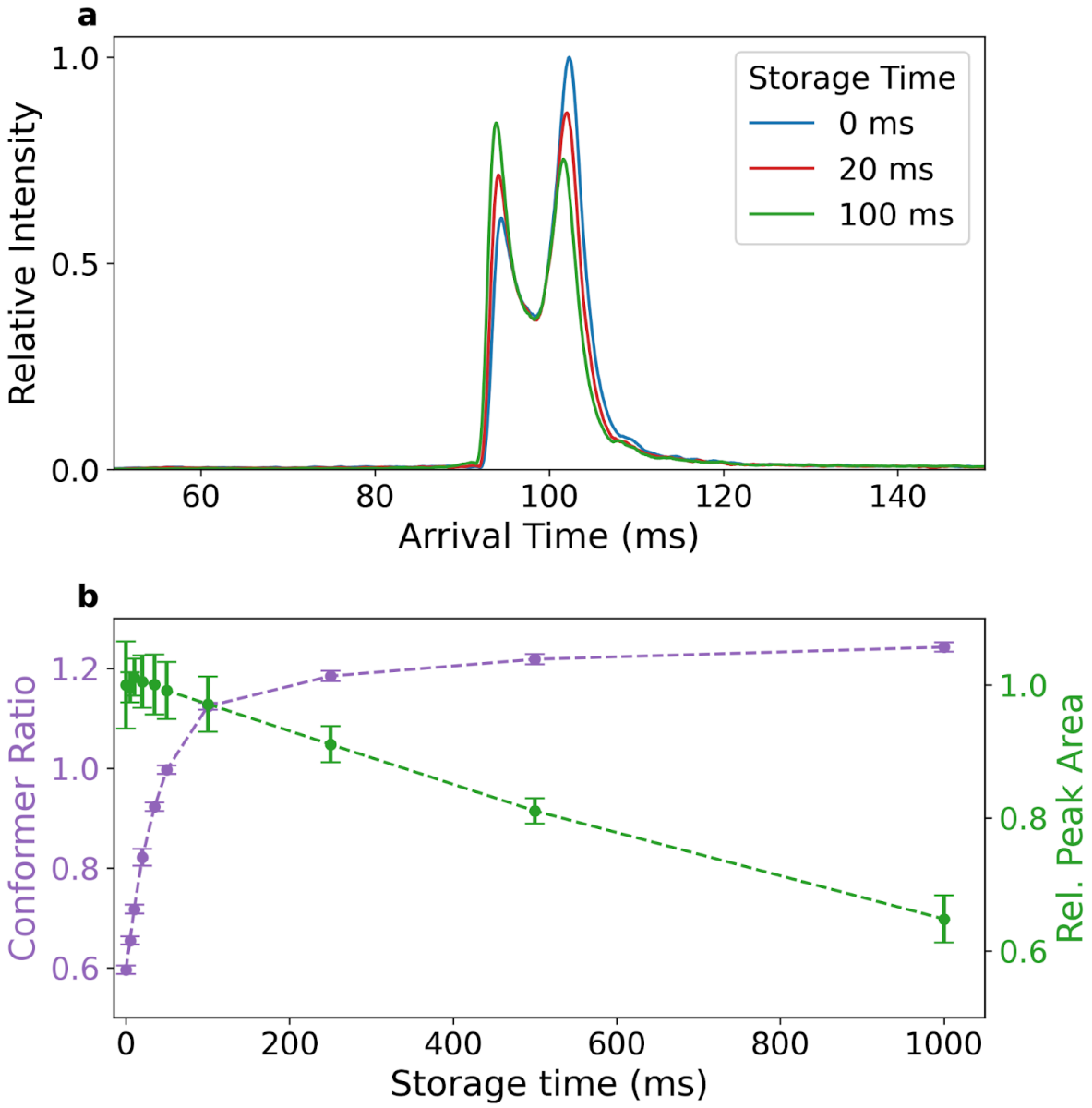

Figure 5.4. (a) Overlaid ATD of bradykinin^{2+} collected with varying storage periods. Arrival times for stored ion populations were adjusted to align spectra. (b) Variations in the ratio between the peak heights (assigned based on arrival time) of the compact and elongated conformers of bradykinin^{2+} as a function of storage time (purple trace). A ratio of >1 would mean that the compact conformer has a greater intensity than the elongated conformer. Additional data regarding the peak heights of the compact and

elongated conformers is shown in Figure 5.S9. The peak area of bradykinin^{2+} as a function of storage time relative to data collected without a storage period (green trace).

The storage data presented in Figure 5.4 suggests that ions are undergoing interconversion while "stationary" within the SLIM. This simultaneously diminishes the role of TW-induced motion as a possible cause of interconversion and points towards factors that impact the ions as they dwell within the SLIM, such as RF. The data contributing to Figure 5.4b are shown in Figure 5.S9 and illustrate that the continued evolution of TW-SLIM experiment may provide insights into the kinetics of these transitions. However, due to the numerous factors that define TW-SLIM analyses (e.g., TW voltage, TW speed, guard voltage, and RF freq and potential), the extension of kinetic measurements from a single set of conditions may be misleading. Ideally, the capacity to change the temperature of the apparatus and associated neutral collision partners would provide a more accurate accounting of the thermodynamics of these transitions.[102]. This subtle but key point aside, Figure 5.5 shows a series of ATD for bradykinin^{2+} collected when operating the SLIM with various RF frequencies and amplitudes. Regardless of RF frequency, the data shown in Figure 5.5 suggests that there exists a clear relationship between RF conditions and the observation of multiple conformers for bradykinin^{2+}. Interestingly, the observance of the compact conformer of bradykinin^{2+} is most pronounced near the middle of the RF V_{pp} explored. Erosion of the compact conformer occurs at the higher and lower ends of the range of RF amplitudes investigated. While comparisons between the data collected at high and low RF amplitudes may prove fruitful, the role of ion loss impacting the observed conformer

ratios cannot be discounted entirely. In many ways, these data illustrate that changing RF parameters can impact the rates of conformer interconversion. Interestingly, recent works by Porter et al.[123] using the CRAFTI[124] technique illustrate that bradykinin^{+2} can adopt a compact conformation following higher energy collisions. While direct mapping between IM techniques and CRAFTI requires great care, the general trends observed using this complementary technique appear to mirror the present observations for bradykinin in the TW-SLIM platform. The data presented in Figures 5.4 and 5.5 suggest that under select circumstances, the kinetics of interconversion from the extended to compact conformer are sufficiently long to be experimentally captured. However, at the extremes of the RF amplitudes, the kinetics and energy landscape between the two conformations prevent facile observation. Ideally, a variable temperature experiment could be deployed toward disentangling the complexities of data interpretation for this system.

Extending these observations to different multiply charged systems, similar trends for substance P^{2+} were also observed (Figure 5.S10), suggesting that the observed interconversion behavior is not solely a result of the chemical and or physical properties of bradykinin^{2+}. Though not thoroughly explored in this work, it is worth noting that similar behaviors can be observed through the modulation of the SLIM guard bias. Such behavior is not entirely surprising, as altering the guard potential changes the physical location of the electric field contours used for ion confinement. In other words, by adjusting the guard bias, it is possible to alter the effective RF and TW voltages experienced by the ion populations. Nonetheless, it is worth considering the relationship

between an ion's position relative to board surfaces and the energies it experiences as it traverses the SLIM. While outside of the scope of this work, these observations raise a number of questions regarding the kinetics at play when transmitting dynamic ion populations throughout SLIM and perhaps suggest that SLIM may serve as a powerful tool for the probing of gas-phase ion kinetics. Additionally, as the applications of SLIM expand, these data suggest that considerations must be made regarding conditions for the analysis of conformationally flexible and labile species.

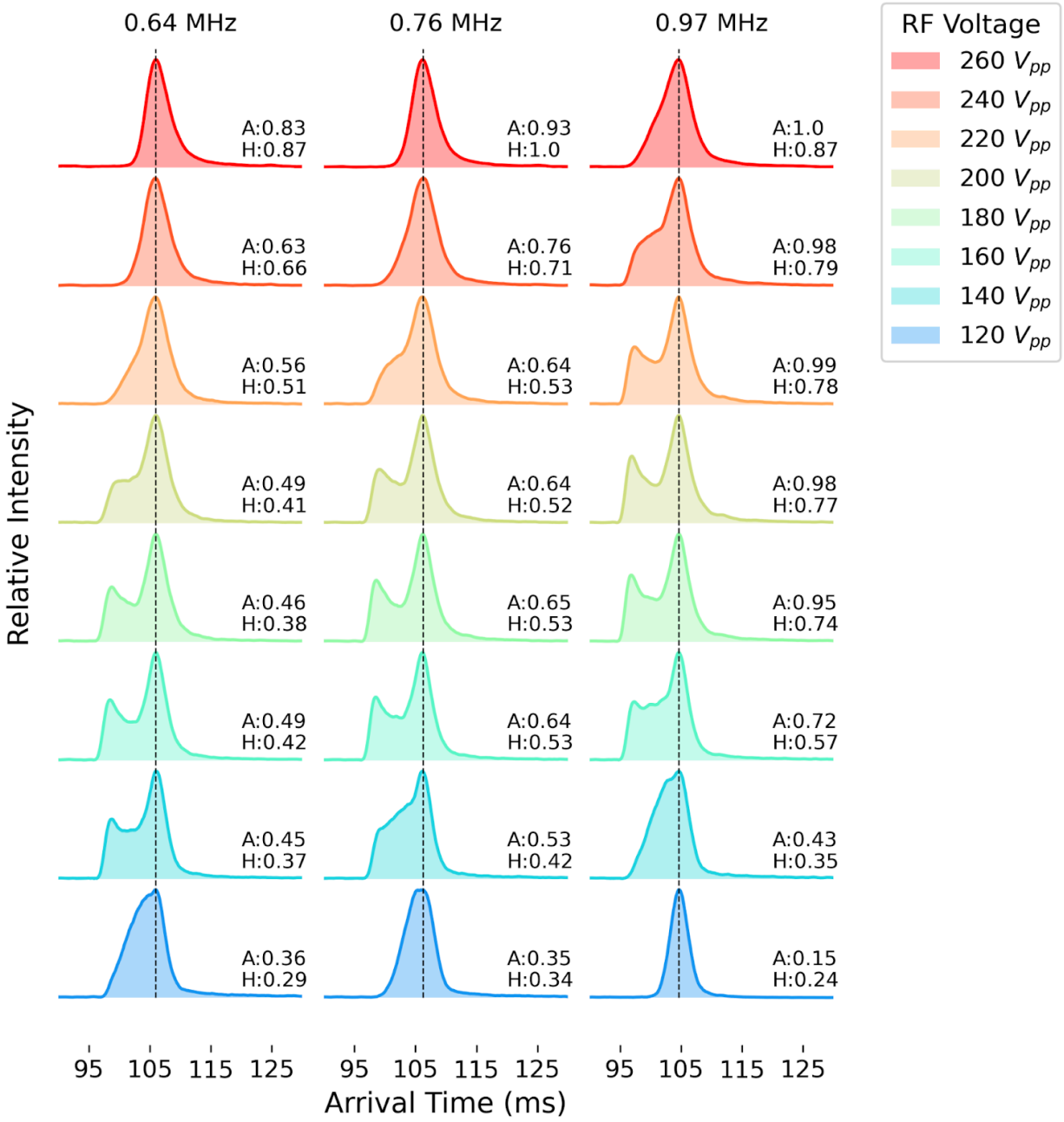

Figure 5.5. ATD of bradykinin2+ collected under various RF conditions. "A" refers to the peak area of the presented spectra relative to the spectra with the greatest area (0.97 MHz, 260 Vp-p). "H" refers to the peak height of the presented spectra relative to the spectra with the greatest height (0.76 MHz, 260 Vp-p).

Matters of interconversion aside, the ATD of substance P in Figure 5.2 also suggests that charge transfer is occurring throughout the presented analyses. The fronting of the substance P^{2+} peak coincides with the arrival of the substance P^{3+} population, which not only suggests that charge transfer is occurring but also that these events happen throughout SLIM analysis. Unlike observations made regarding interconversion, the presence of charge transfer does not seem "tunable" via the modulation of parameters such as RF, suggesting that perhaps it is the result of contaminants within the SLIM chamber. Prior to further discussion, it's important to note that contaminants are not limited to those introduced during the assembly and handling process but include residual solvents from the electrospray process despite a pressure differential and contributions from sources such as outgassing. While precautions may be taken when selecting materials for use in SLIM instrumentation, some degree of outgassing may remain present, especially when utilizing materials that lower the cost of implementation.[125] Furthermore, given that most academic research institutions are not equipped with clean rooms for the assembly of instrumentation, it would benefit those interested in non-commercial SLIM implementation to envision additional stages of differential pumping prior to SLIM separation.

As mentioned previously, the peak shape of substance P^{2+} in Figure 5.2 suggests that charge reduction is occurring continuously throughout the SLIM separation. In order to investigate the relationship between charge reduction and time spent within the SLIM, a series of storage experiments were performed wherein variations in ion population (estimated via the integration of ATD) could be observed as a function of storage time

(Figure 5.6). Although the total time an ion spends within the SLIM system cannot be accurately determined due to uncertainty regarding the time an ion spends on the accumulation board, the use of storage experiments is nonetheless informative in the given context. While used originally as internal calibrants, a closer evaluation of the species in Figure 5.2 illustrates that the substance P^{3+} conformers have ion velocities that are, in some cases, faster than singly charged T4 at *m/z* 242. Using a rough approximation, the ion-neutral collision cross-section of substance P^{3+} is considerably higher than T4 when scaled for charge. However, the magnitude of the force exerted upon these ions is considerably different, and the *efficient* confinement of such ions for extended time periods may require entirely different TW and RF conditions.

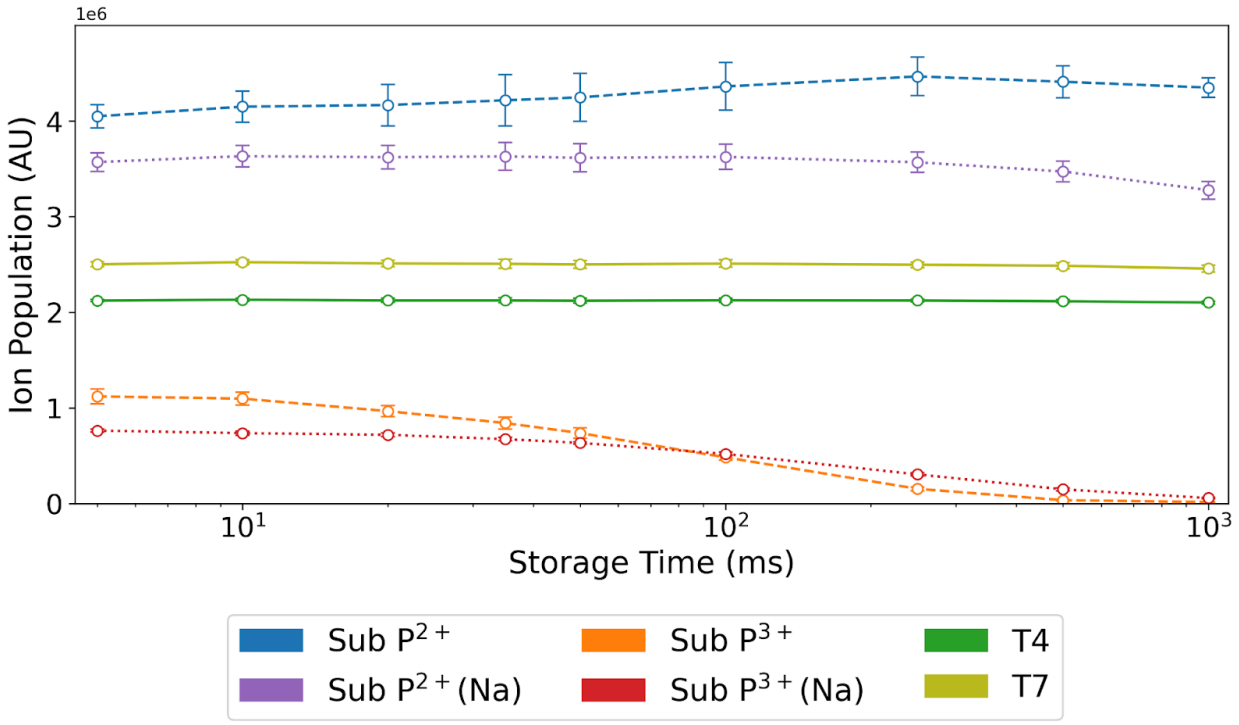

Figure 5.6. Plots of ion population (estimated via the integration of ATD) vs storage time for a number of compounds. The reported ion populations of T4 and T7 were offset by 1.8E6 AU to increase the readability of the figure.

As reported elsewhere,[54] the data shown in Figure 5.6 suggests that in the case of natively charged singly charged species such as tetraalkylammonium ions, SLIM storage across several orders of magnitude does not significantly impact ion populations. However, when storing more dynamic species, clear variations in ion populations can be observed. In the case of substance P, degradation in the substance P^{3+} population coincides with gains in the substance P^{2+} population. While it could be argued that the loss of substance P^{3+} may be related to poor confinement, this alone would not explain the gains in substance P^{2+}, suggesting that charge reduction is, in

fact, occurring as the ATD suggests. Despite being similar to substance P^{2+} and substance P^{3+}, their singly sodiated counterparts behave more statically, perhaps due to the charge-carrying species being less mobile. These observations suggest that experimental conditions that may alter an ion's susceptibility to charge loss[126] may be worth considering for those interested in the analysis of complex species in SLIM. Another influence on the data presented in Figure 5.6 are issues associated with transmitting increasingly disparate species through SLIM. Upon converting from charge states of 3+ to 2+ and 2+ to 1+, an ion's response to the confining RF fields and TW will vary. In the context of the data shown in Figure 5.6, this means that observed losses/gains between species will not necessarily be at a 1:1 ratio as some charge states will not be as effectively confined and or transmitted as others.[52] This is particularly true for the conversion of substance P^{2+} to substance P^{1+}, which was observed, but only to a slight degree (Figure 5.S11).

While previous discussions of charge reduction have focused on its relationship to contamination, it is important to recognize that a second factor, experimental timescale, is also significant. The unique geometry of TW-SLIM has enabled the accumulation of considerably dense ion populations, separation over expansive pathlengths, and the implementation of unique and insightful experiments.[33,41,97] However, it is important to recognize that many of these advancements have coincided with pushing the timescale of SLIM experiments well beyond what is typical for geometries that use stacked-ring ion guides. Stated differently, SLIM experiments occur at pressures (2-4 Torr) and for time periods (hundreds, thousands of ms), which have

yet to be thoroughly explored by the IMS and MS communities. With that in mind, it is unsurprising that charge transfer is being observed and that further investigation into this matter is necessary.

Conclusion

Combined with its capacity for tandem-IM experiments, TW-SLIM offers new and innovative approaches to control ion populations under conditions and timescales previously unrealized. This capability also introduces an entirely new set of technological and chemical challenges. As with many emerging technologies, further implementation of TW-SLIM will inevitably raise important questions as the community deviates further from what defines traditional IMS experiments. In the context of the presented work, a major question that must be answered is how the unique geometry and extended experimental timeframes of TW-SLIM may contribute to behaviors such as interconversion and charge transfer. These latter questions remain imminently important as the TW-SLIM expands to include ion chemistry experiments and as a preparatory tool for spectroscopy.[50] Additionally, given that IMS techniques such as linear-filed SLIM[112,127] and the cyclic system from Waters[45] are exploring similar geometries and timescales, these questions are not limited to those engaging in TW-SLIM research.

With regards to interconversion, the observation that bradykinin^{2+} converts between its compact and elongated states while being stored raises questions and experimental opportunities regarding the energies ions experience within SLIM. Recent work by Kwantwi-Barima et al.[128] has also acknowledged evidence of ion heating in

SLIM, though it should be noted that their investigation focused primarily on ions undergoing accumulation. While further investigation is required to deduce precisely which aspect(s) of the SLIM experiment are responsible for these phenomena, data presented herein suggest that the confining RF fields, and perhaps more broadly the position of the ions with regards to board surfaces, impact the observed interconversion of bradykinin^{2+}. Unlike interconversion, the presence of charge transfer throughout the presented analyses does not appear tunable via parameters such as RF, suggesting that mitigating this behavior may rely on limiting the time spent by an ion within SLIM.

Future efforts that seek to explore the kinetics of interconversion and charge transfer in TW-SLIM will include variable temperature TW-SLIM to disentangle environmental contributions to internal energy from the complex energy deposition mechanism at play using the applied electric fields. Tandem IMS will continue to play prominently in quests to map conformational changes in similar systems, and the broad tunability of the TW-SLIM platform promises to enable an entirely new class of IM and ion chemistry experiments. Furthermore, assuming the implementation of proper experimental controls and the development of a more rigorous theory, the capacity to dynamically alter isomerization rates using TW-SLIM may prove useful in characterizing the behavior of conformationally flexible gas-phase ions.

When considering strategies to limit the time ions spend in SLIM, it's important to recall that ions often spend significant time within SLIM undergoing on-board accumulation as a means of boosting sensitivity. Though the benefits of this approach are well-documented,[33,70,95] those analyzing labile or highly dynamic species may

consider alternative approaches such as the use of ion “dumps”[71] or multiplexing techniques. Approaches that can inject ions via the redirection of a continuous ion beam as opposed to a more traditional gating would not only reduce the time ions spend on the board but would also remove some ambiguity regarding the total time an ion spends within SLIM.[127]

With regards to separation efficiency, optimizing SLIM conditions that enable adequate separation of select compounds of interest while achieving the shortest possible arrival times would alleviate deleterious impacts on ion populations that arise from excessive time within the SLIM. Though counter to much of the development surrounding SLIM, it may also be worth considering limiting the pathlength of a SLIM system to that which provides sufficient separation for particular compounds at the cost of ultra-high resolving powers. Finally, it’s important to recognize that each of the aforementioned strategies sacrifices the flexibility of a SLIM system in exchange for the ability to analyze a select group of analytes more efficiently. Despite these challenges, the exceptional separation power of the TW-SLIM platform offers a new degree of flexibility to simultaneously achieve high-resolution separations and exceptional insights afforded by tandem-IM experiments.

Acknowledgments

This work was supported by the NIH (NIGMS R01GM140129). The authors would like to acknowledge the considerable electronic support provided by GAA Custom

Electronics. Finally, BHC would like to acknowledge Mark Ridgeway for helpful conversations and design inspiration related to the SRIG shown in Figure 5.S3.

Supporting Information

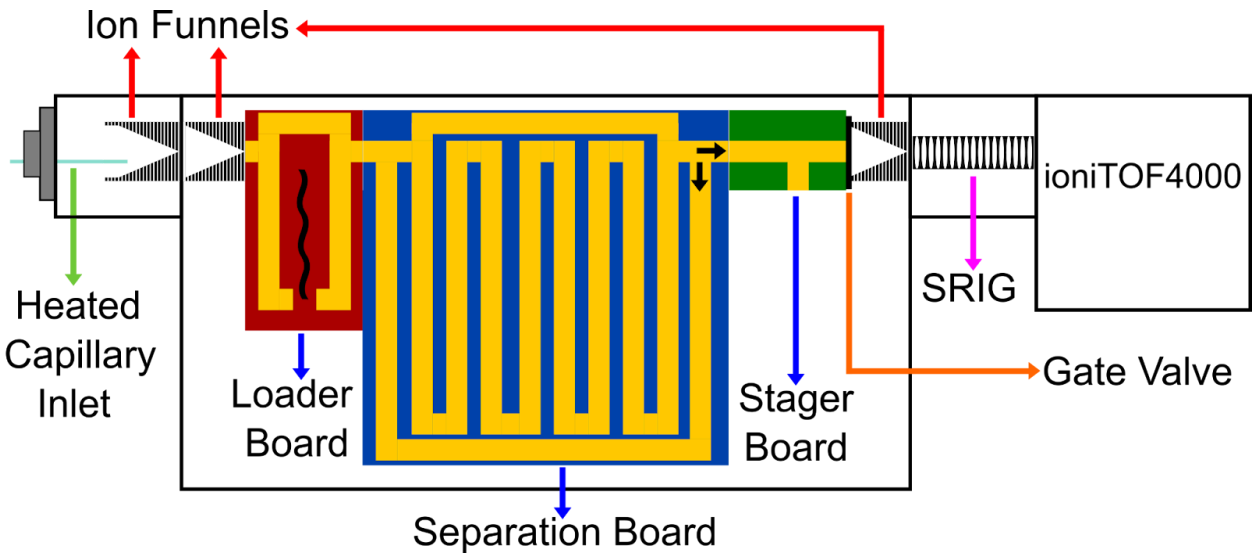

Figure 5.S1. Schematic of the instrument used throughout the presented work. The arrows on the "Separation Board" indicate the possible paths undertaken by ions when they reach this specialized region. Ions exiting the board (path indicated by the horizontal arrow) will travel to the mass spectrometer. Ions that are selected for an additional lap through the board, such as those undergoing tandem-IMS, will follow the path indicated by the vertical arrow.

Overview of Select Instrumental Components

Figure 5.S2 shows photographs of the gate-valve which was implemented to allow for the SLIM chamber to be at atmospheric pressure while the ToF remains at vacuum. The gate-valve allows for rapid SLIM modifications to be made without exposing the ToF to potential contaminants. The design was adapted from work by Tim Esser, PhD.[114]

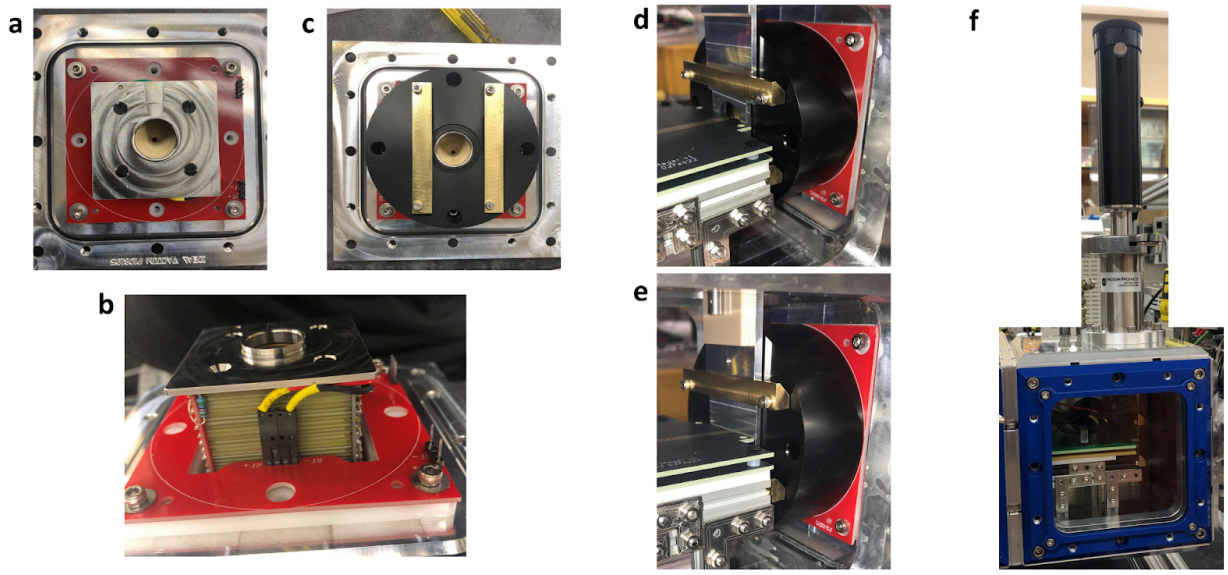

Figure 5.S2. Photographs of the gate-valve and its components. The gate-valve is assembled by first mounting a plate to an ion funnel (a and b) and then encasing the funnel in Delrin housing (c) which is equipped with brass brackets. A blade is then lowered through the brackets and, depending on its position, either allows for ion transmission (d) or creates a seal (e) which allows for the SLIM chamber to be brought up to atmospheric pressure. The position of the blade is controlled using a translator (f) purchased from Ideal Vacuum Products LLC (Albuquerque, New Mexico).

The custom PCB SRIG used to balance the pressure between the SLIM and MS is shown in Figure 5.S3. The DC bias across the SRIG was 10 V (~ 1.3 V/cm). The SRIG is mounted to a PCB flange (Figure 5.S3b) which is pressed between two chambers to create a seal . All electrical connections for the SRIG run through the flange, a portion of which extends beyond the chamber, simplifying the system's electronics.

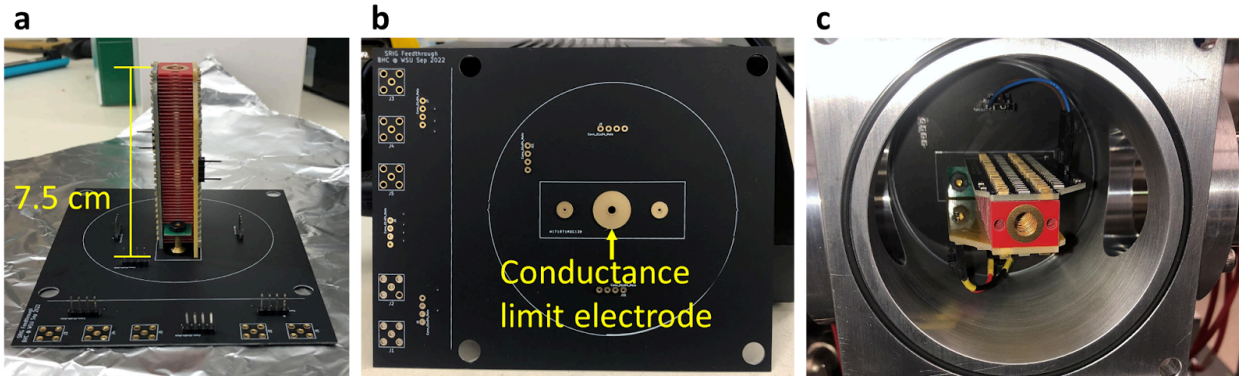

Figure 5.S3. (a) Photograph of the PCB SRIG. (b) Photograph of the custom flange that the SRIG mounts to. The white line on the flange separates the region of the board which extends beyond the instrument (left of the line) from that which is within the chamber (right of the line). (c) Photograph of the SRIG sitting inside the SRIG chamber.

The PCB hexapole, which was designed in-house, transmits ions exiting the SRIG into the lens system of the MS (Figure 5.S4). In order to limit peak broadening in the hexapole, a segmented design was implemented, which enabled for the application of a DC gradient across the hexapole. Prior to the implementation of this segmented hexapole, significant peak broadening occurred due to excessive diffusion in a hexapole which lacked a DC gradient.

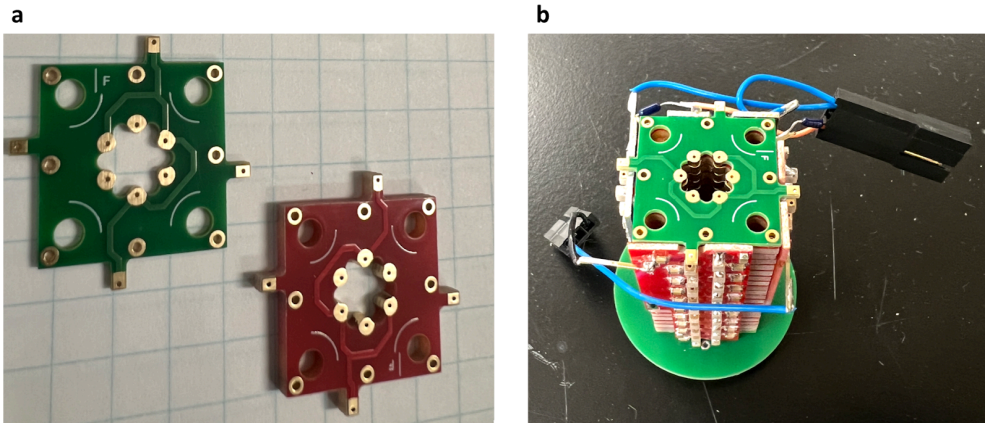

Figure 5.S4. (a) Custom PCB electrodes which are used to assemble the hexapole (b).

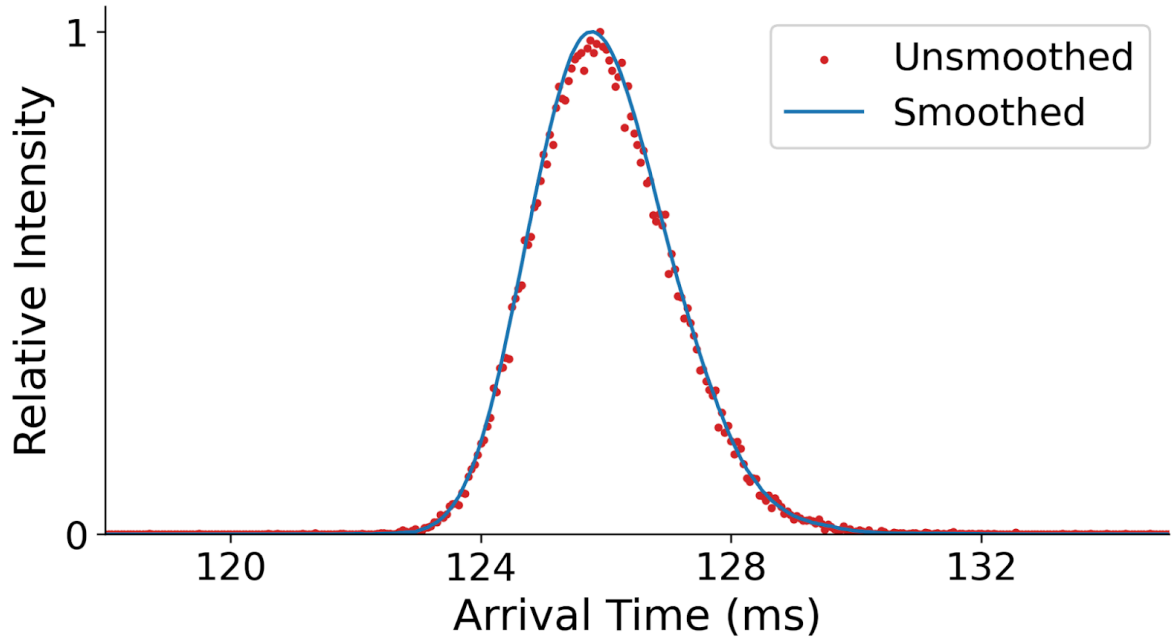

Figure 5.S5. ATD of T5 prior to smoothing (red) and after smoothing (blue) using a Savitzky-Golay smoothing algorithm.

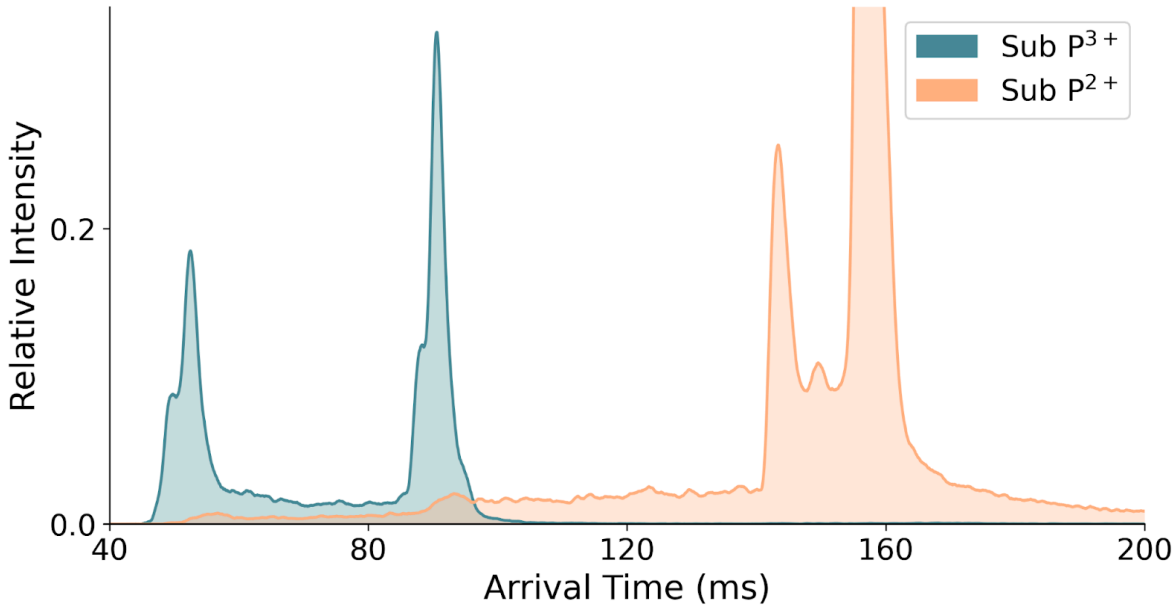

Figure 5.S6. A subsection of the spectra shown in Figure 2 which highlights a noticeable increase in +2 ion current that directly coincides with the +3 ion populations of substance P.

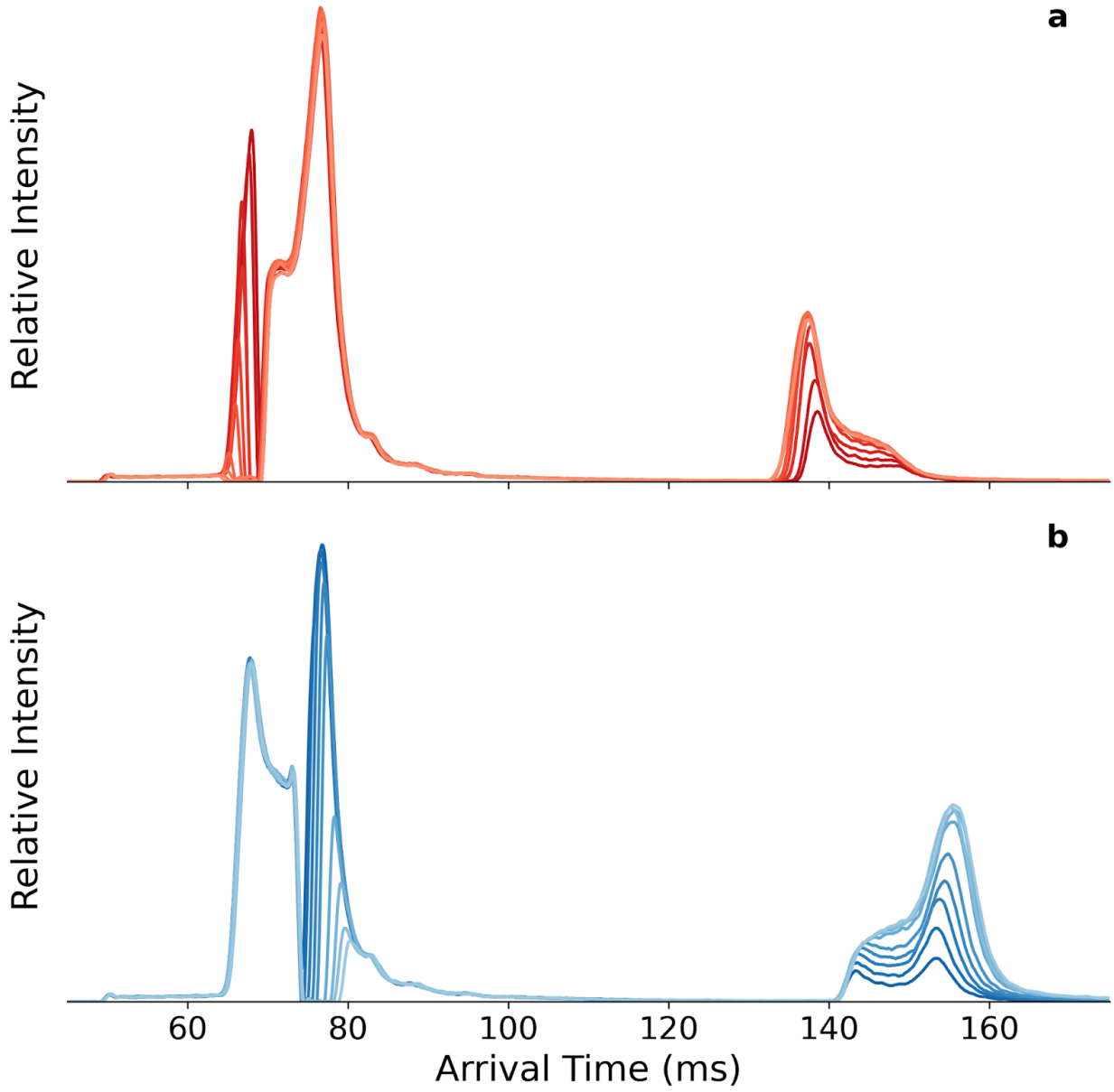

Figure 5.S7. ATD of tandem IMS experiments performed on (a) the compact (earlier arriving) and (b) elongated (later arriving) conformers of bradykinin^{2+}. The apex of the sliced peaks do not align as a result of differences in the start of the slicing as well as the duration of the slice. Unlike experiments shown elsewhere, the following conditions were implemented during the collection of the presented data: TW speed 128 m/s, guard bias 15 V, ToF sampling frequency 25 kHz, number of averages 250.

Table 5.S1. Deviations between the bradykinin^{2+} ion population before (parent) and after (product) being rerouted for tandem IMS analysis via an additional lap through the SLIM. Positive values indicate that the product population was greater than the parent population. The minimal deviation between the two populations suggests that no significant ion loss was experienced by ions traversing the SLIM for an additional lap. The equation used to quantify "deviation" is shown below (eq. 5.1). The data associated with a 3 ms slice of the elongated conformer was excluded due to unusual peak shape, which was attributed to random error.

	Compact Conformer	Elongated Conformer
Slice Width (ms)	Deviation between sliced and product populations (%)	Deviation between sliced and product populations (%)
0.5	1.35	2.05
1	-1.09	4.46
1.5	2.35	6.48
2	2.48	5.54
2.5	2.51	6.74
3	2.70	NA
3.5	4.00	5.23
4	3.47	6.20
4.5	0.97	4.05
5	-2.23	4.48

$$Deviation = \frac{(loss\ in\ parent\ peak\ area) - (gain\ in\ product\ peak\ area)}{(parent\ peak\ area)} * 100\% \qquad \text{(eq. 5.1)}$$

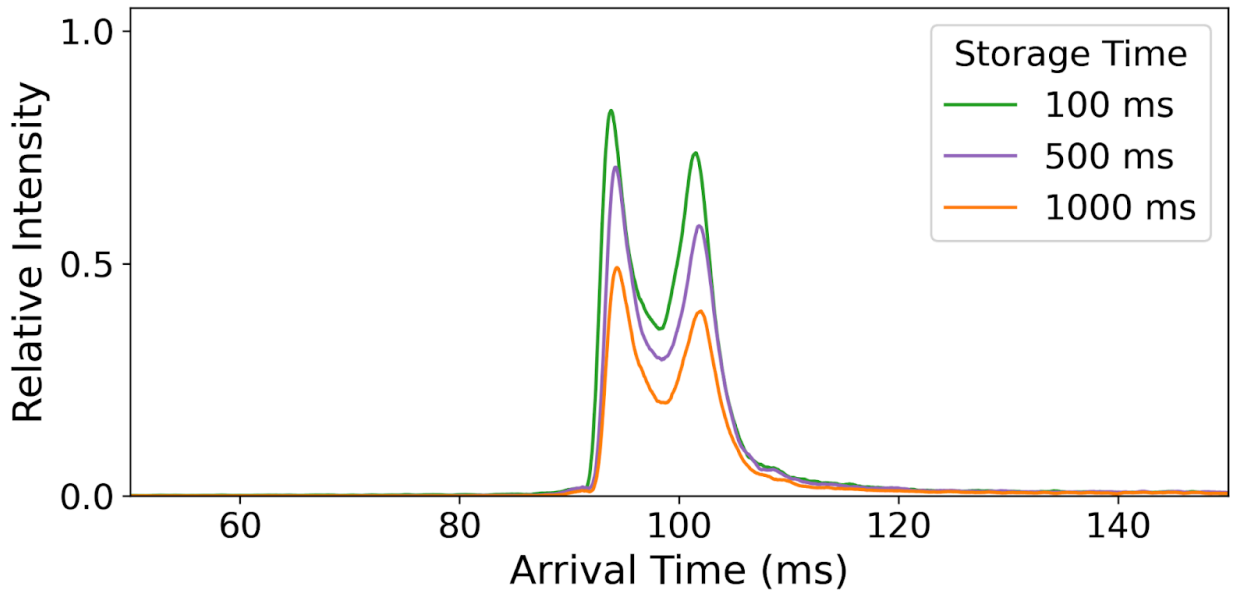

Figure 5.S8. Overlaid ATD of bradykinin^{2+} collected with varying storage periods.

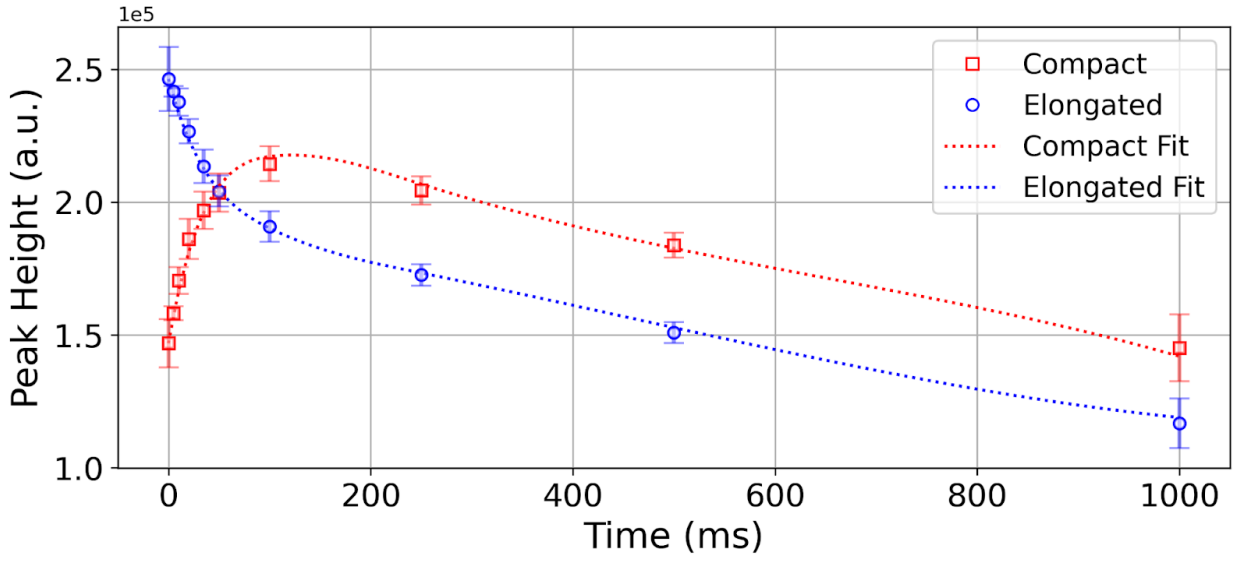

Figure S9. Variations in peak height (assigned based on arrival time) of the compact and elongated conformers of bradykinin2+ as a function of storage time. These data were used to calculate the "conformer ratio" displayed in Figure 4b. The dotted lines represent the fit of the data to the simple interconversion model that accounts for signal depletion as a function of storage time. The precise script used for these fits is shown at the end of the Supporting Information.

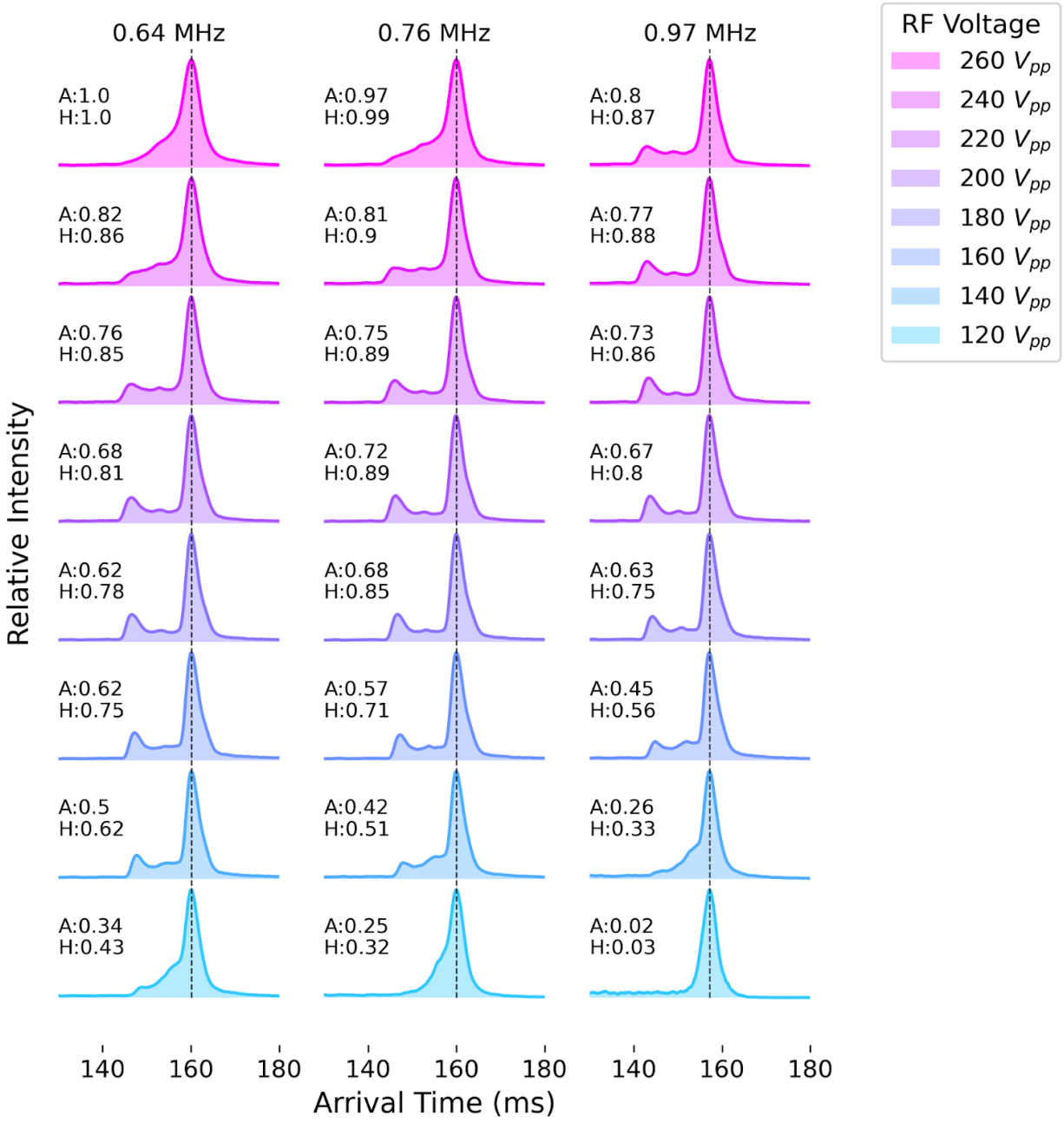

Figure 5.S10. ATD of substance P^{2+} collected under various RF conditions. "A" refers to the peak area of the presented spectra normalized to the spectra with the greatest area (0.64 MHz, 260 Vp-p). "H" refers to the peak height of the presented spectra normalized to the spectra with the greatest height (0.64 MHz, 260 Vp-p).

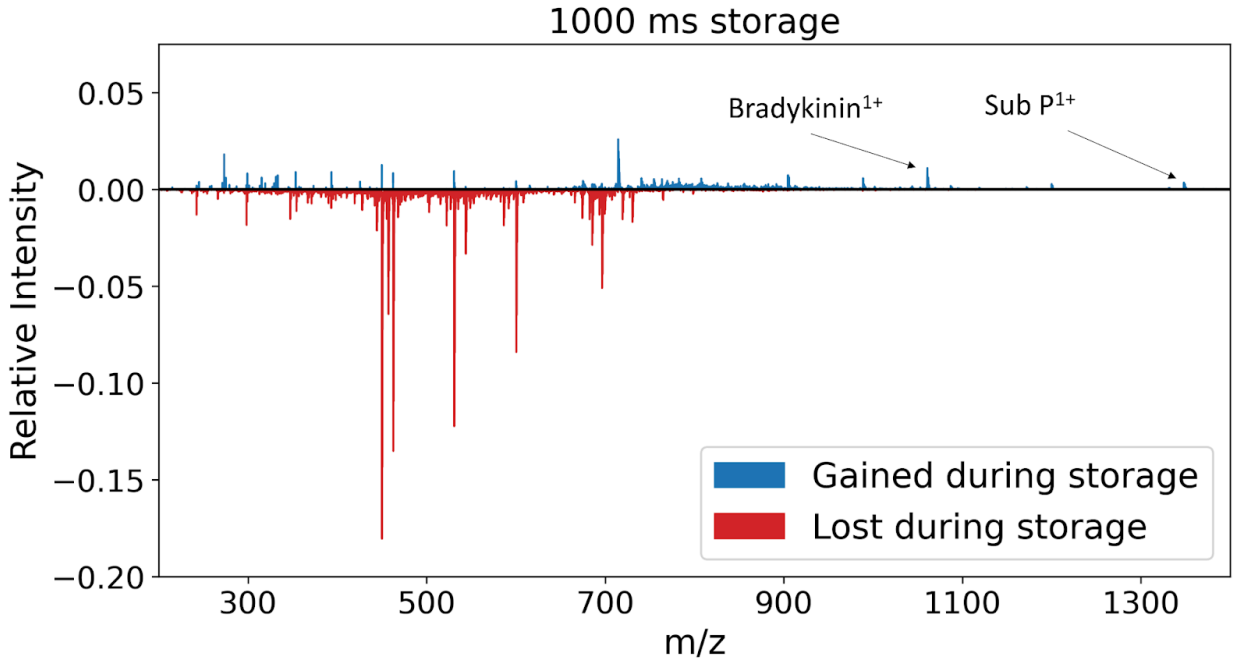

Figure 5.S11. Gains and losses associated with 1000 ms of storage. The spectra shown were generated by subtracting spectra collected when no storage was implemented from spectra where 1000 ms of storage was implemented.

5.4 Broader Impact

The major takeaways from this chapter concern both the development of TW-SLIM platforms as well as insights into the complexities of TW-SLIM analysis. While it would be unreasonable to suggest that this chapter provides a comprehensive blueprint for the development of a TW-SLIM-ToF platform, we nonetheless provide insight into tools and techniques which may simplify similar efforts at other institutions. Building upon work presented in previous chapters, it should be recognized that our work has informed strategies for the development of TW-SLIM instruments which range from simple prototypes to multifaceted platforms capable of tackling complex challenges. Regarding TW-SLIM analysis, the data presented in this chapter suggest that a great deal of consideration is warranted when utilizing this technique for the analysis of labile species. Additionally, it is clear that further investigation into the energies experienced by ions in TW-SLIM is necessary, especially if the technique is to ever see use in a clinical setting wherein it would be used to analyze various biomolecules.

Building upon the work presented in this chapter, future experiments which both quantify the energies experienced by ions in TW-SLIM and deepen our understanding of how each aspect of the experiment contributes to ion heating would be beneficial. Regarding quantification, the use of thermometer ions whose dissociation energies are well studied could provide us with rough estimations of just how “hot” ions in TW-SLIM are.[129,130] While singling out the contributions towards ion heating made by particular aspects of the TW-SLIM experiment (e.g., guard bias, RF conditions, etc.) is a daunting

task, robust data collection and modeling efforts may reveal if any one particular aspect can be tuned to limit ion heating.

CHAPTER SIX: TW-SLIM AS A PLATFORM FOR GAS-PHASE ION CHEMISTRY EXPERIMENTS

6.1 Acknowledgements

The author would like to acknowledge Brain H. Clowers for designing and implementing the reactant gas introduction system and for sharing their knowledge of HDX. The author would also like to acknowledge Haley M. Schramm for aiding in the experimental design process and for sharing their knowledge of HDX.

6.2 Building Towards Gas-phase Ion Chemistry Experiments

For those considering TW-SLIM as a tool for performing gas-phase ion chemistry (GPIC), there are a number of factors which must be taken into account. To begin, the desired functionality of the TW-SLIM must be determined. Recognizing the capacity of TW-SLIM to effectively store ions,[54,95] it is entirely reasonable to design a simple, compact TW-SLIM board whose primary function is to hold the ions as they interact with a desired reactant gas. While this approach may simplify the experiment from a practical standpoint, it ultimately limits the phenomena that can be probed with the system. Numerous reports have shown that shifts in mobility may provide insight into the underlying energetics of GPIC.[131,132] Without sufficient separation in the TW-SLIM, such information may be clouded by ambiguity in the mobility domain. Fortunately, the tools outlined in Chapter 3 can aid in the development of TW-SLIM systems of varying complexity, perhaps even enabling a system to be designed which can operate as either a simple reaction chamber or a system capable of high-powered separations.

Regardless of the desired complexity with regards TW-SLIM, those interested in utilizing the platform for GPIC must also be mindful of potential interaction between dopant gasses and the TW-SLIM boards. Though less expensive than traditional materials such as stainless steel, it should be recognized that PCB are not as inert and may be susceptible to outgassing or undesired chemistry.[125] Given the range of GPIC reactants and PCB materials, the only true solution to this problem is diligent preparation and monitoring for abnormal features during data collection/analysis.

Aside from the TW-SLIM itself, other experimental components must be considered when developing a platform for GPIC. As discussed in Chapter 3, obtaining and maintaining desired pressures throughout a TW-SLIM platform may present issues as the complexity of the system increases. Given that GPIC experiments will almost certainly require a mass spectrometer and additional gas inlets, these issues will be exacerbated. To make matters worse, fluctuations in pressure are particularly damaging to GPIC experiments. Should the concentration of the reactant gas in the TW-SLIM chamber vary significantly over the course of an experiment, the reproducibility of the data will suffer. Additionally, depending on the amount of reactant gas introduced into the system, variations in the total pressure of the TW-SLIM system may induce significant shifts in arrival time. Recalling that information from the mobility domain may be used to deduce GPIC energetics information, considerations must be made to ensure that these deductions are not convoluted by pressure changes.

Moving on from the practical side of instrumentation, the ways in which TW-SLIM can be used to aid in GPIC can be quite powerful, albeit with some drawbacks which

must be considered. Perhaps the biggest advantage of using TW-SLIM for these endeavors is its ability to store ions for user-defined periods, enabling for relatively precise time-based GPIC experiments.[54,95] Given that storage periods in TW-SLIM can be varied by sub-millisecond increments, this approach enables a user to “zoom-in” on a particular time window and analyze the region with a high sampling frequency if desired. Alternatively, given that the duration of storage periods can vary across several orders of magnitude,[54,95] a user could instead observe GPIC taking place over substantially different timescales. It should be noted that aside from TW-SLIM, techniques such as trapping mass spectrometry have enabled time-based GPIC experiments to be conducted. However, these system suffer from limited reactant introduction due to their need for high vacuum conditions which complicates the analysis.[133–135]

Though promising, TW-SLIM storage is not without its drawbacks. As shown in Chapter 5, not all analytes will be effectively stored for extensive periods. In the case of multiply charged species, charge transfer may occur which not only limits the sensitivity of the parent species, but also convolutes the data associated with the product species. Furthermore, conditions (RF frequency, guard bias, etc.) which enable select species to be stored effectively, may not work as well for disparate species. Lastly, while varying ion reaction times is useful, it should be noted that the total exposure time in a TW-SLIM system may be somewhat ambiguous depending on the experimental workflow. Given that on-board accumulation has proven an effective tool for boosting sensitivity,[70,95] it may be tempting to incorporate that approach into a GPIC experiment. That being said,

doing so will make it difficult to ascertain how long ions are exposed to reactants prior to injection, and ultimately their total exposure time. To solve this issue, we developed a fill-inject-sink approach. During the fill period (initiated at “time 0”, t_0), ions are allowed into the TW-SLIM chamber which contains the reactant gas. Eventually, ions which have been allowed into the TW-SLIM chamber will enter the TW-SLIM and arrive at the injection point within the system. Rather than allow ions to accumulate in this region, the injection is synchronized with the arrival of the ions (t_{inj}) so that they pass through with little to no accumulation occurring. To ensure that all ion species reach the injection point at the same time (i.e., no separation takes place) the TW in this region is operated at surfing conditions (low TW speed, high TW amplitude). After the injection period has ended, the injection electrodes are grounded which results in the termination of all ions that did not arrive in time to be injected. Given that we know the time spent by the ions before injection (t_{inj}), are able to measure their arrival time (t_d), and are certain that there are no “leftover” ions due to the sink, we can accurately estimate their exposure time (t_e) to be equivalent to $t_{inj} + t_d$. For the sake of continuity, t_{inj} was held constant throughout all analyses (40 ms).. To be clear, this solution to exposure time ambiguity requires a potential trade-off in sensitivity, which may or may not be feasible for a given analysis.

6.3 Preliminary Results: Hydrogen-Deuterium Exchange in TW-SLIM

Having acquired the prerequisite hardware and familiarity with TW-SLIM, the next step was to perform GPIC experiments. Given our familiarity with gas-phase hydrogen-deuterium exchange (HDX) in DTIMS,[132,136] these experiments represented a logical choice for evaluating our system. Briefly, HDX is a chemical reaction in which bonded hydrogen atoms are replaced by deuterium atoms.[134,137] In the context of IMS, non-deuterated gas-phase ions are exposed to deuterium through interaction with a deuterated dopant gas such as methanol-OD (MeOD). Given that HDX causes shifts in an ion's m/z profile, the magnitude of HDX which occurs throughout a given analysis can be quantified using relative intensities observed in the m/z domain (Figure 6.1).

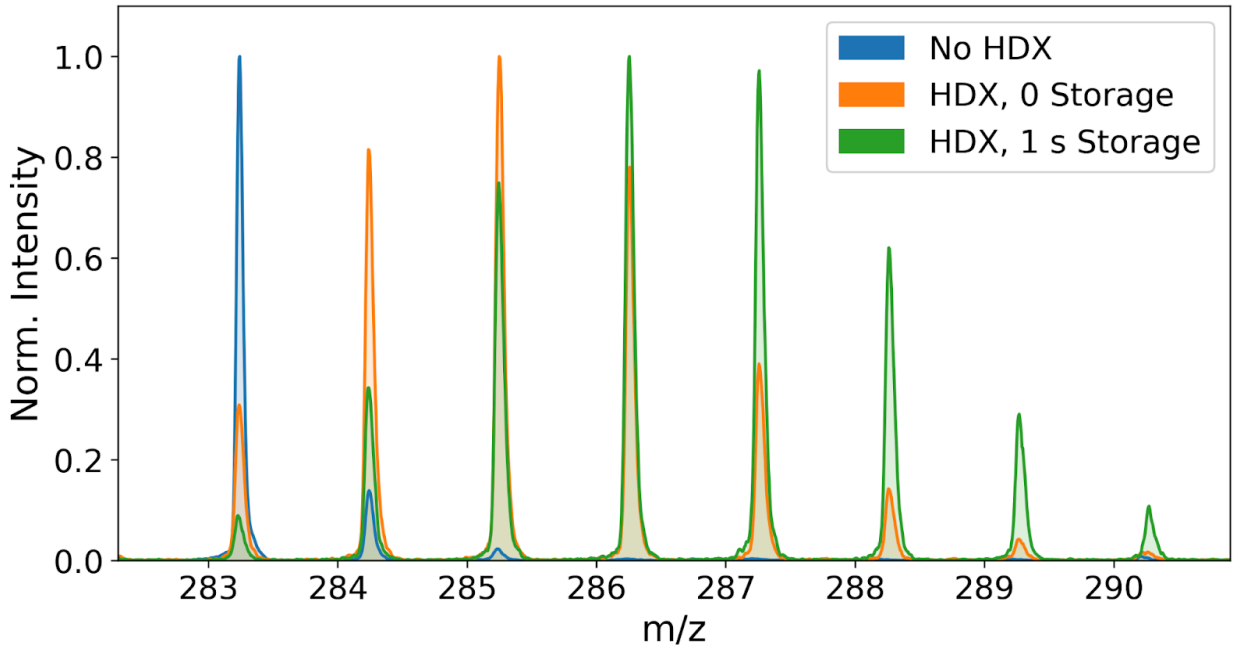

Figure 6.1. Mass spectra of bis-tris propane (BTP) without MeOD in the TW-SLIM chamber (blue) compared to spectra where MeOD vapor was doped into the TW-SLIM chamber (orange, green). The shift in m/z to higher values occurs as a result of HDX

between BTP and MeOD. Increasing the residence time of BTP within the TW-SLIM via storage (green) enables greater deuterium incorporation. Intensities were normalized to increase the readability of the plot. That being said, it should be recognized that HDX reduces intensities as ion populations are dispersed over a wider range of m/z values.

Utilizing the SLIM-ToF platform discussed in Chapter 5, preliminary HDX experiments were performed using MeOD as the dopant gas. After confirming that we could both observe HDX and tune the extent of the deuterium incorporation using our TW-SLIM system (Figure 6.1), our focus then turned to more robust analyses. While storage experiments are unique in that they enable for arbitrary increases in arrival time, other approaches exist to increase the time spent by ions in TW-SLIM. Disregarding surfing conditions, lowering the TW amplitude or increasing TW speed will increase the time it takes for ions to exit TW-SLIM. While modulating these parameters does not provide the same degree of control as storage experiments, there is certainly merit in exploring these approaches for tuning HDX.

Building upon the discussions in Chapter 5 regarding ion heating in TW-SLIM, we were interested in determining whether or not time spent in TW-SLIM is the primary factor in determining the extent of HDX, or if the manner in which ions are delayed is also a factor. Put differently, if an ion population were to spend an equal amount of time in TW-SLIM through either the use of storage or TW modulation, would there be any observable differences between the two with regards to HDX? Could ion heating imparted by the TW impact HDX? Figure 6.2 shows 3 mass spectra for bis-tris propane (BTP, nominal mass: 282 Da) undergoing HDX. Despite varied approaches to

increasing the ions' t_e to approximately 150 ms, no significant differences are present with regards to the degree of HDX which occurred throughout the analyses. While the data shown in Figure 6.2 may suggest that storage and TW modulation are interchangeable with regards to increasing HDX, it must be recognized that BTP is a rather "simple" compound (limited size, singular charge state) and that further investigations involving more complex species are warranted.

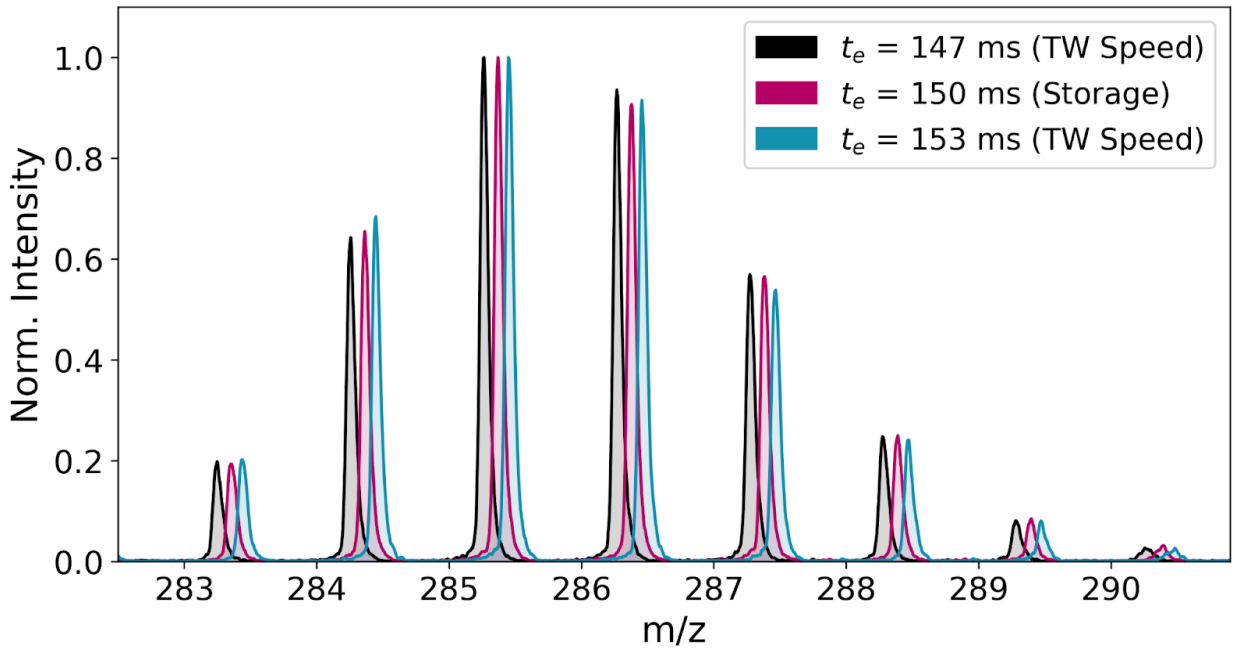

Figure 6.2. Mass spectra of BTP undergoing HDX wherein the exposure time (t_e) was approximately 150 ms. To increase the clarity of the plot, slight offsets were applied to the m/z values of the fuschia and blue spectra. Despite dwelling longer due to a 20 ms storage period (fuschia) as opposed to increasing the TW speed from 174 m/s to 191 m/s (black) and 198 m/s (blue), there does not appear to be any significant differences in the degree of HDX occurring across the three spectra.

Figure 6.3 shows two mass spectra corresponding to the +2 charge state of a custom peptide (N-PGGGGKGGGGKGGGGKGGGGK, nominal mass = 1582 Da) from GenScript Biotech (Piscataway, NJ) undergoing HDX. For the sake of brevity, this peptide will be referred to as PGK. Despite having equivalent t_e, the spectra which corresponds to the use of higher TW speeds (purple) exhibits less HDX than the spectra collected using the storage approach (blue). While at odds with what is shown in Figure 6.2, it should be recognized that numerous factors are at play when evaluating the spectra shown in Figure 6.3 which may explain the observed differences. Unlike BTP which is observed primarily in the +1 charge state, PGK also appears in the +4 and +3 charge states at comparable intensities. Similar to observations reported in Chapter 5, these higher charge states undergo charge transfer, meaning that portions of the +2 population were at one point other species. In the context of HDX, this means that what we denote as the HDX kinetics of the +2 charge state is actually a summation of kinetics between multiple species which convert to the +2 species over the course of the analysis. Recalling discussions from Chapter 5, we know that the extent of charge transfer varies as a function of time spent in TW-SLIM. Given that TW modulation and storage approaches do not impact t_e in the same way (storage delays all ions equally, TW modulation does not), it's possible that the variations in HDX shown in Figure 6.3 result from different degrees of charge transfer and subsequent contributions from species of higher charge states. While further analysis is required in order to decipher these issues and provide insight into potential the role of ion heating in TW-SLIM HDX, these preliminary experiments are nonetheless significant. For starters, they showcase the ability of TW-SLIM to not only serve as a vessel in which GPIC may occur, but also

play a part in influencing the outcomes of the experiments. Furthermore, they show that while TW-SLIM should be considered as a tool for probing GPIC, there remains gaps in our understanding which must be addressed prior to the full-scale adoption of TW-SLIM for these endeavors.

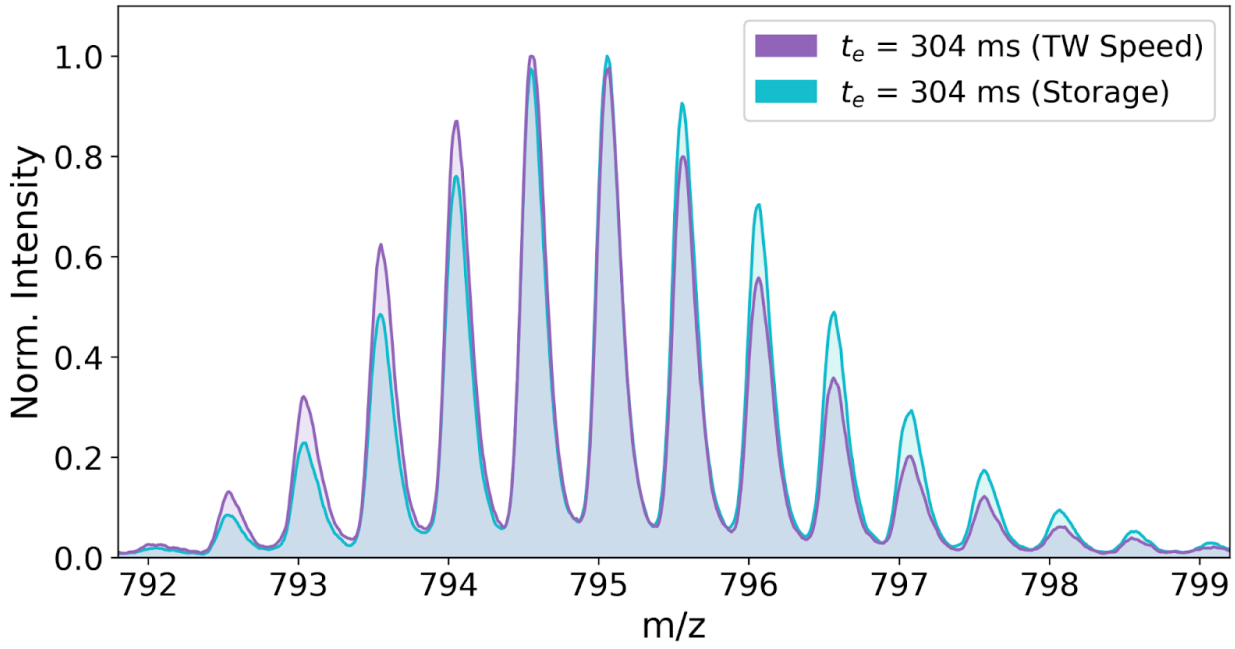

Figure 6.3. Mass spectra of a doubly charged peptide undergoing HDX with t_e of 304 ms. The spectra shown in blue was collected with a 40 ms storage period in place whereas the purple spectra was collected by increasing the TW speed to 198 m/s. Despite having identical exposure times to MeOD, there is a clear difference in the degree of HDX between the two spectra.

6.4 Future Efforts

The immediate goal with regards to TW-SLIM and GPIC is to perform robust analyses based on information gleaned from the preliminary efforts discussed in the previous section. These analyses will include a more in-depth investigation of the storage vs TW modulation phenomena and most importantly incorporate replicates which enable more quantitative conclusions to be drawn. Additionally, approaches which may deconvolute the effects of multiple charge states on HDX will be explored. The results of these more robust experiments and the evaluation of our approaches will be the subject of a future publication.

Beyond our immediate goals with regards to TW-SLIM and GPIC, future endeavors which utilize more advanced instrumentation will be outlined and prepared for. Recognizing that contaminates and pressure fluctuations in the TW-SLIM chamber may limit the reproducibility of HDX and contribute to charge transfer, an ideal system would account for and mitigate these issues. In order to limit the introduction of contaminates through the inlet capillary, housing which encloses the inlet and is supplied with N_2 gas will be implemented. Furthermore, an additional chamber will be added between the inlet and TW-SLIM chambers, further limiting the transmission of ESI solvent downstream. As an added bonus, the author believes that this additional chamber may also limit pressure fluctuations in the TW-SLIM chamber which may arise from gas dynamics in the inlet chamber. A more in-depth discussion regarding future iterations of our TW-SLIM platforms as well as some schematics of these hypothetical instruments can be found in Chapter 7. Lastly, performing other GPIC variants such as

ozonolysis[138,139] will further showcase the utility and flexibility of TW-SLIM as a tool for complex analyses.

CHAPTER 7: CONCLUDING REMARKS AND FUTURE DIRECTIONS

Analytical chemistry offers us unique insights into the world around us. From quantifying pollutants in soil to identifying disease biomarkers in plasma,[140–142] the ability of analytical techniques to reveal what our senses cannot is of profound importance. Owing to an unprecedented degree of flexibility and separation power, TW-SLIM stands out amongst the ever growing suite of analytical techniques and appears poised to redefine the limits ion mobility spectrometry. Key to the continued evolution of TW-SLIM is increased adoption by individuals with varying skill sets and experimental goals who can further mold and develop the technique. With that in mind, a significant portion of my research at WSU was aimed at developing TW-SLIM platforms which can be more easily adopted, providing insights into how best to analyze various species with TW-SLIM, and showcasing the capacity for TW-SLIM to aid in experiments aside from traditional separations.

While TW-SLIM adoption remains limited, it should be noted that numerous R1 institutions have begun experimenting with TW-SLIM as a result of our work. In some instances, research is being performed which utilizes TW-SLIM boards developed at WSU. In other cases, groups are using the tools outlined in *SLIM Tricks* to develop their own TW-SLIM platforms. Regardless of our degree of involvement or the ultimate outcome of the experiments conducted at these institutions, the significance of this development cannot be understated. For the first time since the technique's inception, a foundation upon which independent TW-SLIM research can be built upon has been established.

Aside from making TW-SLIM more accessible, we felt it was important to showcase what we feel to be an underappreciated aspect of TW-SLIM: its ability to aid in gas-phase ion chemistry (GPIC) experiments. Armed with the ability to effectively manipulate and store ions for extended periods at high pressures (2-4 Torr), TW-SLIM is uniquely capable of augmenting and improving GPIC experiments. While the scope of GPIC discussed in this work is limited, it should be recognized that it covers much of the preliminary work upon which future endeavors will be built upon.

In order to tackle increasingly complex challenges, further improvements to our TW-SLIM platform are necessary (Figure 7.1). Beginning with the modifications discussed at the end of Chapter 6, the addition of housing around the inlet capillary and the implementation of a buffer chamber between the inlet and TW-SLIM should reduce contaminants within the system and limit pressure fluctuations. Aside from improving our GPIC experiments, we are also hoping that this will reduce the amount of charge transfer that occurs within our system which we suspect is related to introduction of solvent molecules into the TW-SLIM chamber. The simplest approach to transporting ions through the buffer chamber would be a stacked ring ion guide similar to the one that precedes the ToF (Figure 7.1). That being said, there would certainly be merit in introducing some sort of ion filter prior to TW-SLIM analysis. Similar to the cyclic-IMS system developed by Waters[45] the installation of a quadrupole mass filter prior to the TW-SLIM could greatly enhance the system's capabilities. Though not possible using the chamber layout shown in Figure 7.1, it is nonetheless worth considering how such an approach could enhance TW-SLIM analysis given the inevitable expansion of WSU's

TW-SLIM research. With regards to charge transfer, the ability to exclude higher charge states from analysis would remove the need to deconvolute data associated with the products of charge transfer. Additionally, preventing unwanted species from entering the TW-SLIM and contributing to ion activation during on-board accumulation[128] would be beneficial when analyzing labile species.

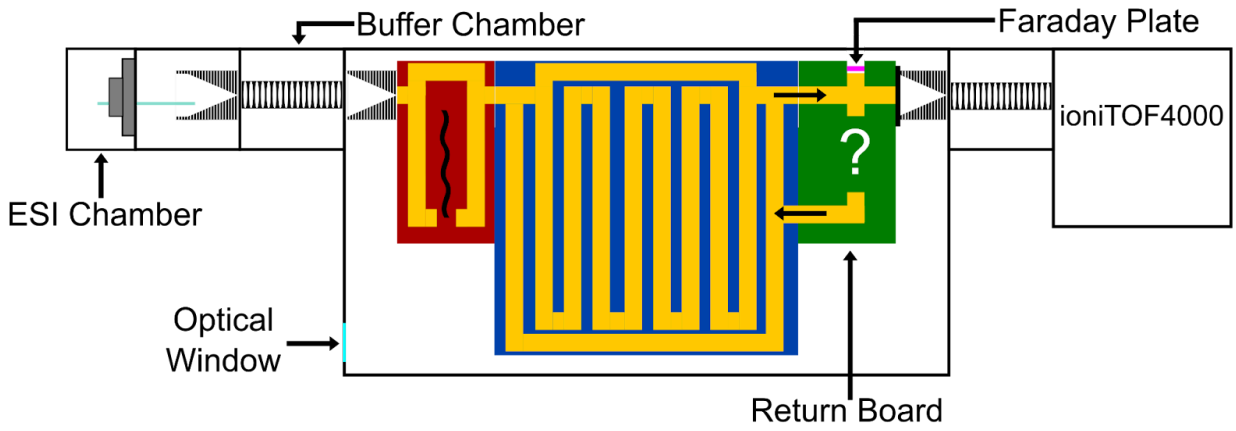

Figure 7.1. Schematic of a hypothetical SLIM-ToF platform which may be implemented at WSU in the future. Major improvements from the original design (Figure 5.S1) are labeled. The ESI and buffer chambers should both decrease the amount of contaminants entering the system and also limit pressure fluctuations in the TW-SLIM chamber. The Faraday plate will make troubleshooting post-SLIM issues easier. The implementation of the return board and optical window will enable this platform to engage in more complex investigations.

Aside from improvements that precede the TW-SLIM, there remains room for further evolution of the TW-SLIM itself as well as the scope of its use. During the process of mating the TW-SLIM with the ToF, it became apparent that procedures for diagnosing issues post-TW-SLIM separation (e.g., diffusion in the hexapole) were necessary. While at first the solution seemed obvious; place a Faraday plate near the

exit of the TW-SLIM, we quickly found that we lacked the space within the vacuum chamber to mount the detector. With that in mind, we began experimenting with the idea of designing TW-SLIM boards that have cutouts in which Faraday plates can be mounted. Fortunately, preliminary testing of this approach has suggested this is a feasible solution and as a result future iterations of our TW-SLIM systems will have Faraday plates near their exits (Figure 7.1).

In addition to modifying the final TW-SLIM board in our system to include a simple detector, we also acknowledge that there's room to enhance the complexity of our system by expanding its functionality. As it stands, the current SLIM-ToF system employs a "stager board" (Figure 5.1) which simply guides ions out of the TW-SLIM as they head towards the ToF. Future versions of the SLIM-ToF will replace the stager board with more complex designs ("Return Board", Figure 7.1) such as those that allow for targeted ion storage and or collision induced dissociation. Additionally, given that the current iteration of the separation board has the capacity to receive ions (Figure 5.1) from the return board, it would be possible to modulate select ion populations and then send them for additional separation. Lastly, specialized plates have been prepared which enable for an optical window to be installed and aligned with the cycling path of the separation board. The aim is to one day augment our SLIM-ToF experiments with the ability to expose ion populations to laser pulses, further showcasing the ability of TW-SLIM to aid in complex analyses.

REFERENCES

(1) Mason, E. A.; McDaniel, E. W. *Transport Properties of Ions in Gases*; John Wiley & Sons: New York, 1988.
(2) Revercomb, H.; Mason, E. Theory of Plasma Chromatography / Gaseous Electrophoresis — A Review. *Anal. Chem.* **1975**, *47* (7), 970–983.
(3) Eicman, G. A.; Karpas, Z.; Hill, H. H. *Ion Mobility Spectrometry*, 3rd ed.; CRC Press: Boca Raton, FL, 2013.
(4) Keller, T.; Keller, A.; Tutsch-Bauer, E.; Monticelli, F. Application of Ion Mobility Spectrometry in Cases of Forensic Interest. *Forensic Sci. Int.* **2006**, *161* (2-3), 130–140.
(5) Puton, J.; Namieśnik, J. Ion Mobility Spectrometry: Current Status and Application for Chemical Warfare Agents Detection. *Trends Analyt. Chem.* **2016**, *85*, 10–20.
(6) Ewing, R. G.; Atkinson, D. A.; Eiceman, G. A.; Ewing, G. J. A Critical Review of Ion Mobility Spectrometry for the Detection of Explosives and Explosive Related Compounds. *Talanta* **2001**, *54*, 515–529.
(7) Metternich, S.; Zörntlein, S.; Schönberger, T.; Huhn, C. Ion Mobility Spectrometry as a Fast Screening Tool for Synthetic Cannabinoids to Uncover Drug Trafficking in Jail via Herbal Mixtures, Paper, Food, and Cosmetics. *Drug Test. Anal.* **2019**, *11* (6), 833–846.
(8) Li, M.; Wang, S.; Xu, C.; Ruan, H.; Wang, W.; Chen, C.; Li, H. Parallel Coupling of Ion Mobility Spectrometry and Ion Trap Mass Spectrometry for the Real-Time Alarm Triggering and Identification of Hazardous Chemical Leakages. *Anal. Chem.* **2021**, *93* (34), 11852–11858.
(9) Fenn, J. B.; Mann, M.; Meng, C. K.; Wong, S. F.; Whitehouse, C. M. Electrospray Ionization for Mass Spectrometry of Large Biomolecules. *Science* **1989**, *246* (4926), 64–71.
(10) Hasin, Y.; Seldin, M.; Lusis, A. Multi-Omics Approaches to Disease. *Genome Biol.* **2017**, *18* (1), 83.
(11) Olivier, M.; Asmis, R.; Hawkins, G. A.; Howard, T. D.; Cox, L. A. The Need for Multi-Omics Biomarker Signatures in Precision Medicine. *Int. J. Mol. Sci.* **2019**, *20* (19). https://doi.org/10.3390/ijms20194781.
(12) Misra, B. B.; Langefeld, C. D.; Olivier, M.; Cox, L. A. Integrated Omics: Tools, Advances, and Future Approaches. *J. Mol. Endocrinol.* **2018**. https://doi.org/10.1530/JME-18-0055.
(13) Bohrer, B. C.; Merenbloom, S. I.; Koeniger, S. L.; Hilderbrand, A. E.; Clemmer, D. E. Biomolecule Analysis by Ion Mobility Spectrometry. *Annu. Rev. Anal. Chem.* **2008**, *1*, 293–327.
(14) Paglia, G.; Kliman, M.; Claude, E.; Geromanos, S.; Astarita, G. Applications of Ion-Mobility Mass Spectrometry for Lipid Analysis. *Anal. Bioanal. Chem.* **2015**, *407*, 4995–5007.
(15) Papadopoulos, G.; Svendsen, A.; Boyarkin, O. V.; Rizzo, T. R. Conformational Distribution of Bradykinin [bk + 2 H]2+ Revealed by Cold Ion Spectroscopy Coupled with FAIMS. *J. Am. Soc. Mass Spectrom.* **2012**, *23* (7), 1173–1181.
(16) Hancock, S. E.; Poad, B. L. J.; Batarseh, A.; Abbott, S. K.; Mitchell, T. W. Advances and Unresolved Challenges in the Structural Characterization of Isomeric Lipids. *Anal. Biochem.* **2017**, *524*, 45–55.
(17) Wu, Q.; Wang, J.-Y.; Han, D.-Q.; Yao, Z.-P. Recent Advances in Differentiation of Isomers by Ion Mobility Mass Spectrometry. *Trends Analyt. Chem.* **2020**, *124*, 115801.
(18) Siems, W. F.; Wu, C.; Tarver, E. E.; Hill, H. H.; Larsen, P. R.; Mcminn, D. G. Measuring the Resolving Power of Ion Mobility Spectrometers. *Anal. Chem.* **1994**, *66*, 4195–4201.
(19) Kemper, P. R.; Dupuis, N. F.; Bowers, M. T. A New, Higher Resolution , Ion Mobility Mass

Spectrometer. *Int. J. Mass Spectrom.* **2009**, *287*, 46–57.
(20) Ridgeway, M. E.; Lubeck, M.; Jordens, J.; Mann, M.; Park, M. A. Trapped Ion Mobility Spectrometry: A Short Review. *Int. J. Mass Spectrom.* **2018**, *425*, 22–35.
(21) Guevremont, R. High-Field Asymmetric Waveform Ion Mobility Spectrometry: A New Tool for Mass Spectrometry. *J. Chromatogr. A* **2004**, *1058* (1-2), 3–19.
(22) Giles, K.; Pringle, S. D.; Worthington, K. R.; Little, D.; Wildgoose, J. L.; Bateman, R. H. Applications of a Travelling Wave-Based Radio-Frequency- Only Stacked Ring Ion Guide. *Rapid Commun. Mass Spectrom.* **2004**, *18*, 2401–2414.
(23) Campuzano, I. D. G.; Giles, K. Historical , Current and Future Developments of Travelling Wave Ion Mobility Mass Spectrometry : A Personal Perspective. *Trends Analyt. Chem.* **2019**, *120*, 115620.
(24) Shvartsburg, A. A.; Smith, R. D. Fundamentals of Traveling Wave Ion Mobility Spectrometry. *Anal. Chem.* **2008**, *80*, 9689–9699.
(25) Kwantwi-Barima, P.; Harrilal, C. P.; Garimella, S. V. B.; Attah, I. K.; Smith, R. D.; Ibrahim, Y. M. Effect of Traveling Waveform Profiles on Collision Cross Section Measurements in Structures for Lossless Ion Manipulations. *J. Am. Soc. Mass Spectrom.* **2022**, *33* (5), 783–792.
(26) Hamid, A. M.; Prabhakaran, A.; Garimella, S. V. B.; Ibrahim, Y. M.; Smith, R. D. Characterization of Applied Fields for Ion Mobility Separations in Traveling Wave Based Structures for Lossless Ion Manipulations (SLIM). *Int. J. Mass Spectrom.* **2018**, *430*, 8–13.
(27) Giles, K.; Williams, J. P.; Campuzano, I. Enhancements in Travelling Wave Ion Mobility Resolution. *Rapid Commun. Mass Spectrom.* **2011**, *25*, 1559–1566.
(28) Hamid, A. M.; Ibrahim, Y. M.; Garimella, S. V. B.; Webb, I. K.; Deng, L.; Chen, T.-C.; Anderson, G. A.; Prost, S. A.; Norheim, R. V.; Tolmachev, A. V.; Smith, R. D. Characterization of Traveling Wave Ion Mobility Separations in Structures for Lossless Ion Manipulations. *Anal. Chem.* **2015**, *87*, 11301–11308.
(29) Webb, I. K.; Garimella, S. V. B.; Tolmachev, A. V.; Chen, T.-C.; Zhang, X.; Cox, J. T.; Norheim, R. V.; Prost, S. A.; LaMarche, B.; Anderson, G. A.; Ibrahim, Y. M.; Smith, R. D. Mobility-Resolved Ion Selection in Uniform Drift Field Ion Mobility Spectrometry/mass Spectrometry: Dynamic Switching in Structures for Lossless Ion Manipulations. *Anal. Chem.* **2014**, *86* (19), 9632–9637.
(30) Webb, I. K.; Garimella, S. V. B.; Tolmachev, A. V.; Chen, T.-C.; Zhang, X.; Norheim, R. V.; Prost, S. A.; LaMarche, B.; Anderson, G. A.; Ibrahim, Y. M.; Smith, R. D. Experimental Evaluation and Optimization of Structures for Lossless Ion Manipulations for Ion Mobility Spectrometry with Time-of-Flight Mass Spectrometry. *Anal. Chem.* **2014**, *86* (18), 9169–9176.
(31) Reinecke, T.; Clowers, B. H. Implementation of a Flexible, Open-Source Platform for Ion Mobility Spectrometry. *HardwareX* **2018**, *4*, e00030.
(32) Kelly, R. T.; Tolmachev, A. V.; Page, J. S.; Tang, K.; Smith, R. D. THE ION FUNNEL : THEORY , IMPLEMENTATIONS , AND APPLICATIONS. *Mass Spectrom. Rev.* **2010**, *29*, 294–312.
(33) Kwantwi-Barima, P.; Garimella, S. V. B.; Attah, I. K.; Ibrahim, Y. M. Evaluating Ion Accumulation and Storage in Traveling Wave Based Structures for Lossless Ion Manipulations. *J. Am. Soc. Mass Spectrom.* **2023**, *34* (12), 2849–2856.
(34) May, J. C.; Leaptrot, K. L.; Rose, B. S.; Moser, K. L. W.; Deng, L.; Maxon, L.; DeBord, D.; McLean, J. A. Resolving Power and Collision Cross Section Measurement Accuracy of a Prototype High-Resolution Ion Mobility Platform Incorporating Structures for Lossless Ion Manipulation. *J. Am. Soc. Mass Spectrom.* **2021**, *32* (4), 1126–1137.
(35) Hamid, A. M.; Garimella, S. V. B.; Ibrahim, Y. M.; Deng, L.; Zheng, X.; Webb, I. K.;

Anderson, G. A.; Prost, S. A.; Norheim, R. V.; Tolmachev, A. V.; Baker, E. S.; Smith, R. D. Achieving High Resolution Ion Mobility Separations Using Traveling Waves in Compact Multiturn Structures for Lossless Ion Manipulations. *Anal. Chem.* **2016**, *88*, 8949–8956.
(36) Merenbloom, S. I.; Glaskin, R. S.; Henson, Z. B.; Clemmer, D. E. High-Resolution Ion Cyclotron Mobility Spectrometry. *Anal. Chem.* **2009**, *81* (4), 1482–1487.
(37) Chen, T.-C.; Ibrahim, Y. M.; Webb, I. K.; Garimella, S. V. B.; Zhang, X.; Hamid, A. M.; Deng, L.; Karnesky, W. E.; Prost, S. A.; Sandoval, J. A.; Norheim, R. V.; Anderson, G. A.; Tolmachev, A. V.; Baker, E. S.; Smith, R. D. Mobility-Selected Ion Trapping and Enrichment Using Structures for Lossless Ion Manipulations. *Anal. Chem.* **2016**, *88* (3), 1728–1733.
(38) Dawson, P. H. Quadrupole Mass Filters with Bent or Bowed Rod Sets. *Int. J. Mass Spectrom. Ion Process.* **1988**, *84* (1), 185–201.
(39) Ilchenko, S.; Cotter, R. J. Collision Energetics in a Tandem Time-of-Flight (TOF/TOF) Mass Spectrometer with a Curved-Field Reflectron. *Int. J. Mass Spectrom.* **2007**, *265* (2-3), 372–381.
(40) Deng, L.; Ibrahim, Y. M.; Hamid, A. M.; Garimella, S. V. B.; Webb, I. K.; Zheng, X.; Prost, S. A.; Sandoval, J. A.; Norheim, R. V.; Anderson, G. A.; Tolmachev, A. V.; Baker, E. S.; Smith, R. D. Ultra-High Resolution Ion Mobility Separations Utilizing Traveling Waves in a 13 M Serpentine Path Length Structures for Lossless Ion Manipulations Module. *Anal. Chem.* **2016**, *88* (18), 8957–8964.
(41) Deng, L.; Webb, I. K.; Garimella, S. V. B.; Hamid, A. M.; Zheng, X.; Norheim, R. V.; Prost, S. A.; Anderson, G. A.; Sandoval, J. A.; Baker, E. S.; Ibrahim, Y. M.; Smith, R. D. Serpentine Ultralong Path with Extended Routing (SUPER) High Resolution Traveling Wave Ion Mobility-MS Using Structures for Lossless Ion Manipulations. *Anal. Chem.* **2017**, *89*, 4628–4634.
(42) Bansal, P.; Yatsyna, V.; Abikhodr, A. H.; Warnke, S.; Faleh, A. B.; Yalovenko, N.; Wysocki, V. H.; Rizzo, T. R. Using SLIM-Based IMS-IMS Together with Cryogenic Infrared Spectroscopy for Glycan Analysis. *Ana* **2020**, *92*, 9079–9085.
(43) Arndt, J. R.; Wormwood Moser, K. L.; Van Aken, G.; Doyle, R. M.; Talamantes, T.; Debord, D.; Maxon, L.; Stafford, G.; Fjeldsted, J.; Miller, B.; Sherman, M. High-Resolution Ion-Mobility-Enabled Peptide Mapping for High- Throughput Critical Quality Attribute Monitoring. *J. Am. Soc. Mass Spectrom.* **2021**, *32*, 2019–2032.
(44) Kedia, K.; Harris, R.; Ekroos, K.; Moser, K. W.; DeBord, D.; Tiberi, P.; Goracci, L.; Zhang, N. R.; Wang, W.; Spellman, D. S.; Bateman, K. Investigating Performance of the SLIM-Based High Resolution Ion Mobility Platform for Separation of Isomeric Phosphatidylcholine Species. *J. Am. Soc. Mass Spectrom.* **2023**, *34* (10), 2176–2186.
(45) Giles, K.; Ujma, J.; Wildgoose, J.; Pringle, S.; Richardson, K.; Langridge, D.; Green, M. A Cyclic Ion Mobility-Mass Spectrometry System. *Anal. Chem.* **2019**, *91*, 8564–8573.
(46) Masson, A.; Kamrath, M. Z.; Perez, M. A. S.; Glover, M. S.; Rothlisberger, U.; Clemmer, D. E.; Rizzo, T. R. Infrared Spectroscopy of Mobility-Selected H+-Gly-Pro-Gly-Gly (GPGG). *J. Am. Soc. Mass Spectrom.* **2015**, *26* (9), 1444–1454.
(47) Wassermann, T. N.; Boyarkin, O. V.; Paizs, B.; Rizzo, T. R. Conformation-Specific Spectroscopy of Peptide Fragment Ions in a Low-Temperature Ion Trap. *J. Am. Soc. Mass Spectrom.* **2012**, *23* (6), 1029–1045.
(48) Khanal, N.; Masellis, C.; Kamrath, M. Z.; Clemmer, D. E.; Rizzo, T. R. Glycosaminoglycan Analysis by Cryogenic Messenger-Tagging IR Spectroscopy Combined with IMS-MS. *Anal. Chem.* **2017**, *89* (14), 7601–7606.
(49) Masellis, C.; Khanal, N.; Kamrath, M. Z.; Clemmer, D. E.; Rizzo, T. R. Cryogenic Vibrational Spectroscopy Provides Unique Fingerprints for Glycan Identification. *J. Am. Soc. Mass Spectrom.* **2017**, *28* (10), 2217–2222.

(50) Ben Faleh, A.; Warnke, S.; Van Wieringen, T.; Abikhodr, A. H.; Rizzo, T. R. New Approach for the Identification of Isobaric and Isomeric Metabolites. *Anal. Chem.* **2023**, *95* (18), 7118–7126.
(51) Yatsyna, V.; Abikhodr, A. H.; Ben Faleh, A.; Warnke, S.; Rizzo, T. R. High-Throughput Multiplexed Infrared Spectroscopy of Ion Mobility-Separated Species Using Hadamard Transform. *Anal. Chem.* **2022**, *94* (6), 2912–2917.
(52) Kinlein, Z.; Clowers, B. H. Evaluating Dynamic Traveling Wave Profiles for the Enhancement of Separation and Sensitivity in Traveling Wave Structures for Lossless Ion Manipulations. *J. Chromatogr. A* **2023**, *1706*, 464207.
(53) Clowers, B. H.; Cabrera, E.; Anderson, G.; Deng, L.; Moser, K.; Van Aken, G.; Debord, J. D. Masked Multiplexed Separations to Enhance Duty Cycle for Structures for Lossless Ion Manipulations. *Anal. Bioanal. Chem.* **2021**, *93*, 5727–5734.
(54) Kinlein, Z. R.; Anderson, G. A.; Clowers, B. H. Accelerating Prototyping Experiments for Traveling Wave Structures for Lossless Ion Manipulations. *Talanta* **2022**, *244*, 123446.
(55) Midey, A. J.; Patel, A.; Moraff, C.; Krueger, C. A.; Wu, C. Improved Detection of Drugs of Abuse Using High-Performance Ion Mobility Spectrometry with Electrospray Ionization (ESI-HPIMS) for Urine Matrices. *Talanta* **2013**, *116*, 77–83.
(56) Steiner, W. E.; Klopsch, S. J.; English, W. A.; Clowers, B. H.; Hill, H. H. Detection of a Chemical Warfare Agent Simulant in Various Aerosol Matrixes by Ion Mobility Time-of-Flight Mass Spectrometry. *Anal. Chem.* **2005**, *77*, 4792–4799.
(57) Morrison, K. A.; Bendiak, B. K.; Clowers, B. H. Assessment of Dimeric Metal-Glycan Adducts via Isotopic Labeling and Ion Mobility-Mass Spectrometry. *J. Am. Soc. Mass Spectrom.* **2018**, *29*, 1638–1649.
(58) Hofmann, J.; Hahm, H. S.; Seeberger, P. H.; Pagel, K. Identification of Carbohydrate Anomers Using Ion Mobility–mass Spectrometry. *Nature* **2015**, *526*, 241–244.
(59) Dwivedi, P.; Bendiak, B.; Clowers, B.; Hill, H., Jr. Rapid Resolution of Carbohydrate Isomers by Electrospray Ionization Ambient Pressure Ion Mobility Spectrometry-Time-of-Flight Mass Spectrometry (ESI-APIMS-TOFMS). *J. Am. Soc. Mass Spectrom.* **2007**, *18*, 1163–1175.
(60) Rister, A. L.; Martin, T. L.; Dodds, E. D. Application of Group I Metal Adduction to the Separation of Steroids by Traveling Wave Ion Mobility Spectrometry. *J. Am. Soc. Mass Spectrom.* **2019**, *30*, 248–255.
(61) May, J. C.; Goodwin, C. R.; Lareau, N. M.; Leaptrot, K. L.; Morris, C. B.; Kurulugama, R. T.; Mordehai, A.; Klein, C.; Barry, W.; Darland, E.; Overney, G.; Imatani, K.; Sta, G. C.; Fjeldsted, J. C.; Mclean, J. A. Conformational Ordering of Biomolecules in the Gas Phase: Nitrogen Collision Cross Sections Measured on a Prototype High Resolution Drift Tube Ion Mobility-Mass Spectrometer. *Anal. Chem.* **2014**, *86*, 2107–2116.
(62) Dugourd, P.; Hudgins, R. R.; Clemmer, D. E.; Jarrold, M. F. High-Resolution Ion Mobility Measurements. *Rev. Sci. Instrum.* **1997**, *68* (2), 1122−1129.
(63) Hines, K. M.; Ross, D. H.; Davidson, K. L.; Bush, M. F.; Xu, L. Large-Scale Structural Characterization of Drug and Drug-Like Compounds by High-Throughput Ion Mobility-Mass Spectrometry. *Anal. Chem.* **2017**, *89*, 9023–9030.
(64) Benton, C. M.; Lim, C. K.; Moniz, C.; Jones, D. J. L. Travelling Wave Ion Mobility Mass Spectrometry of 5-Aminolaevulinic Acid , Porphobilinogen and Porphyrins. *Rapid Commun. Mass Spectrom.* **2012**, *26*, 480–486.
(65) Kliman, M.; May, J. C.; Mclean, J. A. Lipid Analysis and Lipidomics by Structurally Selective Ion Mobility-Mass Spectrometry. *Biochim. Biophys. Acta* **2011**, *1811* (11), 935–945.
(66) Guan, S.; Marshall, A. G. Stacked-Ring Electrostatic Ion Guide. *J. Am. Soc. Mass Spectrom.* **1996**, *7*, 101–106.
(67) Deng, L.; Ibrahim, Y. M.; Garimella, S. V. B.; Webb, I. K.; Hamid, A. M.; Norheim, R. V.;

Prost, S. A.; Sandoval, J. A.; Baker, E. S.; Smith, R. D. Greatly Increasing Trapped Ion Populations for Mobility Separations Using Traveling Waves in Structures for Lossless Ion Manipulations. *Analytical Chemistry* **2016**, *88*, 10143–10150.
(68) Chouinard, C. D.; Nagy, G.; Webb, I. K.; Garimella, S. V. B.; Baker, E. S.; Ibrahim, Y. M.; Smith, R. D. Rapid Ion Mobility Separations of Bile Acid Isomers Using Cyclodextrin Adducts and Structures for Lossless Ion Manipulations. *Anal. Chem.* **2018**, *90*, 11086–11091.
(69) Nagy, G.; Attah, I. K.; Garimella, S. V. B.; Tang, K.; Ibrahim, Y. M.; Baker, E. S.; Smith, R. D. Unraveling the Isomeric Heterogeneity of Glycans : Ion Mobility Separations in Structures for Lossless Ion Manipulations. *Chem. Commun.* **2018**, *54*, 11701–11704.
(70) Deng, L.; Garimella, S. V. B.; Hamid, A. M.; Webb, I. K.; Attah, I. K.; Norheim, R. V.; Prost, S. A.; Zheng, X.; Sandoval, J. A.; Baker, E. S.; Ibrahim, Y. M.; Smith, R. D. Compression Ratio Ion Mobility Programming (CRIMP) Accumulation and Compression of Billions of Ions for Ion Mobility-Mass Spectrometry Using Traveling Waves in Structures for Lossless Ion Manipulations (SLIM). *Anal. Chem.* **2017**, *89*, 6432–6439.
(71) Attah, I. K.; Nagy, G.; Garimella, S. V. B.; Norheim, R. V.; Anderson, G. A.; Ibrahim, Y. M.; Smith, R. D. Traveling-Wave-Based Electrodynamic Switch for Concurrent Dual- Polarity Ion Manipulations in Structures for Lossless Ion Manipulations. *Anal. Chem.* **2019**, *91*, 14712–14718.
(72) Ibrahim, Y. M.; Garimella, S. V. B.; Tolmachev, A. V.; Baker, E. S.; Smith, R. D. Improving Ion Mobility Measurement Sensitivity by Utilizing Helium in an Ion Funnel Trap. *Anal. Chem.* **2014**, *86*, 5295–5299.
(73) Kirk, A. T.; Grube, D.; Kobelt, T.; Wendt, C.; Zimmermann, S. High-Resolution High Kinetic Energy Ion Mobility Spectrometer Based on a Low-Discrimination Tristate Ion Shutter. *Anal. Chem.* **2018**, *90*, 5603–5611.
(74) Kwantwi-barima, P.; Reinecke, T.; Clowers, B. H. Increased Ion Throughput Using Tristate Ion-Gate Multiplexing. *Analyst* **2019**, *144*, 6660–6670.
(75) Nagy, G.; Attah, I. K.; Conant, C. R.; Liu, W.; Garimella, S. V. B.; Gunawardena, H. P.; Shaw, J. B.; Smith, R. D.; Ibrahim, Y. M. Rapid and Simultaneous Characterization of Drug Conjugation in Heavy and Light Chains of a Monoclonal Antibody Revealed by High-Resolution Ion Mobility Separations in SLIM. *Anal. Chem.* **2020**, *92*, 5004–5012.
(76) Hollerbach, A. L.; Li, A.; Prabhakaran, A.; Nagy, G.; Harrilal, C. P.; Conant, C. R.; Norheim, R. V.; Schimelfenig, C. E.; Anderson, G. A.; Garimella, S. V. B.; Smith, R. D.; Ibrahim, Y. M. Ultra-High-Resolution Ion Mobility Separations Over Extended Path Lengths and Mobility Ranges Achieved Using a Multilevel Structures for Lossless Ion Manipulations Module. *Anal. Chem.* **2020**, *92*, 7972–7979.
(77) Wang, X.; Wu, B.; Gao, R.; Zhou, S.; Wu, Y.; Yu, J.; Tang, K. A New Ion Funnel for Improving the Transmission of Low Mass Ions. *Int. J. Mass Spectrom.* **2021**, *470*, 116702.
(78) Clowers, B. H.; Ibrahim, Y. M.; Prior, D. C.; Danielson, W. F.; Belov, M. E.; Smith, R. D.; Division, B. S.; Northwest, P.; Box, P. O. Enhanced Ion Utilization Efficiency Using an Electrodynamic Ion Funnel Trap as an Injection Mechanism for Ion Mobility Spectrometry. *Anal. Chem.* **2008**, *80*, 612–623.
(79) Greer, C.; Kinlein, Z.; Clowers, B. H. SLIM Tricks: Tools, Concepts, and Strategies for the Development of Planar Ion Guides. *J. Am. Soc. Mass Spectrom.* **2023**, *34* (8), 1715–1723.
(80) Attah, I. K.; Garimella, S. V. B.; Webb, I. K.; Nagy, G.; Norheim, R. V.; Schimelfenig, C. E.; Ibrahim, Y. M.; Smith, R. D. Dual Polarity Ion Confinement and Mobility Separations. *J. Am. Soc. Mass Spectrom.* **2019**, *30*, 967–976.
(81) Garimella, S. V. B.; Hamid, A. M.; Deng, L.; Ibrahim, Y. M.; Webb, I. K.; Baker, E. S.; Prost, S. A.; Norheim, R. V.; Anderson, G. A.; Smith, R. D. Squeezing of Ion Populations and

Peaks in Traveling Wave Ion Mobility Separations and Structures for Lossless Ion Manipulations Using Compression Ratio Ion Mobility Programming. *Anal. Chem.* **2016**, *88*, 11877–11885.
(82) Price, J.; Goble, T. 10 - Signals and Noise. In *Telecommunications Engineer's Reference Book*; Mazda, F., Ed.; Butterworth-Heinemann, 1993; pp 10–11 – 10–15.
(83) Roscioli, K. M.; Davis, E.; Siems, W. F.; Mariano, A.; Su, W.; Guharay, S. K.; Hill, H. H., Jr. Modular Ion Mobility Spectrometer for Explosives Detection Using Corona Ionization. *Anal. Chem.* **2011**, *83* (15), 5965–5971.
(84) Zhang, X.; Quinn, K.; Cruickshank-Quinn, C.; Reisdorph, R.; Reisdorph, N. The Application of Ion Mobility Mass Spectrometry to Metabolomics. *Curr. Opin. Chem. Biol.* **2018**, *42*, 60–66.
(85) Ben-Nissan, G.; Sharon, M. The Application of Ion-Mobility Mass Spectrometry for Structure/function Investigation of Protein Complexes. *Curr. Opin. Chem. Biol.* **2018**, *42*, 25–33.
(86) Bonneil, E.; Pfammatter, S.; Thibault, P. Enhancement of Mass Spectrometry Performance for Proteomic Analyses Using High-Field Asymmetric Waveform Ion Mobility Spectrometry (FAIMS). *J. Mass Spectrom.* **2015**, *50* (11), 1181–1195.
(87) Liu, F. C.; Ridgeway, M. E.; Park, M. A.; Bleiholder, C. Tandem-Trapped Ion Mobility Spectrometry/mass Spectrometry (tTIMS/MS): A Promising Analytical Method for Investigating Heterogenous Samples. *Analyst* **2022**, *147* (11), 2317–2337.
(88) Michelmann, K.; Silveira, J. A.; Ridgeway, M. E.; Park, M. A. Fundamentals of Trapped Ion Mobility Spectrometry. *J. Am. Soc. Mass Spectrom.* **2015**, *26* (1), 14–24.
(89) Moser, K. L. W.; Wormwood Moser, K. L.; Van Aken, G.; DeBord, D.; Hatcher, N. G.; Maxon, L.; Sherman, M.; Yao, L.; Ekroos, K. High-Defined Quantitative Snapshots of the Ganglioside Lipidome Using High Resolution Ion Mobility SLIM Assisted Shotgun Lipidomics. *Analytica Chimica Acta*. 2021, pp 77–87. https://doi.org/10.1016/j.aca.2020.12.022.
(90) Dodds, J. N.; May, J. C.; McLean, J. A. Correlating Resolving Power, Resolution, and Collision Cross Section: Unifying Cross-Platform Assessment of Separation Efficiency in Ion Mobility Spectrometry. *Anal. Chem.* **2017**, *89* (22), 12176–12184.
(91) Zimmermann, S.; Barth, S.; Baether, W. K. M.; Ringer, J. Miniaturized Low-Cost Ion Mobility Spectrometer for Fast Detection of Chemical Warfare Agents. *Anal. Chem.* **2008**, *80* (17), 6671–6676.
(92) May, J. C.; McLean, J. A. The Influence of Drift Gas Composition on the Separation Mechanism in Traveling Wave Ion Mobility Spectrometry: Insight from Electrodynamic Simulations. *Int. J. Ion Mobil. Spectrom.* **2003**, *16* (2), 85–94.
(93) Williamson, D. L.; Nagy, G. Evaluating the Utility of Temporal Compression in High-Resolution Traveling Wave-Based Cyclic Ion Mobility Separations. *ACS Meas. Au* **2022**. https://doi.org/10.1021/acsmeasuresciau.2c00016.
(94) Sheehan; Yost. What's the Most Meaningful Standard for Mass Spectrometry: Instrument Detection Limit or Signal-to-Noise Ratio. *Curr Trends Mass Spectrom*.
(95) Huntley, A. P.; Hollerbach, A. L.; Prabhakaran, A.; Garimella, S. V. B.; Giberson, C. M.; Norheim, R. V.; Smith, R. D.; Ibrahim, Y. M. Development of a Structure for Lossless Ion Manipulations (SLIM) High Charge Capacity Array of Traps. *Anal. Chem.* **2023**, *95* (9), 4446–4453.
(96) Habibi, S. C.; Nagy, G. General Method to Obtain Collision Cross-Section Values in Multipass High-Resolution Cyclic Ion Mobility Separations. *Anal. Chem.* **2023**, *95* (20), 8028–8035.
(97) Wojcik, R.; Nagy, G.; Attah, I. K.; Webb, I. K.; Garimella, S. V. B.; Weitz, K. K.; Hollerbach,

A.; Monroe, M. E.; Ligare, M. R.; Nielson, F. F.; Norheim, R. V.; Renslow, R. S.; Metz, T. O.; Ibrahim, Y. M.; Smith, R. D. SLIM Ultrahigh Resolution Ion Mobility Spectrometry Separations of Isotopologues and Isotopomers Reveal Mobility Shifts due to Mass Distribution Changes. *Anal. Chem.* **2019**, *91*, 11952–11962.

(98) Stow, S. M.; Causon, T. J.; Zheng, X.; Kurulugama, R. T.; Mairinger, T.; May, J. C.; Rennie, E. E.; Baker, E. S.; Smith, R. D.; McLean, J. A.; Hann, S.; Fjeldsted, J. C. An Interlaboratory Evaluation of Drift Tube Ion Mobility-Mass Spectrometry Collision Cross Section Measurements. *Anal. Chem.* **2017**, *89* (17), 9048–9055.

(99) Picache, J. A.; Rose, B. S.; Balinski, A.; Leaptrot, K. L.; Sherrod, S. D.; May, J. C.; McLean, J. A. Collision Cross Section Compendium to Annotate and Predict Multi-Omic Compound Identities. *Chem. Sci.* **2019**, *10* (4), 983–993.

(100) Merenbloom, S. I.; Koeniger, S. L.; Valentine, S. J.; Plasencia, M. D.; Clemmer, D. E. IMS-IMS and IMS-IMS-IMS/MS for Separating Peptide and Protein Fragment Ions. *Anal. Chem.* **2006**, *78* (8), 2802–2809.

(101) Kirk, A. T.; Raddatz, C.-R.; Zimmermann, S. Separation of Isotopologues in Ultra-High-Resolution Ion Mobility Spectrometry. *Anal. Chem.* **2017**, *89* (3), 1509–1515.

(102) Poyer, S.; Comby-Zerbino, C.; Choi, C. M.; MacAleese, L.; Deo, C.; Bogliotti, N.; Xie, J.; Salpin, J.-Y.; Dugourd, P.; Chirot, F. Conformational Dynamics in Ion Mobility Data. *Anal. Chem.* **2017**, *89* (7), 4230–4237.

(103) Wyttenbach, T.; Pierson, N. A.; Clemmer, D. E.; Bowers, M. T. Ion Mobility Analysis of Molecular Dynamics. *Annu. Rev. Phys. Chem.* **2014**, *65*, 175–196.

(104) Le Fèvre, A.; Dugourd, P.; Chirot, F. Exploring Conformational Landscapes Using Trap and Release Tandem Ion Mobility Spectrometry. *Anal. Chem.* **2021**, *93* (9), 4183–4190.

(105) Bull, J. N.; Scholz, M. S.; Carrascosa, E.; Bieske, E. J. From E to Z and Back Again: Reversible Photoisomerisation of an Isolated Charge-Tagged Azobenzene. *Phys. Chem. Chem. Phys.* **2017**, *20* (1), 509–513.

(106) Ibrahim, Y. M.; Hamid, A. M.; Cox, J. T.; Garimella, S. V. B.; Smith, R. D. Ion Elevators and Escalators in Multilevel Structures for Lossless Ion Manipulations. *Anal. Chem.* **2017**, *89* (3), 1972–1977.

(107) Morsa, D.; Gabelica, V.; De Pauw, E. Effective Temperature of Ions in Traveling Wave Ion Mobility Spectrometry. *Anal. Chem.* **2011**, *83* (14), 5775–5782.

(108) Merenbloom, S. I.; Flick, T. G.; Williams, E. R. How Hot Are Your Ions in TWAVE Ion Mobility Spectrometry? *J. Am. Soc. Mass Spectrom.* **2012**, *23* (3), 553–562.

(109) Li, A.; Conant, C. R.; Zheng, X.; Bloodsworth, K. J.; Orton, D. J.; Garimella, S. V. B.; Attah, I. K.; Nagy, G.; Smith, R. D.; Ibrahim, Y. M. Assessing Collision Cross Section Calibration Strategies for Traveling Wave-Based Ion Mobility Separations in Structures for Lossless Ion Manipulations. *Anal. Chem.* **2020**, *92*, 14976–14982.

(110) Allen, S. J.; Bush, M. F. Radio-Frequency (rf) Confinement in Ion Mobility Spectrometry: Apparent Mobilities and Effective Temperatures. *J. Am. Soc. Mass Spectrom.* **2016**, *27* (12), 2054–2063.

(111) Allen, S. J.; Eaton, R. M.; Bush, M. F. Structural Dynamics of Native-Like Ions in the Gas Phase: Results from Tandem Ion Mobility of Cytochrome c. *Anal. Chem.* **2017**, *89* (14), 7527–7534.

(112) Zercher, B. P.; Hong, S.; Roush, A. E.; Feng, Y.; Bush, M. F. Are the Gas-Phase Structures of Molecular Elephants Enduring or Ephemeral? Results from Time-Dependent, Tandem Ion Mobility. *Anal. Chem.* **2023**, *95* (25), 9589–9597.

(113) Eldrid, C.; Ujma, J.; Kalfas, S.; Tomczyk, N.; Giles, K.; Morris, M.; Thalassinos, K. Gas Phase Stability of Protein Ions in a Cyclic Ion Mobility Spectrometry Traveling Wave Device. *Anal. Chem.* **2019**, *91* (12), 7554–7561.

(114) Esser, T. A Cryogenic Mass Spectrometer for Action Spectroscopy of Single Nanoparticles. PhD, University of Leipzig, 2019.
(115) Glaskin, R. S.; Ewing, M. A.; Clemmer, D. E. Ion Trapping for Ion Mobility Spectrometry Measurements in a Cyclical Drift Tube. *Anal. Chem.* **2013**, No. 85, 7003–7008.
(116) Silveira, J. A.; Ridgeway, M. E.; Park, M. A. High Resolution Trapped Ion Mobility Spectrometery of Peptides. *Anal. Chem.* **2014**, *86* (12), 5624–5627.
(117) Gidden, J.; Bowers, M. T. Gas-Phase Conformational and Energetic Properties of Deprotonated Dinucleotides. *The European Physical Journal D - Atomic, Molecular, Optical and Plasma Physics* **2002**, *20* (3), 409–419.
(118) Valentine, S. J.; Counterman, A. E.; Clemmer, D. E. Conformer-Dependent Proton-Transfer Reactions of Ubiquitin Ions. *J. Am. Soc. Mass Spectrom.* **1997**, *8* (9), 954–961.
(119) Myung, S.; Badman, E. R.; Lee, Y. J.; Clemmer, D. E. Structural Transitions of Electrosprayed Ubiquitin Ions Stored in an Ion Trap over ~10 Ms to 30 S. *J. Phys. Chem. A* **2002**, *106* (42), 9976–9982.
(120) Freitas, M.; Marshall, A. Rate and Extent of Gas-Phase Hydrogen/deuterium Exchange of Bradykinins: Evidence for Peptide Zwitterions in the Gas Phase. *Int. J. Mass Spectrom.* **1999**, *182-183*, 221–231.
(121) Schaaff, T. G.; Stephenson, J. L.; McLuckey, S. A. The Reactivity of Gaseous Ions of Bradykinin and Its Analogues with Hydro- and Deuteroiodic Acid. *J. Am. Chem. Soc.* **1999**, *121* (38), 8907–8919.
(122) Ewing, N. P.; Pallante, G. A.; Zhang, X.; Cassady, C. J. Gas-Phase Basicities for Ions from Bradykinin and Its Des-Arginine Analogues. *J. Mass Spectrom.* **2001**, *36* (8), 875–881.
(123) Porter, S.R., Arslanian, A. J., Mismash, N. J., Dearden, D. V. Activation and Relaxation of Protein Ions Observed in an FT-ICR MS. In *71st ASMS Conference on Mass Spectrometry and Allied Topics*; 2023.
(124) Pope, B. L.; Joaquin, D.; Hickey, J. T.; Mismash, N.; Heravi, T.; Shrestha, J.; Arslanian, A. J.; Anupriya; Mortensen, D. N.; Dearden, D. V. Multi-CRAFTI: Relative Collision Cross Sections from Fourier Transform Ion Cyclotron Resonance Mass Spectrometric Line Width Measurements. *J. Am. Soc. Mass Spectrom.* **2021**, *33* (1), 131–140.
(125) Giles, K.; Ujma, J.; Harrison, J.; Chande, B.; Scambler, G. Ion Guide. 20220216045:A1, July 7, 2022. https://patentimages.storage.googleapis.com/55/e9/02/b5026f1d6bfbb4/US20220216045A1.pdf (accessed 2023-12-11).
(126) Ieritano, C.; Rickert, D.; Featherstone, J.; Honek, J. F.; Campbell, J. L.; Blanc, J. C. Y. L.; Schneider, B. B.; Hopkins, W. S. The Charge-State and Structural Stability of Peptides Conferred by Microsolvating Environments in Differential Mobility Spectrometry. *J. Am. Soc. Mass Spectrom.* **2021**, *32* (4), 956–968.
(127) Eaton, R. M.; Zercher, B. P.; Wageman, A.; Bush, M. F. A Flexible, Modular Platform for Multidimensional Ion Mobility of Native-like Ions. *J. Am. Soc. Mass Spectrom.* **2023**, *34* (6), 1175–1185.
(128) Kwantwi-Barima, P.; Garimella, S. V. B.; Attah, I. K.; Zheng, X.; Ibrahim, Y. M.; Smith, R. D. Accumulation of Large Ion Populations with High Ion Densities and Effects Due to Space Charge in Traveling Wave-Based Structures for Lossless Ion Manipulations (SLIM) IMS-MS. *J. Am. Soc. Mass Spectrom.* **2024**. https://doi.org/10.1021/jasms.3c00389.
(129) Carpenter, J. E.; McNary, C. P.; Furin, A.; Sweeney, A. F.; Armentrout, P. B. How Hot Are Your Ions Really? A Threshold Collision-Induced Dissociation Study of Substituted Benzylpyridinium “Thermometer” Ions. *J. Am. Soc. Mass Spectrom.* **2017**, *28* (9), 1876–1888.

(130) Collette, C.; De Pauw, E. Calibration of the Internal Energy Distribution of Ions Produced by Electrospray. *Rapid Commun. Mass Spectrom.* **1998**, *12* (4), 165–170.
(131) Kwantwi-Barima, P.; Hogan, C. J., Jr; Clowers, B. H. Deducing Proton-Bound Heterodimer Association Energies from Shifts in Ion Mobility Arrival Time Distributions. *J. Phys. Chem. A* **2019**, *123* (13), 2957–2965.
(132) Schramm, H. M.; Tamadate, T.; Hogan, C. J.; Clowers, B. H. Ion-Neutral Clustering Alters Gas-Phase Hydrogen-Deuterium Exchange Rates. *Phys. Chem. Chem. Phys.* **2023**, *25* (6), 4959–4968.
(133) Poad, B. L. J.; Pham, H. T.; Thomas, M. C.; Nealon, J. R.; Campbell, J. L.; Mitchell, T. W.; Blanksby, S. J. Ozone-Induced Dissociation on a Modified Tandem Linear Ion-Trap : Observations of Different Reactivity for Isomeric Lipids. *J. Am. Soc. Mass Spectrom.* **2010**, *21*, 1989–1999.
(134) Suckau, D.; Shi, Y.; Beu, S. C.; Senko, M. W.; Quinn, J. P.; Wampler, F. M., 3rd; McLafferty, F. W. Coexisting Stable Conformations of Gaseous Protein Ions. *Proc. Natl. Acad. Sci. U. S. A.* **1993**, *90* (3), 790–793.
(135) Campbell, S.; Rodgers, M. T.; Marzluff, E. M.; Beauchamp, J. L. Deuterium Exchange Reactions as a Probe of Biomolecule Structure. Fundamental Studies of Gas Phase H/D Exchange Reactions of Protonated Glycine Oligomers with D2O, CD3OD, CD3CO2D, and ND3. *J. Am. Chem. Soc.* **1995**, *117* (51), 12840–12854.
(136) Schramm, H. M.; Tamadate, T.; Hogan, C. J.; Clowers, B. H. Evaluation of Hydrogen-Deuterium Exchange during Transient Vapor Binding of MeOD with Model Peptide Systems Angiotensin II and Bradykinin. *J. Phys. Chem. A* **2023**, *127* (42), 8849–8861.
(137) Valentine, S. J.; Clemmer, D. E. H/D Exchange Levels of Shape-Resolved Cytochrome c Conformers in the Gas Phase. *J. Am. Chem. Soc.* **1997**, *119* (15), 3558–3566.
(138) Thomas, M. C.; Mitchell, T. W.; Harman, D. G.; Deeley, J. M.; Nealon, J. R.; Blanksby, S. J. Ozone-Induced Dissociation : Elucidation of Double Bond Position within Mass-Selected Lipid Ions. *Anal. Chem.* **2008**, *80*, 303–311.
(139) Poad, B. L. J.; Zheng, X.; Mitchell, T. W.; Smith, R. D.; Baker, E. S.; Blanksby, S. J. Online Ozonolysis Combined with Ion Mobility-Mass Spectrometry Provides a New Platform for Lipid Isomer Analyses. *Anal. Chem.* **2018**, *90*, 1292–1300.
(140) Castelli, F. A.; Rosati, G.; Moguet, C.; Fuentes, C.; Marrugo-Ramírez, J.; Lefebvre, T.; Volland, H.; Merkoçi, A.; Simon, S.; Fenaille, F.; Junot, C. Metabolomics for Personalized Medicine: The Input of Analytical Chemistry from Biomarker Discovery to Point-of-Care Tests. *Anal. Bioanal. Chem.* **2022**, *414* (2), 759–789.
(141) Hoefer, I. E.; Steffens, S.; Ala-Korpela, M.; Bäck, M.; Badimon, L.; Bochaton-Piallat, M.-L.; Boulanger, C. M.; Caligiuri, G.; Dimmeler, S.; Egido, J.; Evans, P. C.; Guzik, T.; Kwak, B. R.; Landmesser, U.; Mayr, M.; Monaco, C.; Pasterkamp, G.; Tuñón, J.; Weber, C.; ESC Working Group Atherosclerosis and Vascular Biology. Novel Methodologies for Biomarker Discovery in Atherosclerosis. *Eur. Heart J.* **2015**, *36* (39), 2635–2642.
(142) He, D.; Luo, Y.; Lu, S.; Liu, M.; Song, Y.; Lei, L. Microplastics in Soils: Analytical Methods, Pollution Characteristics and Ecological Risks. *Trends Analyt. Chem.* **2018**, *109*, 163–172.